ALMA MATER STUDIORUM - UNIVERSITÀ DI BOLOGNA

SCHOOL OF ENGINEERING AND ARCHITECTURE

DEPARTMENT OF CIVIL, CHEMICAL, ENVIRONMENTAL AND
MATERIALS ENGINEERING

Master's Degree in Chemical and Process Engineering
Sustainable Technologies and Biotechnologies for Energy and Materials

THESIS

in
Polymer Science and Technology

NATURAL WAX-BASED WATER VAPOUR BARRIER COATINGS ON PLA FOR MAP FOOD PACKAGING

CANDIDATE: SUPERVISOR:
Lorenzo Tomei   Prof. Andrea Saccani

                                              ASSISTANT SUPERVISORS:
                                              Prof.ssa Annamaria Celli
                                              Dr. Siegfried Fürtauer
                                              Prof.ssa Laura Sisti

Academic Year 2019/2020
Session III

Acknowledgments

Table of Contents

Abbreviations

ASTM: American Society for Testing Materials

DSC: Differential Scanning Calorimetry

ESBO: Epoxidized Soybean Oil

EU: European Union

FAME: Fatty Acid Methyl Esters

FAO: Food and Agriculture Organization

FTIR: Fourier Transform Infrared Spectroscopy

MAP: Modified Atmosphere Packaging

RH: Relative Humidity

SDG: Sustainable Development Goals

WVP: Water Vapour Permeability

WVTR: Water Vapour Transmission Rate

Polymers

HDPE: High Density Polyethylene

PA: Polyamide

PBAT: Polybutylene adipate-*co*-terephthalate

PBS: Polybutylene succinate

PCL: Polycaprolactone

PE: Polyethylene

PEF: Polyethylene furanoate

PET: Polyethylene terephthalate

PHAs: Polyhydroxyalkanoates

PLA: Polylactide acid

PP: Polypropylene

PS: Polystyrene

PTT: Polytrimethylene terephthalate

PVC: Polyvinyl chloride

Natural waxes

BEE: Beeswax

CND: Candelilla wax

CRB: Carnauba wax

RB: Rice bran wax

SF: Sunflower wax

Objectives

This thesis will focus on the description of the experimental work concerning the modification of natural waxes and the development of innovative bio-based materials in order to improve the water vapour barrier properties of PLA food packaging trays.

Fresh packaged foods require specific concentration of H_2O and O_2 in order to maintain the organoleptic properties unaltered throughout their shelf-life. PLA is a very promising bio-based polymer that is bound to become more and more relevant for a sustainable packaging manufacturing. However, its gas and vapour barrier properties are not enough to comply with the requirements of MAP packaging of fresh foodstuffs. The use of waxes from natural renewable sources such as plants (*e.g.*, candelilla wax, carnauba wax, rice bran wax, sunflower wax) or animals (*e.g.*, beeswax) could tackle down the permeation of water vapour through the packaging without affecting its bio-based content. The core of this thesis is enhancing the thermo-mechanical properties of natural waxes so that they can undergo thermoforming and ensuring proper adhesion to the PLA substrate. Chemical modifications of waxes have been performed to produce in-house wax-based alkyd resins that should provide the desired properties to address the two main problems cited just above. Films of the synthesised materials are produced in order to assess their water vapour permeability.

The work has been carried out as a part of the PLA4MAP project in the *Materialentwicklung* (Materials Development) department at the *Fraunhofer-Institut für Verfahrenstechnik und Verpackung IVV* (Institute for Process Engineering and Packaging) in Freising, Germany.

1. Introduction

Packaging is an essential element in our modern society and its relevance will keep rising due to the challenging necessity to develop a more sustainable industrial economy, able to provide an environmentally responsible supply for a strikingly increasing worldwide demand. This issue is especially sensitive to food, whose total loss, as reported in 2011 by FAO (Food and Agricultural Organization) [1], was roughly estimated to be around one-third of edible parts of food globally produced for human consumption. More recent data estimate a 13.8% loss of total food produced worldwide between farming and retail [2]. When considering an estimated increase of 2 billion people in the next 30 years that would lead to 9.7 billion people in 2050 [3], the urgency to create sustainable and potentially circular food economy is becoming significantly vital. Supranational organizations and both national and international policymakers are making a considerable effort to outline regulations and guidelines to tackle down the problem. The United Nations have adopted the 17 Sustainable Development Goals (*SDGs*) in September 2015 as crucial items of their 2030 Agenda for Sustainable Development. The EU Commission has fostered the Green New Deal as a pact to make Europe climate neutral by 2050.

Packaging could play a pivotal role in the implementation of the previously cited policies. In fact, it is designed not merely to fulfil the distribution and the safeguard of various products effectively and efficiently, but also to help the final consumer to avoid misuse and waste of the product.

The main goal of designing a packaging solution is the protection and preservation of products from external strains such as: light, impacts, vibrations, high or low temperatures, unwanted odours, dust, physical damage, moisture, gases, chemical agents and microorganisms. In addition, the endurance of the packaged products is remarkably important since both food quality and freshness must fulfil specific standards for safety and health of consumers. Packaging is then fundamental in increasing the so-called *shelf-life* of products, thus extending the period during which the food is still edible and consequently reducing potential wastes due to improper storage. One of the main challenges of packaging is trying to protect food

products as long as possible from deterioration. The most prevailing causes of quality alteration are oxidative phenomena in combination with metabolic and microbial deterioration. They could happen in each of the food manufacturing steps: production, transportation, storage and retail. It is of striking importance that packaging can preserve both quality and safety standards because a potential inability in proper food preservation would affect consumers' decision-making on buying packaged products and their health. In addition, it would cast a dark shadow on the entire food supply chain [4].

The main requirements for food packaging are reported in TABLE 1.

Table 1 – Packaging requirements

• Protection from surrounding environment
• Prevention from loss and waste
• Mechanical and chemical resistance
• Extended shelf-life
• Quality and safety preservation
• Provide information about the product

1.1 Sustainable Plastics: a Prevailing Drive for Packaging Applications

The packaging world has been continuously dominated by fossil-based plastics over the last half-century. In fact, traditional plastics derived from petroleum fractioning and refining (e.g., PE, PP, PET, PVC, PS) have been massively used for protecting goods and products due to their incredible advantageous combination of flexibility, lightness, strength, stability, impermeability and ease of sterilization. Moreover, short of either geo-political or oil market crisis, fossil-based plastics are economic and easily scalable at industrial level. In 2018 the global production of plastics reached 359 Mt, whereas in Europe alone almost 62 million tonnes of plastics were manufactured. The packaging sectors absorbs a considerably large 40% of the 51.2 Mt of the total EU plastics converters demand [5]. However, the strong dependence of traditional plastics manufacturing on fossil fuels and the increasingly

overwhelming issue of single-use packaging disposal have cast a light on the urgency to find less ecologically burdening solutions on both technological and policy-making levels [6]. In 2017 roughly 77 Mt of packaging waste were generated in Europe and plastics occupied almost 19% thereof [7]. According to the renowned *Ellen McArthur Foundation*, the main three principles for establishing a *New Plastics Economy* are the following (SEE FIGURE 1) [8]:

- Create an effective after-use plastic economy
- Reduce leakage of plastics into natural systems
- Decouple plastics from fossil feedstocks
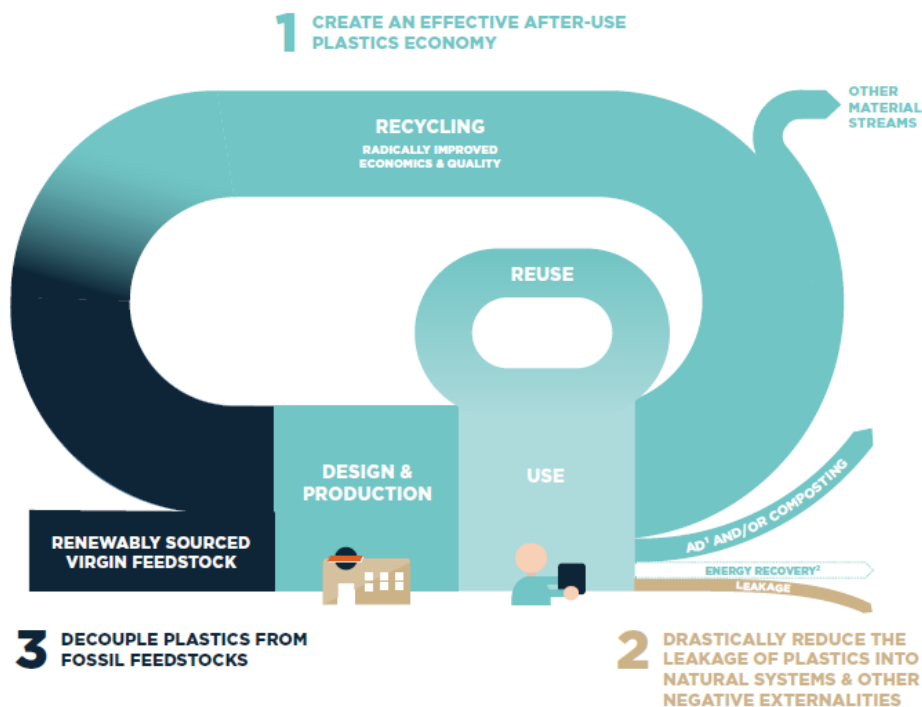
Figure 1 – The New Plastics Economy and its three pillars

The first two points are intrinsically related to end stage of plastics lifecycle. The typical strategies to manage the disposal of fossil-based plastics are reported in TABLE 2. However, over the years a consistent awareness has risen and since 2006 the amount of recycled plastic waste has more than doubled, while landfilling has become less and less relevant, as displayed in FIGURE 2. In order to achieve a circular economy for plastics, the landmark goal of *zero landfilling* should be reached [5].

Table 2 – Strategies for disposal of plastics

Strategy	Pros	Cons
Landfilling or water dispersion	Most straightforward and most economic	High ecological hazard for flora and fauna, health risk for human beings
Incineration	Energy recovery	Greenhouse gases and toxic and/or carcinogenic emissions to air
Recycling	Lifecycle extension and reduction of waste environmental impact	Reduction of plastic mechanical properties (i.d., downcycling); inefficiency of separation techniques for different plastic types
Composting	Production of fertilizers	Complicated and time-consuming; presence of by-products (e.g., additives)
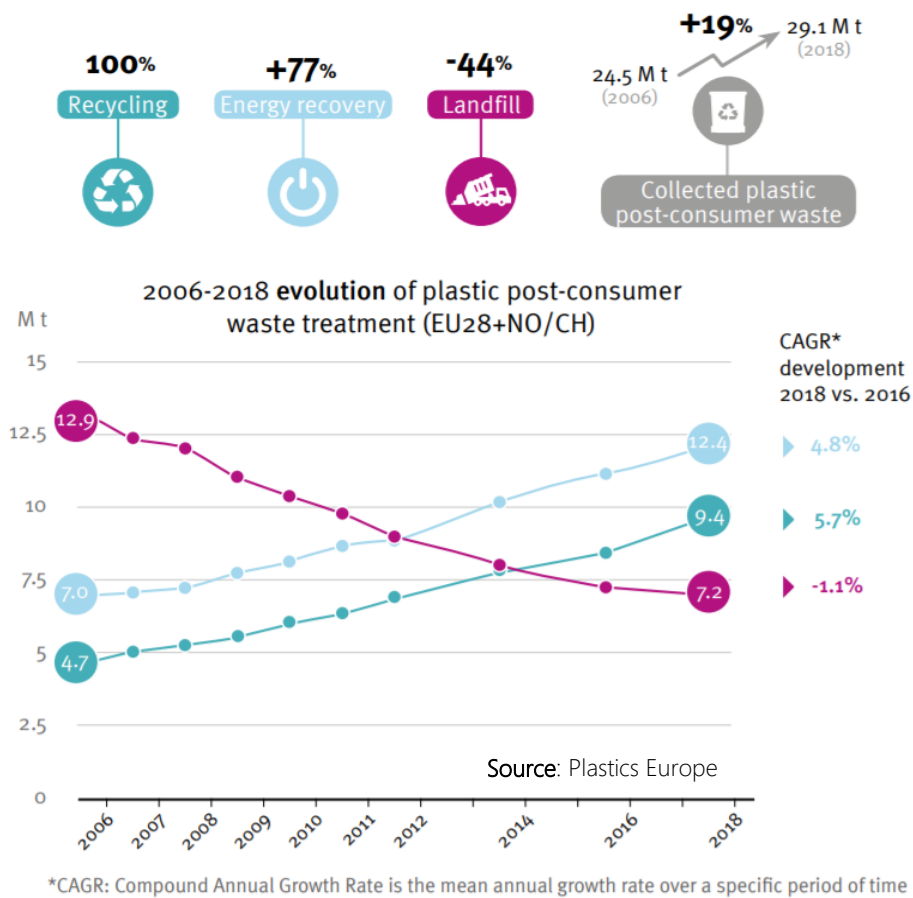
Figure 2 – Time evolution of strategies of disposal

The third and last point is strictly related to the starting raw materials, instead. The focus of this thesis is centred on this latter goal and the development of innovative materials based on renewable sustainable resources is highly of interest. The claim of *renewability* consists in the capacity of a given resource to be replenished by means of a naturally occurring and repetitive biological process. This must take place in a relatively small time in comparison with a human timescale. Fossil fuels usually take millions of years to be formed. Two further important concepts which are related to both the selection of raw materials and the end-of-life of packaging are the *biodegradability* and the *compostability* of the material itself. In fact, a biodegradable material is naturally degraded in simpler metabolites (*e.g.*, H_2O, CO_2, CH_4 and biomass) by microorganisms (*e.g.*, bacteria or fungi) present in the surrounding ambient. No artificial control is operated on this process and the degradation rate is strongly variable depending on the environmental conditions. On the other hand, *compostability* is by no means a synonym of *biodegradability*, since it consists in a very finely controlled degradation process in terms of temperature, aeration and humidity. Compliance with EN 13432 is assumed as a good criterion for assessing the industrial compostability of a given material [9].

Lastly, another fundamental notion is the definition of a *bio-based* material. EN 16575 defines a *bio-based* material as *wholly or partly derived from biomass*, which can be any material of biological origin. Bio-based materials can be called renewable only if a new crop at least balances the harvest.

In order to avoid any misunderstanding, the following TABLE 3 sums up all the different key-features of the previous definitions.

Table 3 – Distinction between bioplastic-related definitions

Renewable	Naturally cyclically replenished on human timescale
Biodegradable	Naturally degraded by microorganisms in the environment
Compostable	Artificially degraded under controlled conditions (EN 13432)
Bio-based	Wholly or partly derived from biomass (EN 16575)

Bioplastics display an interesting range of the properties just cited above. *European Bioplastics* – the association representing the interests of the bioplastics industry along the entire value chain in Europe – defines bioplastics as *a family of materials which are either bio-based, biodegradable or features both properties*. The overlapping of properties is reported in FIGURE 3 [10].
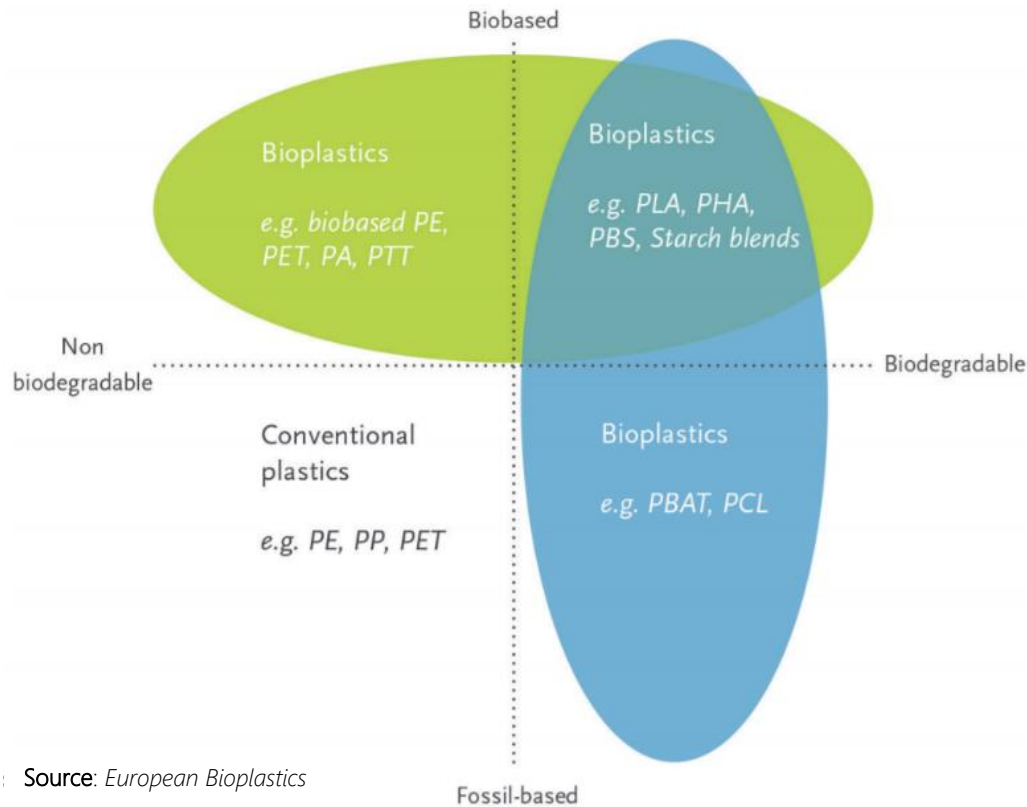
Source: *European Bioplastics*

Figure 3 – Material coordinate system of bioplastics: biodegradability vs. bio-based

The market of bioplastics is still small when compared to traditional fossil-based plastics, but it is increasing each year. All the reported market data and FIGURES 4-7 are provided by *European Bioplastics* [11]. In 2019 the 2.11 Mt global production of bioplastics represented a modest 0.59% of the global share of manufactured plastics. Nevertheless, when considering the increase of bioplastics manufacturing over the following years up to 2024, a remarkable +14.8% is forecast (FIGURE 4). Moreover, the most likely field of application for bioplastics is identified in packaging, which represents almost 54% of the share (FIGURE 5). The global production capacities for each given material is reported in FIGURE 6.

6
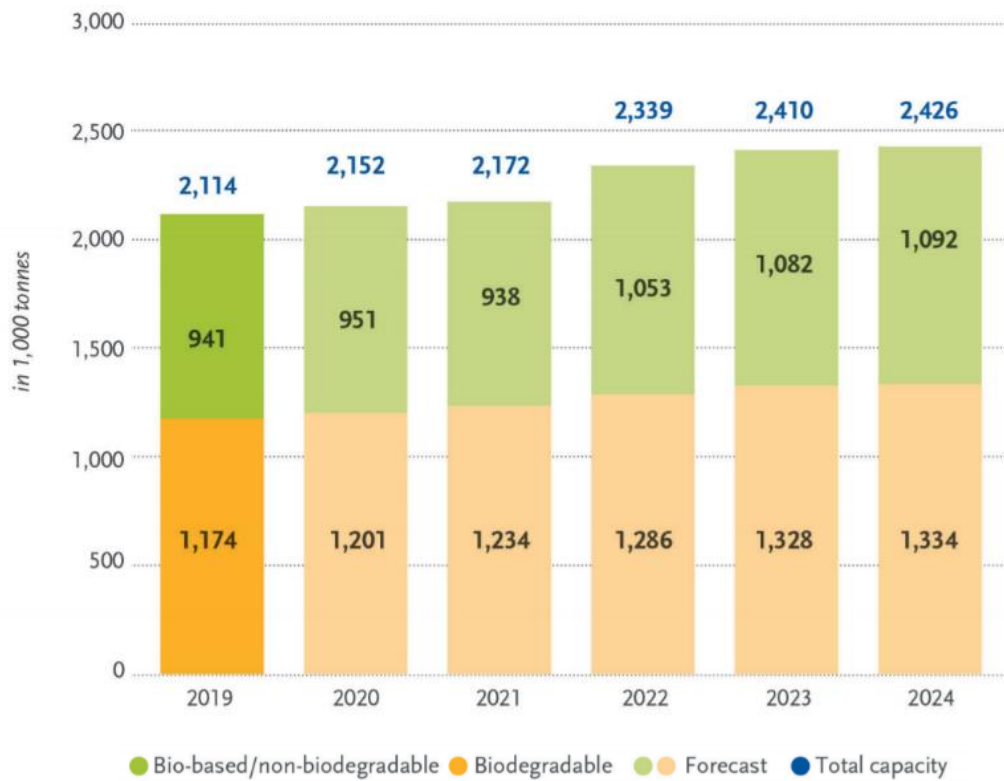
Figure 4 – Global production of bioplastics (2019-2024)
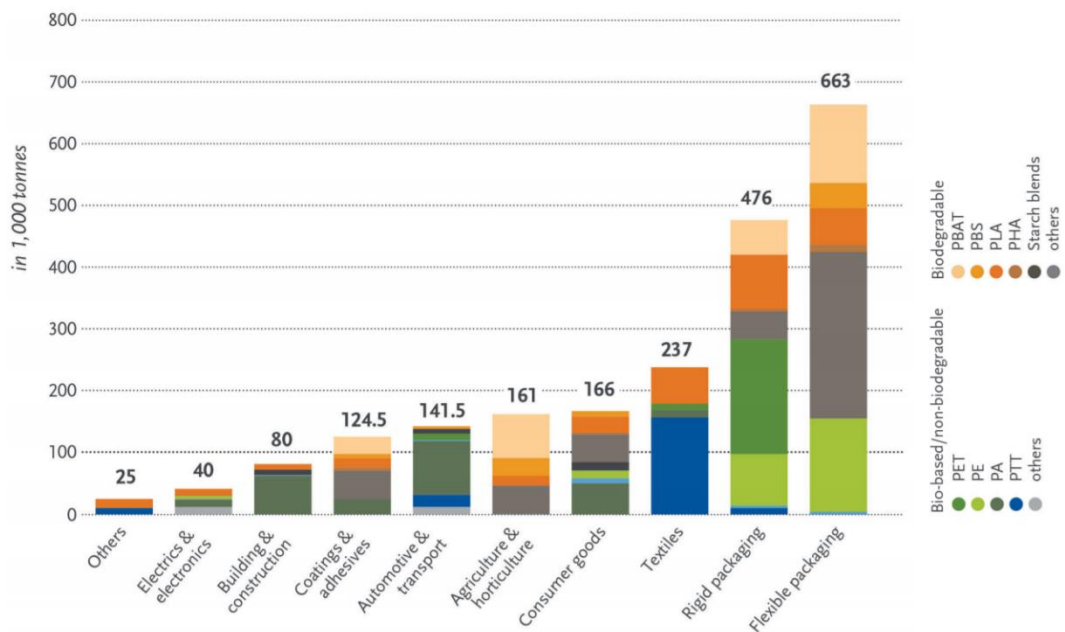
Figure 5 – Market segments for different bioplastics (2019)
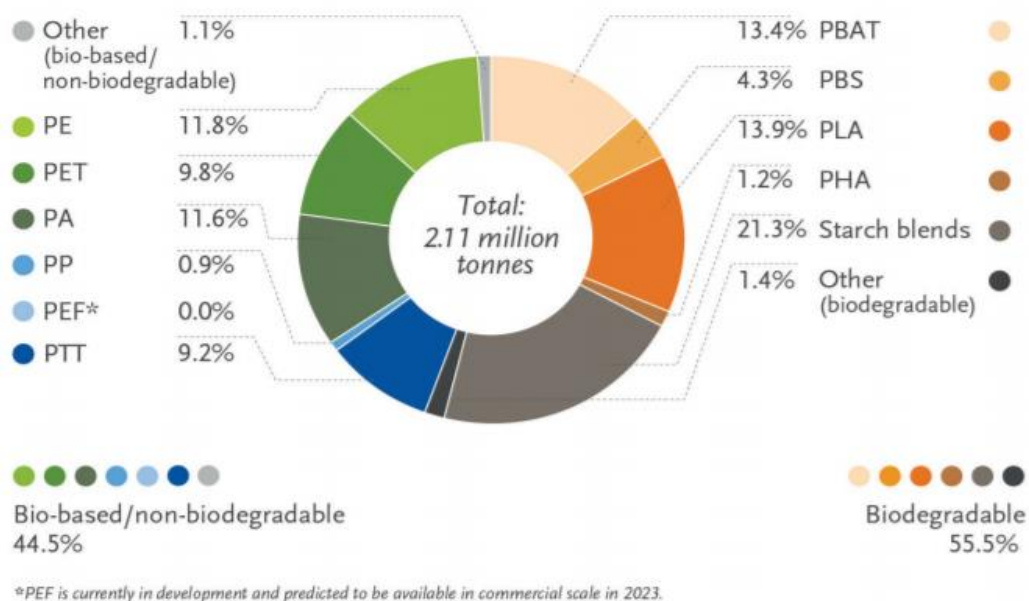
Figure 6 – Different polymeric materials for bioplastics (2019)

A very interesting trend is that the land required to grow the renewable feedstocks for bioplastics production accounts approximately for a remarkably minute 0.02% of the global 4.8 billion hectares allocated to agriculture in 2019. Even more interesting is that the estimated land use share will remain around 0.02% over the following years (FIGURE 7). Thus, despite the global market growth, there is no significant competition with renewable feedstock for feed and food. Nonetheless, bioplastics are forecast to become in relevant competition with food crops in the future, when their production capacity will rise and substitute the majority of fossil-based materials.
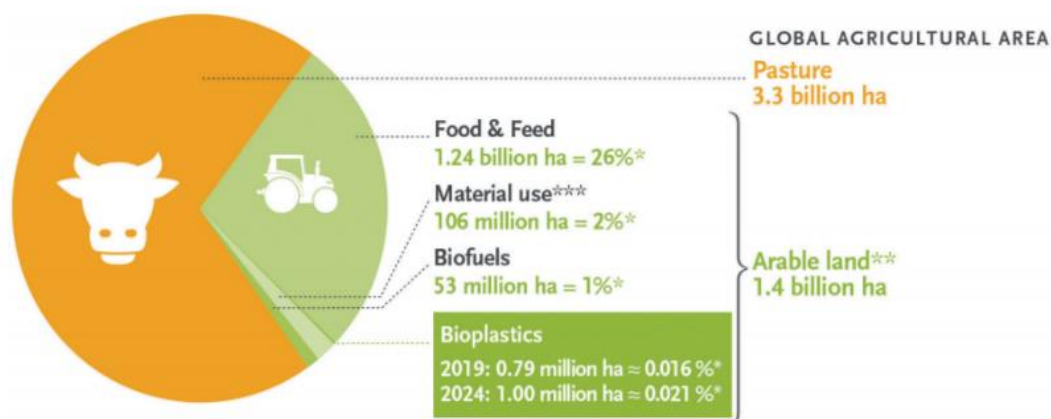
Figure 7 – Land use estimation for bioplastics (2019-2024)

In conclusion to this section, according to the *Sustainable Packaging Coalition –* an international pool of packaging industries – a packaging can be defined as *sustainable* if the requirements reported in TABLE 4 are fulfilled [12].

Table 4 – Definition of sustainable packaging

A sustainable packaging:
A. is beneficial, safe and healthy for individuals and communities throughout its lifecycle.
B. meets market criteria for performance and cost.
C. is sourced, manufactured, transported and recycled using renewable energy.
D. optimizes the use of renewable or recycled source materials.
E. is manufactured using clean production technologies and best practices.
F. is made from materials which remain safe for human life throughout the entire lifecycle.
G. is physically designed to optimize materials and energy.
H. is effectively recovered and utilized in biological and/or industrial closed loop cycles.

1.2 Modified Atmosphere Packaging: a Longer Shelf-Life for Oxygen-Sensitive Foodstuffs

Each packaged food requires proper optimal conditions to avoid the acceleration of biological degradation. That is why the selected materials must display the required barrier properties against undesired vapours and gases such as H_2O (trigger for microbial growth that may damage the product) and O_2 (trigger for oxidative degradation phenomena) to avoid decaying phenomena over the expected time of storage. Likewise, a well-designed packaging should keep the organoleptic food properties unaltered so that the final consumer can taste the product at its best potentially even long after its manufacturing. Generally speaking, the better the barrier properties of a packaging material, the longer the shelf-life of the packaged

product, thus the better the food quality and the higher the economic value of both the packaging and the product.

The *shelf-life* can be described as a finite period after production – or even after maturation or aging in specific cases – and packaging of a given food product during which a required standard of quality must be preserved under precisely delineated conditions of storage. In the European Union, food companies are required to attribute a shelf-life to their products under defined storage conditions in compliance with Regulation 1169/2011. This law defines the date of minimum food durability as *"the date until which the food retains its specific properties when properly stored"* (Ch. I, Art. 2, Par. 2.r). In the case of highly perishable food which are capable of undergoing microbial degradation during storage and thus constituting immediate danger to human health, the date of minimum durability shall be substituted with the "*use by*" date (Ch. IV, Sect. 2, Art. 24, Par. 1) [13].

A very challenging task is prolonging the shelf-life of fresh foodstuffs such as meat, fish, dairy and baked products, fruits and vegetables. This is because any fresh product will display a certain metabolic activity even when the harvesting is completed. The necessary energy to sustain such activities is obtained from oxidation of carbohydrates into CO_2, H_2O and heat. This phenomenon is called *respiration* and it continues as long as enough nutrient reserves and moisture content are present in the food itself. Respiration favours a deterioration of food which is undesired for both quality, safety and aesthetic standards. Reducing the *respiration rate* will allow a reduction of loss of energy reserves and thus an extension of the shelf-life of packaged foodstuffs. *Modified Atmosphere Packaging* (or MAP) is a preservation strategy aiming at extending the shelf-life of O_2-sensitive fresh food products by optimizing the gaseous packaging headspace. The main three gases involved in MAP are O_2, CO_2 and N_2 (the so-called *tri-gas* MAP) and the key concept is a reduction in O_2 vapour pressure to reduce the respiration rate by increasing CO_2 content and balancing N_2 to reach the desired packaging design pressure. However, the headspace gaseous composition is strongly dependent on the packaged products and the storage temperature [14]–[16].

1.3 PLA: a Renewable Journey From Corn to Packaging

It has been previously highlighted how crucial the re-design of a new plastic economy is for sustainable production and consumption. Moreover, it has been observed that biodegradable packaging solutions developed on bio-based and renewable raw materials are a very compelling and interesting strategy to tackle the problem. Nonetheless, these environmentally-friendly materials still present some challenges in terms of mechanical, thermal and barrier performance when compared with traditional fossil-based materials. A solution could be to chemically functionalize the polymers to impart specific properties like hydrophobicity, since most biopolymers have a tendency of being naturally hydrophilic. Another strategy could be to create bio-composite materials, in which biopolymers function as matrix and the dispersed phase is to improve mechanical, thermal and barrier performance. In the case of films, multilayer films could be designed to impart a specific function to each specific layer. However, the latter two scenarios must be carefully dealt with, since increasing the complexity of the packaging system could affect the biodegradability of the final material [17], which is one of the main value propositions of biopolymers.

In order to understand the most interesting biopolymers which are available for food packaging applications, a due classification is reported in FIGURE 8. A broad and preliminary separation is based upon the origin of raw materials, while a finer and secondary division is focused on the chemical nature of the polymer itself.
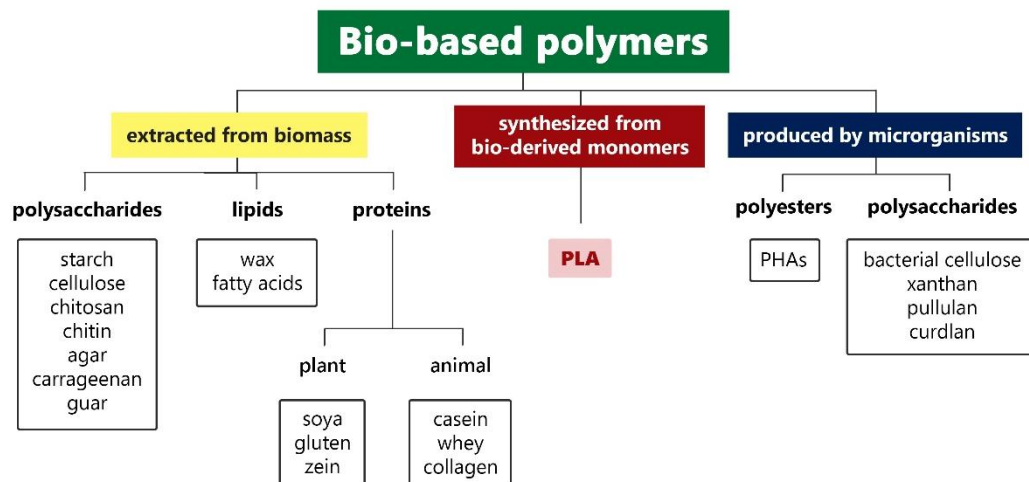
Figure 8 – Biopolymers classification

Polysaccharides, polyamides (e.g., proteins) and polyesters (e.g., PLA, PHAs) are the three main polymeric structures of interest in the field of biopolymers. Polyesters play a pivotal role since their hydrolysable ester bonds enhance their potential biodegradability. Commercially available polyesters are reported in TABLE 5 with their polymer structure.

Among the family of polyesters, PLA occupies a paramount position in terms of packaging applications. In fact, PLA is a high-modulus and high-strength thermoplastic produced from renewable raw materials. It can be processed on conventional equipment for fossil-based thermoplastics. Parts can be moulded and formed, films can be drawn and fibres can be spun and PLA products are both biodegradable and compostable. The degradation of PLA is due to hydrolysis of ester bonds and enzyme catalysis is not really necessary. The degradation rate depends on different variables such as the dimensions of the product, the morphology or the temperature. However, its degradation time can be estimated between six months and two years when disposed in the environment. If we consider that conventional plastics such as PS and PE require 500 to 1,000 years for degradation, PLA has an incredible advantage in terms of environmental sustainability [18]. The building block of PLA is lactic acid (2-hydroxy propionic acid), which is industrially produced by fermentation of carbohydrate-rich substrates such as maize.

The lifecycle of PLA is reported in FIGURE 9. It is highlighted how promising it is as a biopolymer since a theoretical *closed-loop* could be obtained by complete recovery of starting monomers by simple hydrolysis of the bioplastics used for a given packaging.

Marketwise, PLA occupies an important role in the bioplastics segment. According to European Bioplastics, it displays 13.9% share of 2.11 Mt of global bioplastics produced in 2019 (see FIGURE 6).

Table 5 – Commercially available bio-polyesters

Polyester	Abbreviation	Polymer structure
Poly(lactic acid)	PLA	
Polyhydroxyalkanoates	PHAs	 R is the lateral chain that distinguishes each single polyhydroxyalkanoate
Polycaprolactone	PCL	
Poly(butylene succinate)	PBS	
Poly(butylene succinate-*co*-adipate)	PBSA	
Bio-poly(ethylene terephthalate)	Bio-PET	
Poly(butylene adipate-*co*-terephthalate)	PBAT	
Poly(ethylene furanoate)[1]	PEF	
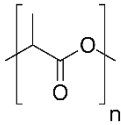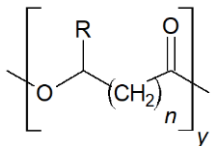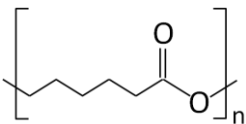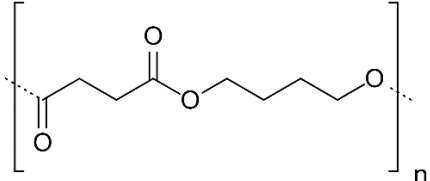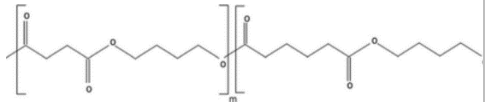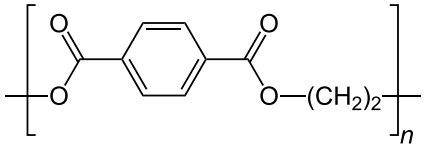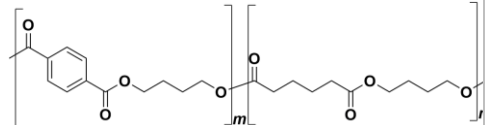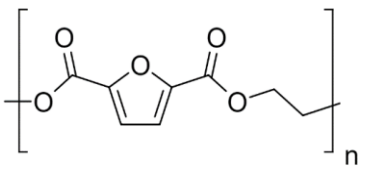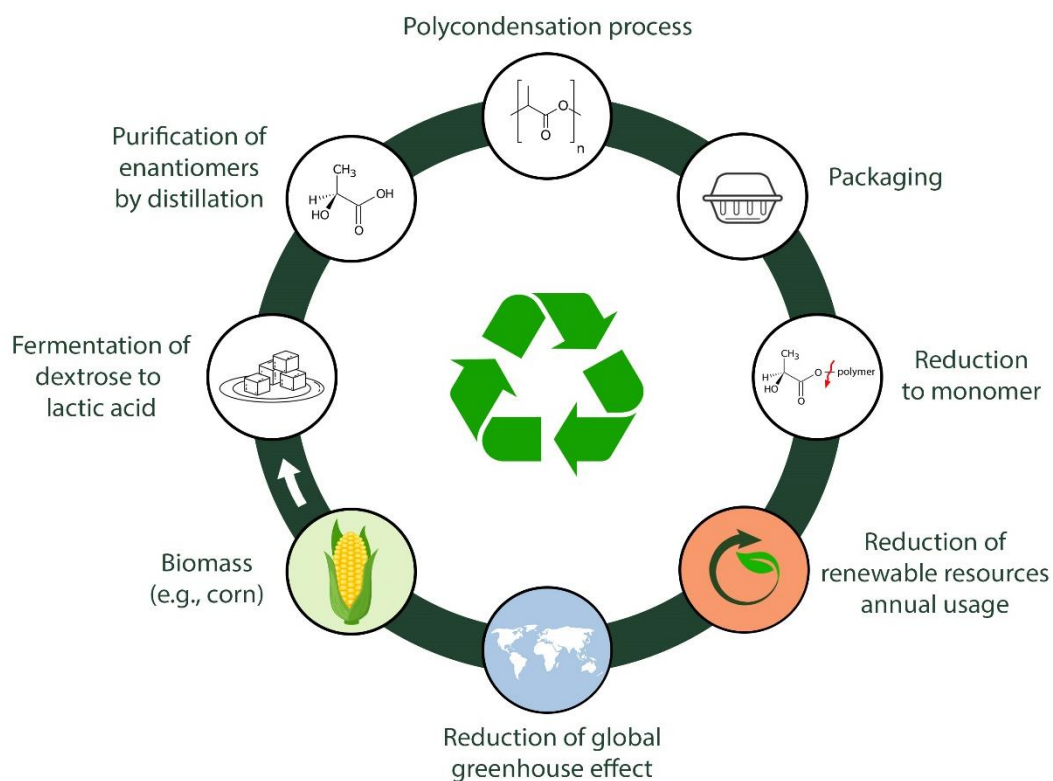
Figure 9 – PLA lifecycle

Asia and North America are the two major regions producing PLA. 50% of the worldwide PLA capacity is located in North America with NatureWorks LLC being the major producer for PLA in the past and expected to be the same in the future. The Asian market does not display a large producer such as NatureWorks LLC. However, the fragmented small manufacturers add up to 47% of the worldwide PLA capacity. Europe has a minor PLA production of the remaining 3% share, which is provided by Corbion, Sulzer Chemtech AG and thyssenkrupp Industrial Solutions AG (formerly known as Uhde-Inventa Fischer AG). Capacity addition in 2019 for PLA is coming from the addition of Guangzhou Bio-plus Materials Technology Co., Ltd. capacity of 10,000 t/a in China. In the next five years till the end of 2024 a capacity increase of about 24,000 t/yr in Asia is expected. PLA production capacity in 2019 is in total around 300,000 t/yr. Due to an enduring increase of PLA production capacities until the end of 2024, the operating rate of PLA facilities is estimated to be around 90%. From this an actual production of

around 270,000 t/yr of PLA in 2019 is evaluated [19]. The market trend of previous years and the estimations of the coming years are reported in FIGURE 10, while the main producers along with their market shares for 2019 are reported in FIGURE 11.
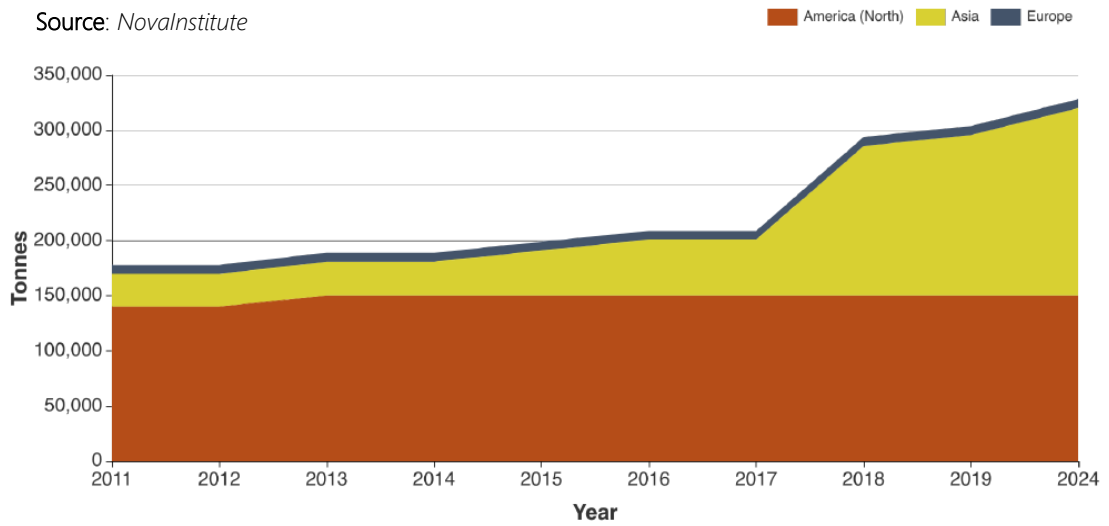
Figure 10 – Global PLA production in three key regional markets (2011-2024)
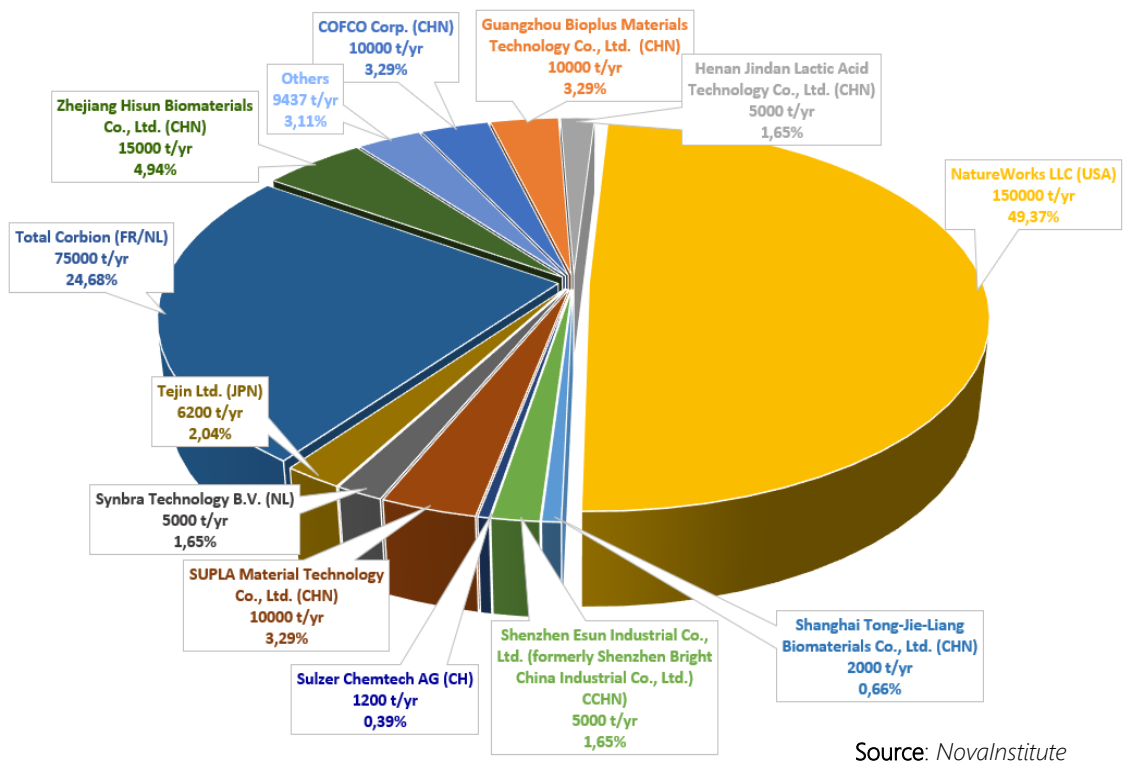
Figure 11 – PLA Global Manufacturers, Production Capacities and Market Shares (2019)

1.3.1 How PLA Is Produced

Lactic acid (LA) is the simplest hydroxyl acid with an asymmetric carbon atom. It is a chiral molecule and two optically active configurations exist: the L-lactic acid and the D-lactic acid (see FIGURE 12). When LA is produced through anaerobic respiration in animal muscle tissue, only the L- configuration will exist. On the other hand, bacteria are able to produce the D- enantiomer as well, then yielding a racemic mixture thereof.
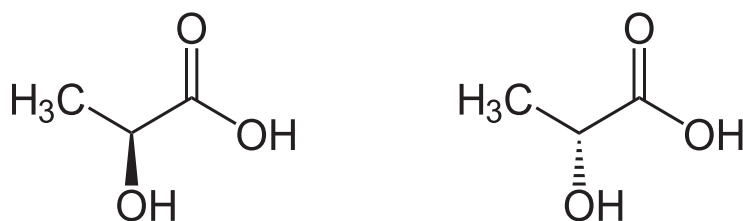
Figure 12 – L-lactic acid (left) and D-lactic acid (right) enantiomers

The majority of LA is obtained through bacterial lactic fermentation operated by different species of the *Lactobacillus* genus. The carbon substrate for bacterial growth is dependent on the given strain of *Lactobacillus* and usually simple carbohydrates from agri-food by-products are used, as reported in TABLE 6.

Table 6 – Carbon sources for lactic fermentation

Substrate	Source
Glucose, maltose, dextrose	Corn or potato starch
Sucrose	Cane or beet sugar
Lactose	Cheese whey

TABLE 7 reports different common agricultural wastes and products utilised as substrate and the corresponding fermenting microorganism, along with the mass yield of LA per unitary gram of substrate [20].

16

Table 7 – Agri-food sources, microorganisms and LA yield

Substrate	Microorganism	LA yield
Cassava bagasse	*L. delbrueckii NCIM 2025, L. casei*	0.9-0.98 g/g
Wheat starch	*Lactococcus lactis* and *Lactobacillus delbrueckii*	0.93-0.95 g/g
Corn starch	*L. amylovorous NRRL B-4542*	0.935 g/g
Barley	*Lactobacillus casei NRRLB-441*	0.87-0.98 g/g
Potato starch	*Rhizopus oryzae, R. arrhizuso*	0.87-0.97 g/g
Cellulose	*Lactobacillus coryniformis ssp. Torquens*	0.89 g/g
Corn, rice, wheat starches	*Lactobacillus amylovorous ATCC 33620*	< 0.70 g/g
Wheat and rice bran	*Lactobacillus sp.*	0.129 g/g
Corn cob	*Rhizopus sp. MK-96-1196*	0.090 g/g
Pre-treated wood	*Lactobacillus delbrueckii*	0.048-0.062 g/g

Packaging and technical applications require PLA to have high molecular weight in order to display compelling mechanical performance. Three distinct solution pathways exist to synthesize high molecular weight PLA of at least 100000 Da and they are all reported in TABLE 8 and graphically explained in FIGURE 13 [14], [18], [20]–[22].

Table 8 – Methods for high molecular weight PLA polymerization

Method of synthesis	Pros	Cons
Direct polycondensation	Most straightforward and most economic	Desirable molecular weight for technical applications is difficult to reach
Azeotropic dehydrative condensation	Energy recovery	Greenhouse gases and toxic and/or carcinogenic emissions to air
Ring-opening polymerization (ROP) through lactide formation	Lifecycle extension and reduction of waste environmental impact	Reduction of mechanical properties
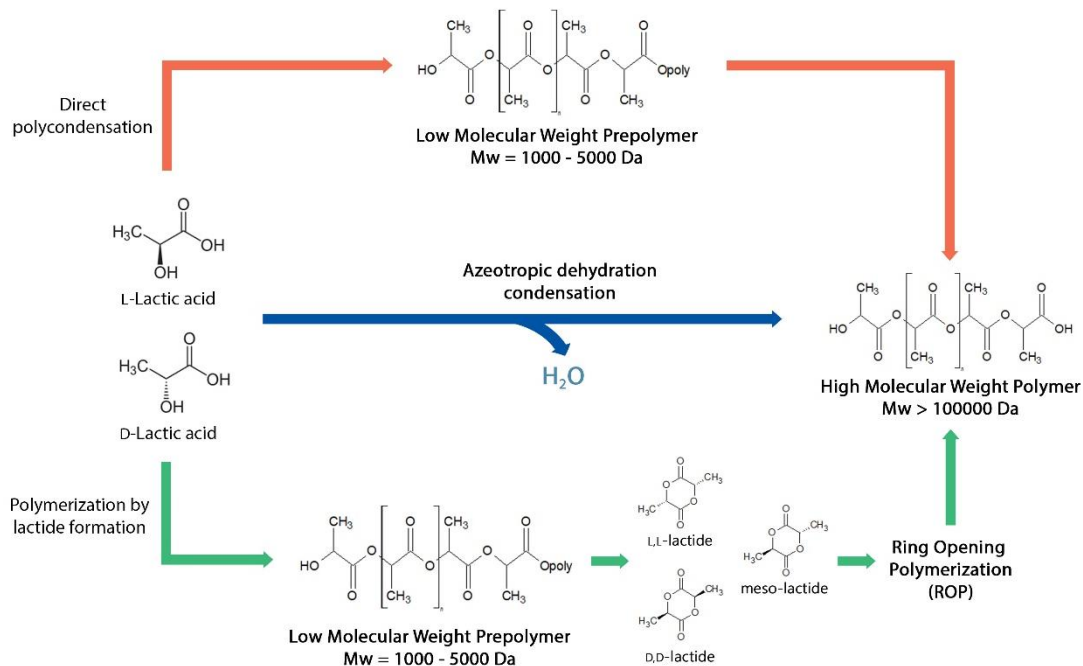
Figure 13 – Available routes for high molecular weight PLA synthesis

1.3.2 The Main Properties of PLA

When considering high molecular weight PLA, its properties are mainly dictated by the stereochemical configuration, the molecular mass, the processing and the annealing temperatures (*i.e.*, the thermal history of the polymer). All these parameters directly affect the crystallinity and its rate. Crystallinity is quite fundamental when considering physical, mechanical and barrier properties. When PLA is quenched, the polymer will display an amorphous morphology which is desirable for producing optically transparent films, yet not for higher mechanically, thermally and gas barrier demanding applications. In order to obtain semi-crystalline PLA, it is essential that stereoregularity is preserved so that chains can arrange themselves in orderly structured crystallites.

Table 9 – Properties of commercial amorphous PLA grade

Characteristic	Unit	Value
Physical:		
Mw	g/mol	66000
Solid density	g/cm^3	1.252
Melt density	g/cm^3	1.073
T_g	°C	55
T_m	°C	165
Specific heat	J/(kg·°C)	
190 °C		2060
100 °C		1955
55 °C		1590
Thermal conductivity	W/(m·°C)	
190 °C		0.195
109 °C		0.197
48 °C		0.111
Optical:		
UV light transmission		
190 to 220 nm		< 5 %
225 to 250 nm		85 %
> 300 nm		95 %
Visible light transmission		95 %
Colour		
L*		90.64 ± 0.21
a*		-0.99 ± 0.01
b*		-0.50 ± 0.04
Mechanical:		
Tensile strength	MPa	59
Elongation at break	%	7
Elastic modulus	MPa	3500
Shear modulus	MPa	1287
Poisson's ratio		0.36
Yield strength	MPa	70
Flexural strength	MPa	106
Unnotched Izod	J/m	195
Notch Izod impact	J/m	26
Rockwell hardness	HR	88
Heat deflection temp.	°C	55
Vicat penetration	°C	59
Ultimate tensile strength	MPa	73
Percent of elongation	%	11.3
Young's modulus	MPa	1280

Therefore, enantiomeric purity is very important and the presence of meso-lactides (see FIGURE 12) tends to favour the formation of amorphous PLA. As a rule of thumb, the crystallization half-time of PLA increases about 40% for every 1 wt% meso-lactide in the reaction medium. Moreover, even 8 wt% of D-lactide in PLLA (*i.e.*, PLA synthesised from L-lactic acid) will completely suppress the crystallization rate and amorphous PLA will be produced [21]. The rate of

crystallization can be enhanced by adding nucleating agents in order to reduce the surface free energy barrier for nucleation and thus favouring crystallization to take place at higher temperature upon cooling. [18], [21].

The practical properties of PLA display a quite variable range of values depending on the given grade required for the given application. A very general widely-used commercial amorphous injection mould grade (96:4 L-D isomer ratio content) PLA produced by NatureWorks LLC. is reported in TABLE 9 [22].

In terms of processability, it is very interesting to report the two following images that describe the metastable states of both high molecular weight *amorphous* (FIGURE 14) and *semi-crystalline* (FIGURE 15) PLA.
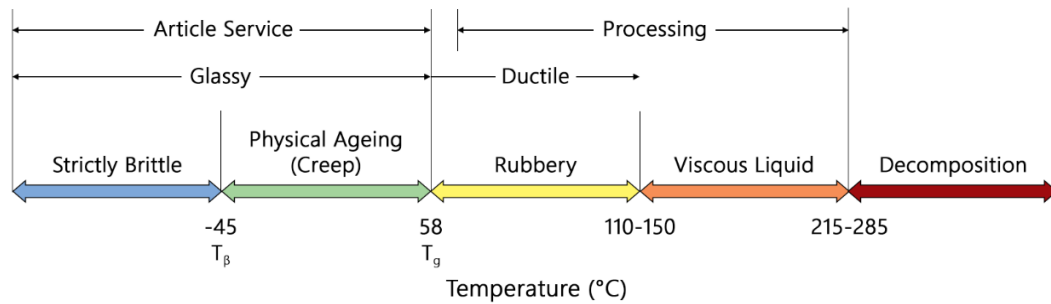
Figure 14 – Metastable states and processing temperature ranges for amorphous PLA
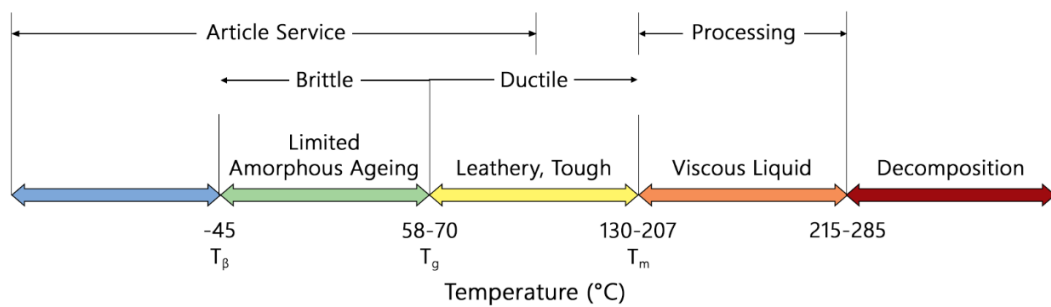
Figure 15 – Metastable states and processing temperature ranges for semi-crystalline PLA

When considering PLA for food packaging applications, gas barrier properties play a fundamental role in the tailoring of the desired properties. The material property to be considered in this sense is the *permeability*, which in mere terms describes the

tendency of a given material to allow the transfer of a given gas or vapour throughout[2].

The most direct comparing polymer is PET, being PLA its most promising renewable and bio-based *competitor*. The permeability coefficients for the three main gases or vapours of interest in food applications (*i.e.*, O_2, H_2O and CO_2) are reported in TABLE 10 for both polymers. All the permeability coefficients are expressed in (kg·m)/(m^2·s·Pa). On the one hand, it is evident that both water vapour and CO_2 barrier properties are not comparable with PET properties, since they are an order of magnitude higher. On the other hand, O_2 barrier properties are somehow comparable to PET, since they have at least the same order of magnitude [20]. The following section will be dedicated to a very interesting natural solution that could be used to enhance the resistance to water vapour permeation, which is fundamental to preserve the freshness of foods and prevent decomposition.

Table 10 – Barrier properties of PLA in comparison to PET

	PLA	PET
P_{O_2} [(kg · m)/(m^2 · s · Pa)]		
25 °C, 0% RH	9.0×10^{-14}	6.2×10^{-14}
25 °C, 30% RH	12.4×10^{-14}	3.0×10^{-14}
25 °C, 60% RH	4.9×10^{-14}	4.7×10^{-14}
25 °C, 90% RH	2.0×10^{-14}	2.4×10^{-14}
P_{H_2O} [(kg · m)/(m^2 · s · Pa)]		
20 °C, 50% RH	9.63×10^{-14}	1.1×10^{-15}
P_{CO_2} [(kg · m)/(m^2 · s · Pa)]		
25 °C, 0% RH	1.99×10^{-17}	1.73×10^{-18}
45 °C, 0% RH	3.35×10^{-17}	3.17×10^{-18}

1.4   Natural Waxes: Man's First Plastic

Waxes have been known for quite a long time. The earliest scientific proof of their use by humans dates back to ca. 3000 B.C. in ancient Egypt for mummification. They were initially used by human beings as casting mould models, pigment

---

[2] For a more detailed description of the physics of mass transfer and the mathematical treatment of membrane fundamentals, see ANNEX I.

carriers and surface protection. However, waxes were already utilized long before humans by nature as a formidable barrier to water that fulfil several needs. For instance, plants secrete waxes to control both evaporation and hydration in their cuticles to adapt to different ambient conditions, whereas bees produce beeswax to build honeycombs. However, *wax* is quite a generic term because waxes consist of a varied and complex mixture of organic compounds in highly different compositions from wax to wax. A precise definition of wax is therefore not possible. However, the most convincing and comprehensive definition has been stated by the *Deutsche Gesellschaft für Fettwissenschaft*, whose most relevant points are reported in TABLE 11 [23].

Table 11 – A practical definition of wax

A wax:

A. Must have a drop point[3] (*mp*) > 40 °C.

B. Must have a melt viscosity that must not exceed 10000 mPa·s at 10 °C above *mp*.

C. Should be polishable under slight pressure and have a strongly temperature-dependent consistency and solubility.

D. At 20 °C must be kneadable or hard-to-brittle, coarse-to-finely crystalline, transparent-to-opaque, but not glassy or highly viscous or liquid.

E. Above 40 °C should melt without decomposition.

F. Above *mp* the viscosity should exhibit a strongly negative temperature dependence and the liquid should not tend to stringiness.

G. Should normally melt roughly in the range 50-90 °C (in exceptional cases up to 200 °C).

H. Generally burns with a soothing flame after ignition.

I. Can form pastes or gels and are poor conductors of heat and electricity.

---

[3] The *drop point* is the temperature at which a wax passes from a semi-solid to a liquid state under specific test conditions. It represents the wax resistance to heat and the standard test procedures are defined in ASTM D-566 and D-2265.

1.4.1 What Waxes Are: a Characterization of the Types of Interest

The classification of waxes can be based upon different criteria such as origin, chemical, physical and engineering features or applications. The most straightforward is to divide waxes into two main groups depending on their source: natural and synthetic. Further subdivisions can exist and they are schematically reported in FIGURE 16.
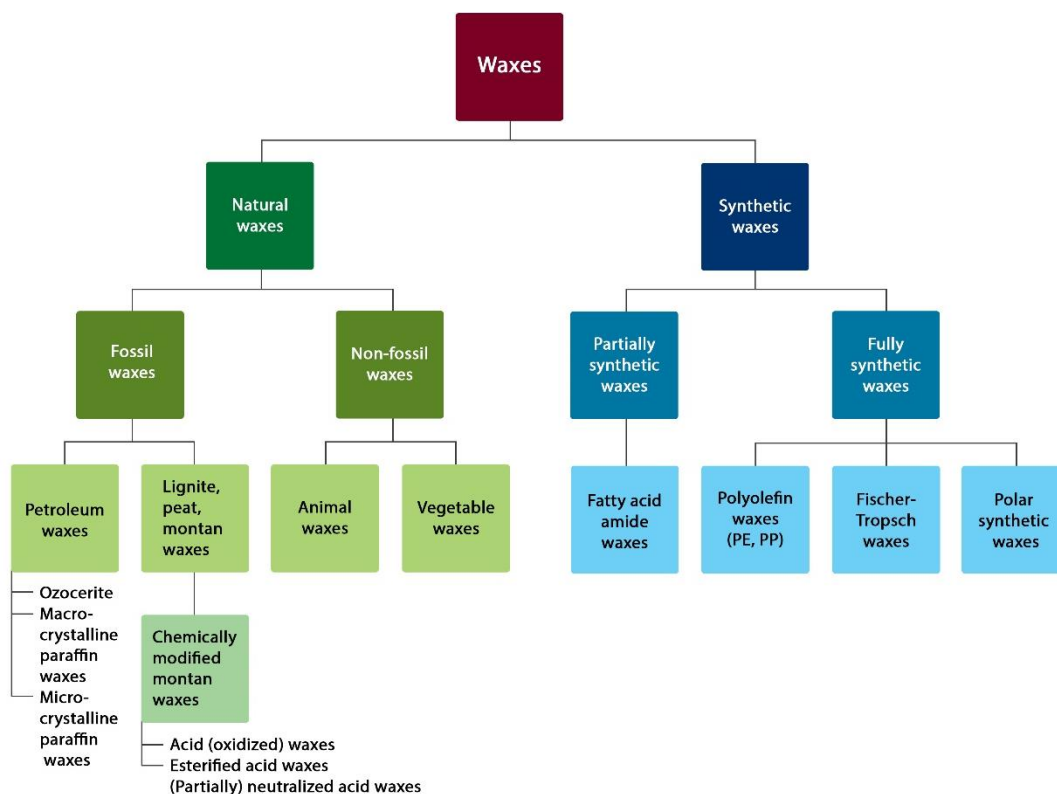
Figure 16 – Classification of waxes

The focus of this work is centred on the use of natural waxes and especially biologically synthesised non-fossil waxes, which are also known as *recent natural waxes* [23]. This type of waxes mainly consists of complex blends of organic compounds, whose main components typically are esters of long-chain aliphatic alcohols and acids. These fatty alcohols and fatty acids mostly belong to homologous series in the $C_{16} - C_{36}$ range and the esters having even-numbered carbon atoms are predominant. Free fatty acids and alcohols are present in highly varying contents and they are typically consistent with those present in the corresponding esters. Depending on the given wax, smaller quantities of esters

derived from acids and alcohols with odd-numbered carbon atoms as well as bifunctional components such as diols, hydroxycarboxylic and dicarboxylic acids are present. In addition, aromatic acids such as cinnamic, 4-hydroxycinnamic and ferulic acids can be present in certain types of wax. Homologous *n*-alkanes in the $C_{15} - C_{37}$ range are usual components of recent natural waxes as well, especially those with odd-numbered carbon atoms. Glycerides, phytosterols, terpenes, rosins, long-chain carbonyl compounds and other minor components such as flower pigments are present in very small, almost negligible amounts. A proper characterization of a given wax type should be performed by means of advanced chromatography techniques coupled with mass spectrometry to avoid thermal decomposition at high temperature [23], [24].

Carnauba, beeswax and candelilla are the most predominant waxes in the market, whereas rice bran and sunflower waxes are quite interesting for the scope of this work. Three sources of waxes are displayed in FIGURE 17. The most common recent natural waxes are reported in TABLE 12 along with other minor less commercially widespread types.

Source: *KahlWax*

Figure 17 – Three sources of waxes of interest (clockwise from top left):
bees, carnauba palm and rice bran.

Table 12 – Biological waxes and their sources

Natural wax	Source
Vegetable	
Alfalfa wax	*Medicago sativa*
Candelilla wax	*Euphorbia cerifera/antisyphilitica*
Caranday wax	*Copernicia alba*
Carnauba wax	*Copernicia prunifera*
Cotton wax	*Gossypium* (GENUS)
Dammar wax	*Dipterocarpacee shorea/hopea*
Douglas fir wax	*Pseudotsuga menziesii*
Esparto wax	*Stipa tenacissima, Lygeum spartum*
Flax wax	*Linum usitatissimum*
Hemp wax	*Cannabis sativa*
Japan wax	*Toxicodendrum vernicifluum/succedaneum*
Jojoba oil	*Simmondsia chinensis*
Ocatillo wax	*Fouquieria splendens*
Oleander wax	*Nerium oleander*
Ouricury wax	*Syagrus coronata*
Raffia wax	*Raphia* (GENUS)
Rice wax	*Oryza* (GENUS)
Retamo wax	*Bulnesia retama*
Sisal wax	*Agave sisalana*
Sugarcane wax	*Saccharum* (GENUS)
Tea wax	*Camellia sinensis*
Animal	
Beeswax	*Apis* (GENUS)
Chinese wax	*Ceroplastes ceriferus, Ericerus pela*
Spermaceti	*Physeter macrocephalus*
Lanolin	*Ovis aries*

As stated previously, natural waxes are complex blends of several different organic compounds and a complete and consistent characterization is usually problematic to have, sometimes even among different samples of the same type of wax. However, it is important to assess at least composition ranges so that the chemical nature of different waxes is noted. This allows to evaluate and understand each material property of waxes and how to improve them and functionalize them for specific applications. Compositions of some types of the waxes just cited above are reported in TABLE 13.

Table 13 – Composition of wax types of interest

Wax	n-Alkanes	Esters	Free alcohols	Free acids	Unsaturated molecules	Other	Reference
Beeswax	C_{23} – C_{31} 15 wt%	C_{34} – C_{36} 35 % monoesters 12% diesters (from diols) 24 % hydroxy esters	NR[4]	8 wt%	Monounsaturated fatty acids 7.8 wt%	NR	[24], [25]
Candelilla	C_{29} – C_{33} 49-50 wt%	20-29 wt%	12-14 wt%	7-9 wt%	NR	Mineral matter 1 wt%	[26]
	C_{29} – C_{33} 92 wt%	NR	NR	NR	NR	Triterpenols 7 wt%	[27]
Carnauba	0.3-1 wt%	38-40 wt%	10-12 wt%	NR	NR	*p*-OH cinnamate esters 20-23 wt%	[28]
	NR	C_{50} – C_{62} *C_{54} esters fatty acids:* C_{20} 17 wt%, C_{22} 61 wt%, C_{24} 22 wt % *C_{56} esters fatty acids:* C_{22} 11 wt%, C_{24} 84 wt%, C_{26} 5 wt%	C_{32}	NR	NR	NR	[24], [29]
Rice bran	NR	*C_{54} esters fatty acids:* C_{16}– C_{20} 1 wt%, C_{22} 28 wt%, C_{24} 69 wt % *C_{56} esters fatty acids:* C_{22} 29 wt%, C_{24} 70 wt%	NR	NR	NR	NR	[29]
	NR	C_{44} – C_{64}	C_{24} – C_{40} C_{22} – C_{24}		Fatty acids: 16:1 0.2 wt% 18:1 2.7 wt%	NR	[24], [30]

---

[4] NR: not reported

1.4.2 Hydrophobicity and Thermo-Mechanical Properties: an Utmost Natural Protection From Water

It has already been stated that waxes act as a natural barrier to humidity and water for plants. This is arguably their most relevant property, which is simply due to the chemical nature of waxes themselves. Since they consist mainly of a mix of long-chain esters, hydrocarbons, fatty acids and alcohols, waxes are intrinsically *lipophilic* materials. *Similia similibus solvuntur*, water – and polar compounds as well – will not be miscible or soluble at all with waxes. Apart from the chemical nature itself, the chain length, the molar mass distribution and the presence of branching will affect the properties of the waxes as well. On the one hand, the longer the chains, the higher the values of melting and softening points, hardness and melt viscosity. On the other hand, the higher the degree of branching, the lower the drop point. When considering wax presenting polar groups such as carboxyl, ester and amide groups, intermolecular forces are enhanced by ionic interactions which tend to stabilize the structure and thus increase both drop point and hardness. Many waxes display good absorption and ability to bind solvents. This allows to have hot wax solutions that guarantee stable and homogeneous adhesives on cooling. Shiny, glossy, hard and mechanically resistant wax films can be obtained by coating a given surface and allowing the solvent to evaporate. Waxes having polar groups can form stable dispersions in water, whenever a suitable emulsifier or surfactant is added. This is a very interesting field of research, especially in terms of sustainable and green industrial processes. In addition to the just cited applications, waxes can also be used for mould releasing, regulating viscosity, lubrication, adjusting consistency, fine-tuning the drop point, binding, adapting compatibility and flexibility, combustion and illumination. Several examples of application are reported in TABLE 14 along with their corresponding industrial sector [23]. Barrier properties are yet another set of most fundamental properties in terms of food packaging applications. Generally speaking, waxes are extremely well-performing natural H_2O barriers due to their intrinsic lipophilic chemical nature. Water vapour permeability data for beeswax, candelilla and carnauba are reported in TABLE 15 along with some other reference polymer materials for comparison [31], [32].

Table 14 – Wax applications and corresponding industrial sectors

Industrial sector	Application
Adhesives, hot-melts	Viscosity regulation, lubricants, surface hardening
Building	Modification of bitumen, anti-graffiti treatment
Candles	Fuel, drop point regulation
Ceramics and metal	Binders for sintering
Cosmetics	Binders and consistency regulators, for ointments, pastes, creams, lipsticks
Electrical and electronics industries	Release agents, insulating materials, etching bases
Explosives	Stabilization
Foods	Citrus fruit and cheese coating, chewing gum base, confectionery
Matches, pyrotechnics	Impregnation, fuel
Medicine and pharmaceuticals	Molding and release agents in dental laboratories, retardants, surface hardening of pills
Office equipment	Dispersing agents and binders for carbon paper and self-duplicating paper, anti-offsets for toners for photocopiers
Paints and coatings	Matting, surface protection
Paper and cardboard	Surface hardening
Plastics	Lubricants (PVC), release agents (PA), pigment carriers
Polishes	Surface protection of leathers, floors, cars
Printing inks	Improvement of rub resistance, slip
Recycling	Compatibilizing
Rubber industry	Release agents enhancing rigidity, surface hardening

Mechanical and thermal properties of waxes are highly dependent on the wax itself. However, as reported in TABLE 11, waxes are usually soft and malleable materials at room temperature or above and they melt in the temperature range 50-90 °C. This is why natural waxes involves issue when the goal is to use them in packaging

Table 15 – WVP of three natural waxes (in italic) and other reference polymer materials

Material	Temperature (°C)	Relative Humidity[5] (%)	Permeability coefficient [(kg·m)/(m²·s·Pa)]
Beeswax	25	100→0	5.81×10^{-17}
Candelilla wax	25	100→0	1.76×10^{-17}
Carnauba wax	25	100→0	3.33×10^{-17}
Paraffin wax	25	100→0	2.20×10^{-17}
PP	23	85→0	5.66×10^{-18}
HDPE	23	85→0	$4,31 \times 10^{-18}$
PET	23	85→0	2.43×10^{-17}
PLA	23	85→0	2.46×10^{-16}

applications, since they should sustain thermo-mechanical stresses during the processing, the storage and the handling of the packaging. Very basic mechanical and thermal properties for beeswax and carnauba wax are reported in TABLE 16 [33]–[35]. For further details on the waxes used in this present work, see MATERIALS AND METHODS (SECTION 3.1.1).

Table 16 – Thermo-mechanical properties for two main natural waxes of reference

Wax	Elastic modulus (MPa)	Compressive strength (MPa)	T_m (°C)
Beeswax	75.84	0.87	62–65
Carnauba wax	1806.42	18.77	82–86

The following chapter will display the focus of this thesis in further detail. In fact, the actual project and the wax modification solutions designed in order to improve the thermo-mechanical properties of several selected natural waxes for coating of PLA thermoformed trays for MAP food packaging applications will be described.

---

[5] The value refers to difference in humidity between the conditioning cabinet and the gravimetric chamber for water vapour permeability testing. See SECTION 3.3.4.3 for further details.

2. Natural Waxes for Food Packaging: PLA4MAP at Fraunhofer IVV

The research project is publicly funded by the *Bundesministerium für Ernährung und Landwirtschaft* (Federal Ministry of Food and Agriculture) (FIGURE 18).

The goal of the project is the development of PLA trays with enhanced barrier properties to protect sensitive foodstuffs for MAP packaging applications. The focus is related to meat products, dairy produce and baked goods that require special solutions to maintain the freshness and the organoleptic

Source: *Fraunhofer IVV*

Figure 18 – PLA4MAP logo

properties as long as possible. The PLA4MAP project is driven towards a bio-based, recyclable packaging system that comprises a deep-drawn composite PLA-based thermoformed container and a PLA sealing film. For MAP applications, specific oxygen and water vapor permeabilities must not be exceeded. That is why the packaging is designed as a multi-layered system in which a bio-based protein layer for improving O_2 permeability and a natural wax layer for improving H_2O vapour permeability are placed in-between two PLA layers. A hot-melt layer will function as an adhesive between the hydrophilic protein-based layer and the hydrophobic wax-based layer. To improve the barrier properties of the PLA lid film, a thin transparent inorganic layer will be deposited, which will not interfere with the recycling process. An additional PLA layer will be laminated to ensure sealing properties. For a better understanding of the multi-layered system, see FIGURE 19.

The components and chemical structure of the selected formulations will be improved to enable processing on commercial production lines and achieve sufficient mechanical resistance and stability. The new food packaging concept will be checked both in terms of mechanical recyclability and solvent-based

recyclability. In addition, the recycled materials will be evaluated for compliance with food legislation and for their use for a variety of applications. The project results will be published in a user manual to promote market penetration [36].

The relevant milestones set for the project and their corresponding expected achievements over time are reported in TABLE 17.
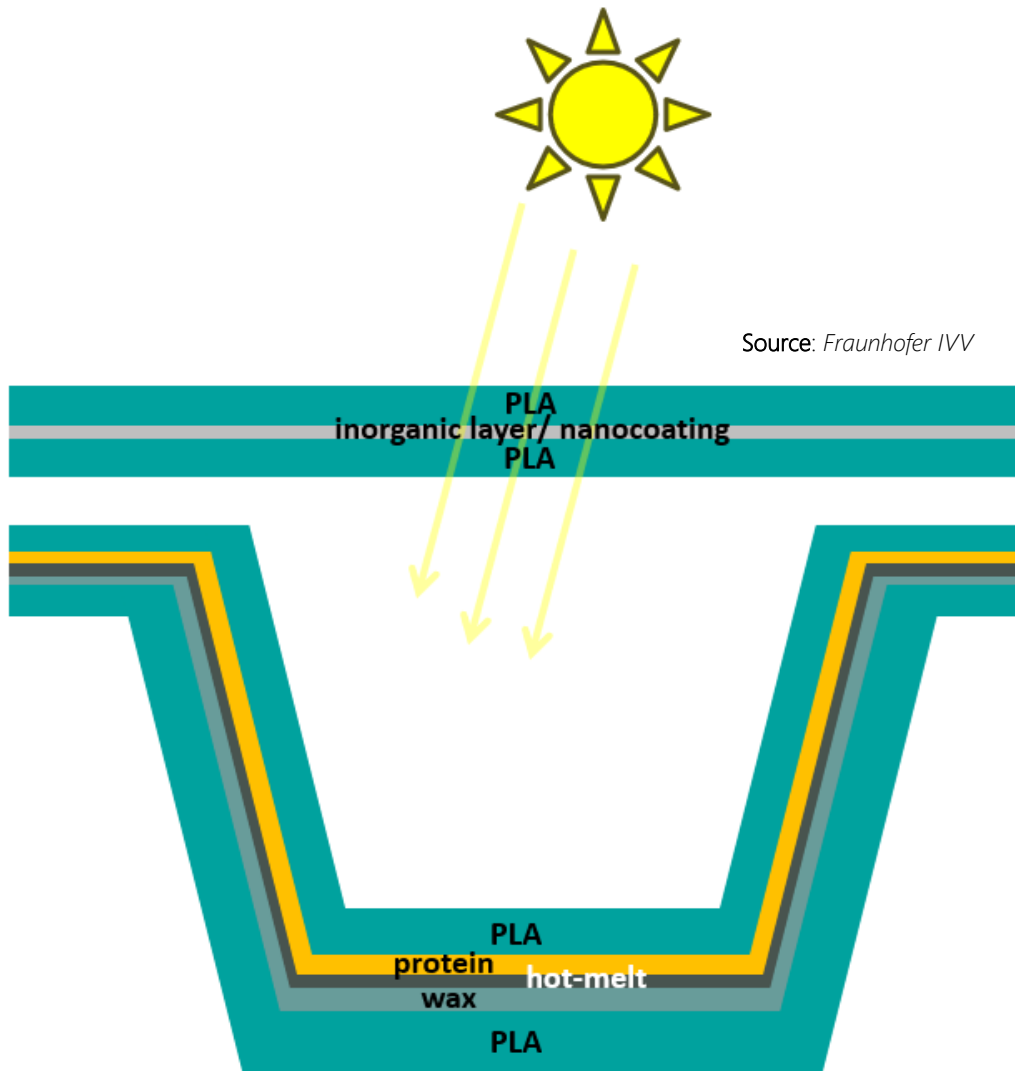
Figure 19 – PLA4MAP multi-layered packaging system

Milestone	Description	Expected time of achievement
M1	Significant change (p-value < 5%) in the melting point of the wax mixture by at least one chemical-physical modification strategy.	Month 12
M2	Coherent coating film of the wax formulation with uniform layer thickness distribution without tearing of the layer during the thermoforming process. The forming process can also be carried out after a storage period of the film (2 weeks).	Month 19
M3	Availability of film samples with a water vapour transmission rate of less than 10 (g/m²·d) and an oxygen transmission rate of less than 10 cm³/(m²·d·bar) (both under standard conditions 23°C/50% RH for oxygen and 23°C/85% RH for water vapour) with good processability of the coating materials. Thermoformed trays show comparable values, depending on material thickness.	Month 22
M4	Achievement of high recycled qualities, which are again suitable for extrusion and thermoforming processes and thus technically close the material cycle (without consideration of conformity).	Month 28

2.1 Improvement of Thermo-Mechanical Properties of Natural Waxes

The previous section described the overall PLA4MAP project. However, this very thesis is centred around the development of enhanced natural wax thermo-mechanically stable coatings to improve water vapour barrier properties of PLA. The three main goals in this work are reported below in TABLE 18.

Table 18 – Project goals of this experimental work

Project goal	Description
G1: Increase melting point and scratch resistance of wax formulation	Natural waxes lack of thermal stability (low melting points) and scratch resistance (softness). This can be overcome by formulation, chemical modification and crosslinking, preferentially with food packaging approved additives. The scratch resistance and thermal stability is necessary for subsequent hot melt lamination and thermoforming (follow-up activities).
G2: Maintain the water vapour barrier close to the value of natural waxes	Natural waxes already have a quite sufficient water vapour barrier [<2 $(g \cdot 100\mu m)/(m^2 \cdot d)$], comparable to PP [~1 $(g \cdot 100\mu m)/(m^2 \cdot d)$]. The blending with other components and chemical modification should not significantly affect the barrier against water vapour.
G3: Achieve sufficient adhesion on PLA substrate	The similar polarities of PLA surface and wax layer will lead to sufficient wetting. However, it can be expected that the interaction forces are quite weak and the coatings can easily be removed from the substrate. The aim is therefore to increase this adhesion by modifying the PLA surface and subsequently covalently bonding to the components of the wax barrier layer.

2.2 Cross-Linking: a Strategy to Create Polymer Networks

In order to achieve project goals several strategies can be designed. The key-concept at the basis of the improvement of waxes thermo-mechanical properties is to functionalize them to obtain the desired performance without compromising the barrier effect to water vapour. This involves a fine-tuning of properties that should interfere as less as possible with the underlying desired hydrophobic chemical nature of waxes. The most promising strategy has been identified in favouring the formation of *cross-linked* structures that allow to obtain a harder and more thermal-
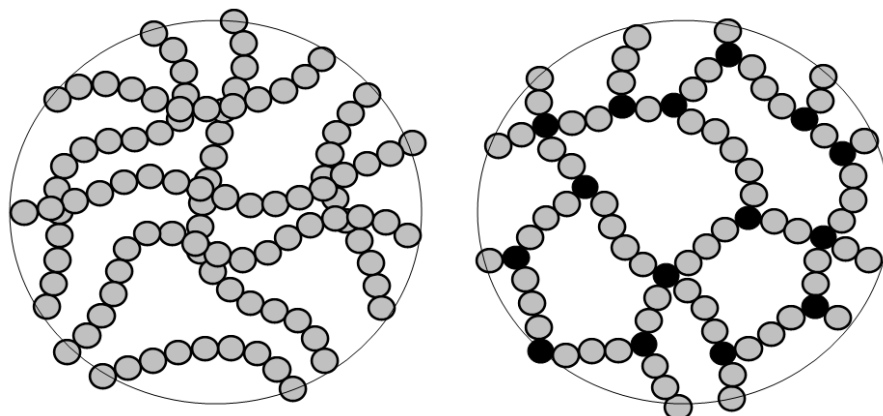
Figure 20 – What cross-linking means: individual free linear polymer chains (left) undergo cross-linking (black dots imply that the chains are covalently bond one to each other) to yield a 3D rigid network (right)

resistant material. Cross-linking is the process of *covalently* bonding atoms from two distinct polymer chains by means of shorter polymer chains that branch out from the latter. This phenomenon will favour the formation of complex and tightly bound 3D polymeric networks and the material is then said to be a *thermoset* (FIGURE 20). In fact, when heated to high temperatures, the polymer will not melt, but will directly degrade to carbonaceous matter, since the polymeric chains do not have enough degrees of freedom to rotate like a thermoplastic polymer does while undergoing melting. The strong chemical nature of C-C primary covalent bonds allows thermosets to be more resistant to higher thermal and mechanical stresses than thermoplastics. The higher the degree of cross-linking, the better the thermo-mechanical performance at the expense of increased brittleness.

The desired goal is to obtain a certain degree of cross-linking in the wax-based material of interest so that G1 and G2 are achieved, without affecting the viscosity and workability to obtain a proper homogeneous coating on the PLA substrate. Cross-linking can be triggered by several strategies and the most interesting for our purpose are displayed in TABLE 19. The rationale behind the selection of a given strategy is both to guarantee that the required performance is achieved and to obtain a coating material to be as much sustainable and bio-based as possible. Thus, this work will be mostly focused on the development of wax-based bio-alkyd resins, whose basic chemistry and properties are briefly described in the following section.

Table 19 – Strategies for cross-linking

Cross-linking strategy	Description
Autoxidation	In presence of atmospheric O_2 or radicals, C=C double bonds could spontaneously form cross-linked network. High temperature, high pressure, initiators (e.g., peroxides) and irradiation (electron beam, UV light, …) accelerate consistently the process.
Formulation with chemical cross-linkers	The wax could be blended with compounds presenting functional groups for cross-linking such as: • C=C double bonds (e.g., linseed oil) • Hydroxy groups (e.g., castor oil) • Epoxy groups (e.g., ESBO)
Preparing wax-based resins	The wax is not simply blended with a cross-linkable compound, but it is actually part of the 3D network via chemical bonding.

2.2.1 Alkyd Resins: From Paintings to Wax-Based Bio-Coatings

An *alkyd* is a polyester resin that is constituted by the three monomers reported in FIGURE 21, whereas a very common alkyd based on *Glyptal* (the very first conceptual alkyd resin based on glycerol and phthalic anhydride) and linseed oil is reported in FIGURE 22.

The word *alkyd* comes from the respelling of the crasis of the words **alc**ohol and ac**id**, which are the two essential components in the resin. In fact, according to ASTM, an alkyd is *a synthetic resin made from polyhydric alcohols and polybasic acids; generally modified with resins, fatty oils or fatty acid* [37].

Alkyd resins are widely used for surface coatings (paints, enamels, lacquers, and varnishes) in which they function as binders and constitute a tough, continuous film that homogeneously adheres to the given substrate.

The mechanical and thermal properties of alkyd resins are highly dependent on the mixture of polyol, diacid/acid anhydride and oil. However, as a rule of thumb, T_g is often lower than most commercially available commodity polymer (for further
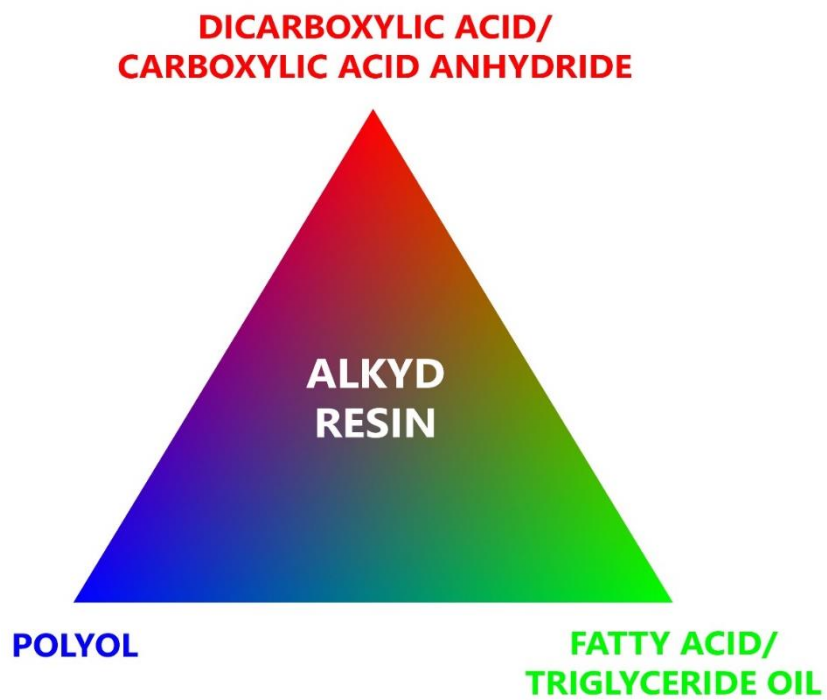
Figure 21 – Composition triangle of a generic alkyd resin
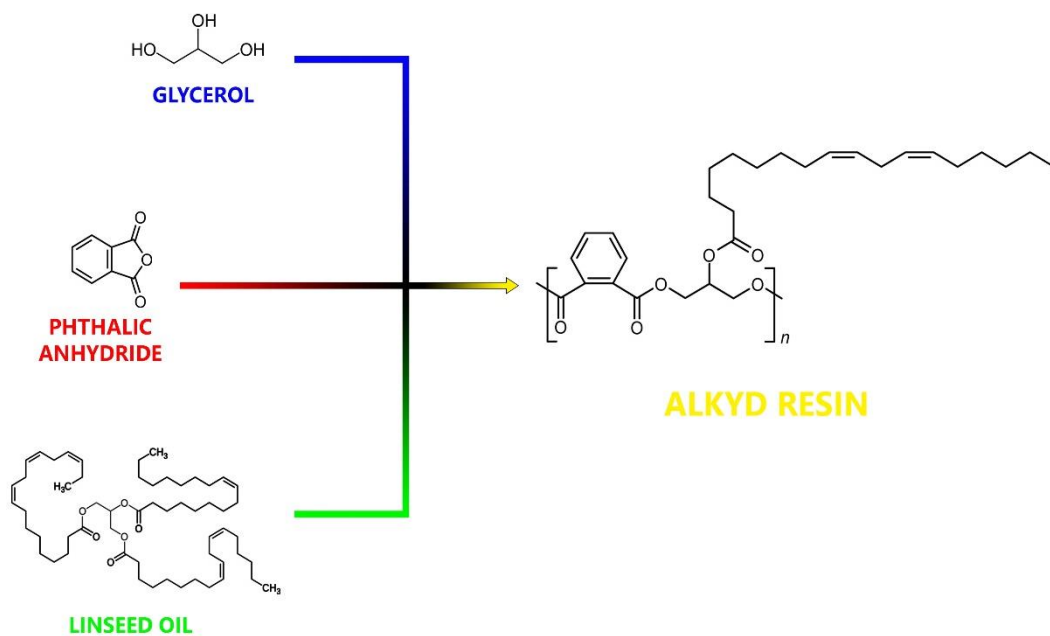
Figure 22 – A most typical alkyd resin

detail see the DATA AND RESULTS chapter to check the properties of some in-house synthesised alkyd resins). Thus, alkyd resins are typically highly viscous and tacky materials which involve issues in their handling and coating. Once coated, alkyds are typically cured to favour cross-linking. This process yields a hardened and glossy lacquer that provides good resistance to water and scratching. Cross-linking is triggered by the presence of double bonds that can favour further polymerization and the formation of 3D networks in presence of O_2. The resin is *drying* if the double bonds are already present in the alkyd structure by means of *polyunsaturated* fatty acids – which are often derived from vegetable *drying* oils such as linseed or castor oils. If not, the resin is *non-drying* and a cross-linking agent is to be blended to favour curing.

The typical technological route to produce alkyds is displayed in FIGURES 23-24.
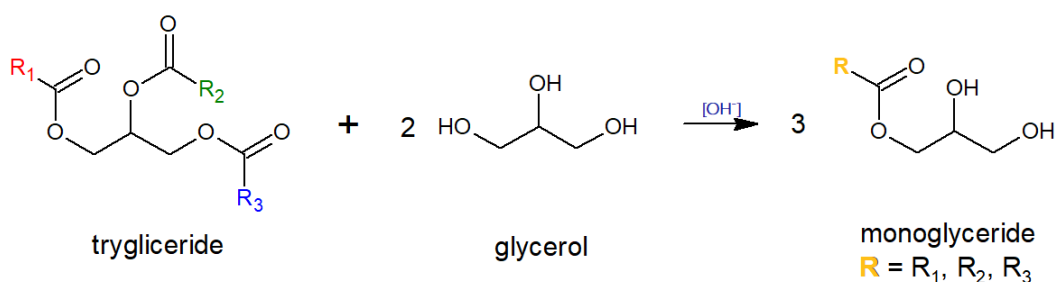
Figure 23 – First stage: theoretical alcoholysis of triglycerides
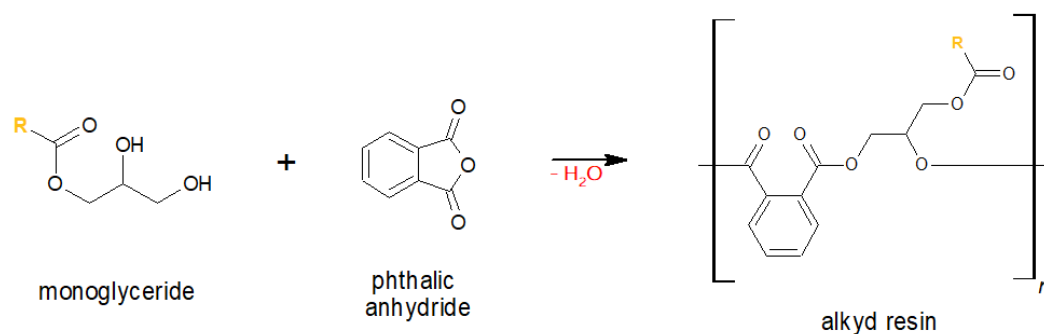
Figure 24 – Second stage: esterification with dicarboxylic acid/acid anhydride

The first step involves the base-catalysed *alcoholysis* (or *transesterification*) of fatty acids or triglycerides with pure glycerol in order to obtain *mono*glycerides. These prepolymers contain two free hydroxyl groups that can be esterified with the carboxyl groups of dicarboxylic acids – or their corresponding acid anhydrides, equivalently – to form polyesters by polycondensation. The removal of H_2O during the esterification of the prepolymer is of utmost importance. The more efficient its

removal from the reaction medium, the larger the shift of the reaction equilibrium towards products and thus the higher the yield of alkyd resin. Plus, the high temperatures employed in the esterification (i.e., ca. 200-250 °C) involve instant vaporization of water, which may favour the formation of undesired foamy materials. In order to avoid undesired and uncontrolled cross-linking due to high temperatures and O_2 presence in the reaction headspace, inert atmosphere can be maintained. For further details about how the reactions have been carried out, see MATERIALS AND METHODS, PROTOCOLS (SECTION 3.3.2).

The core concept of this experimental work of this thesis is trying to substitute the triglycerides from vegetable oils with natural wax esters. In fact, the substitution is theoretically possible since triglycerides consist of esters of glycerol and three fatty acids, whereas wax esters are constituted by fatty alcohol and fatty acids. The practical difficulties pivot around the actual feasibility to *transesterify* the wax esters with glycerol to obtain monoglycerides and shift the equilibrium towards the products (FIGURE 25).

R = fatty acid alkyl chain (C16-C24)
R' = fatty alcohol alkyl chain (C20-C40)
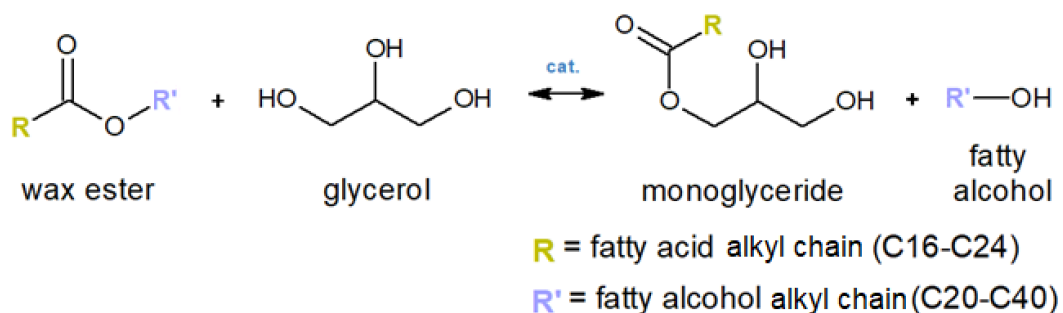
Figure 25 – Transesterification of wax esters

Despite the hypothetical issues regarding the actual synthesis of wax-based alkyd resins, the potentially high bio-based content in the overall material makes it remarkably appealing for sustainable packaging solution. In fact, glycerol can be obtained from transesterification of vegetable oils as a by-product of bio-diesel manufacturing. Wax is abundant in natural sources as reported in SECTION 1.4. Dicarboxylic acids or their acid anhydrides such as succinic acid/anhydride, itaconic acid/anhydride or maleic acid/anhydride can be bio-synthesised. Therefore, a wax-based alkyd resin could be potentially 100 percent bio-based and its

components are food-grade approved as well, which is vital in terms of food packaging applications. That is why this solution has been selected as the most promising and compelling in the logic of this thesis as a part of the PLA4MAP project at Fraunhofer IVV.

3. Materials and Methods

All the reagents and the materials used in the experiments, all the instruments operated for measuring the fundamental properties, and all the procedures and the protocols adopted for polymer synthesis and analysis are reported here in detail.

3.1 Materials

3.1.1 Natural Waxes

All the natural waxes used in this work were supplied by German manufacturer Kahl GmbH & Co. KG along with the main properties of interest (TABLE 20). Images of the waxes as received are reported in FIGURE 26.

Table 20 – Natural waxes used in the experimental work

Abbr.	Product	m.p. (°C)	a.v. (mg KOH/g)	s.v. (mg KOH/g)	e.v. (mg KOH/g)
BEE	KahlWax 8109 Yellow Food Beeswax	62 – 65	17 – 24	87 – 104	70 – 80
CND	KahlWax 2039L Candelilla	68 – 73	12 – 22	43 – 65	31 – 43
CRB	KahlWax 2442 Carnauba	82 – 86	2 – 7	78 – 95	71 – 88
RB	KahlWax 2811 Rice	79 – 85	< 15	65 – 95	< 70
SF	KahlWax 6607L MB Sunflower	74 – 80	2 – 8	75 – 95	73 – 78

m.p.: melting point; **a.v.**: acid value; **s.v.**: saponification value; **e.v.**: ester value

Beeswax   Candelilla wax   Carnauba wax   Rice bran wax   Sunflower wax

Figure 26 – All the natural waxes supplied by KahlWax GmbH

3.1.2 Polyols

Glycerol was selected as the main polyol of interest, both for its known chemistry and for its potential as a bio-based building block. However, other solutions have been investigated as well, which are all reported in TABLE 21. Molecular structures of all the selected polyols are reported in FIGURE 27.

Table 21 – Polyols used in the experimental work

Abbr.	Product	Conc.	CAS-Nr.	Producer
Branched-resin polyols				
GLY	Glycerol	99%	56-81-5	ChemSolute (Th. Geyer)
PTOL	Pentaerythritol	98%	115-77-5	Sigma Aldrich
SRB	D(-)–Sorbitol	99%	50-70-4	ChemSolute (Th. Geyer)
Linear-resin polyols				
EG	Ethylene glycol	99.5%	203-473-3	Riedel-de Haën
PG	Propylene glycol	s.g.*	57-55-6	Amresco
PEG 400	Polyethylene glycol 400	s.g.*	25322-68-3	Th. Geyer
PEG 10000	Polyethylene glycol 10000	s.g.*	25322-68-3	Sigma Aldrich

* synthesis-grade
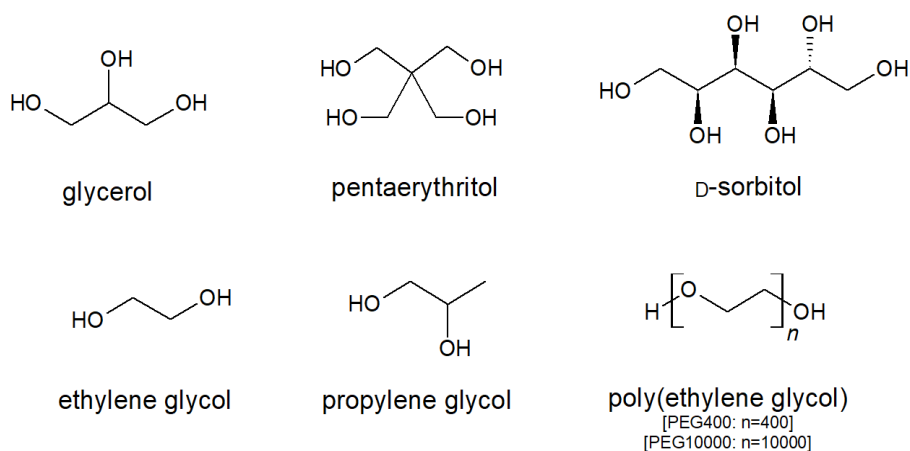
Figure 27 – Polyols used in the experimental work

42

3.1.3 Acid Anhydrides

Four different anhydrides have been selected for the synthesis of the wax-based alkyd resins. Succinic, maleic and itaconic anhydrides have been selected for their potential bio-based production. Phthalic anhydride has been selected due to its common use in traditional alkyds, despite it is not food-grade approved (TABLE 22). Molecular structures of the selected acid anhydrides are reported in FIGURE 28.

Table 22 – Acid anhydrides used in the experimental work

Abbr.	Product	Conc.	CAS-Nr.	Producer
SUC	Succinic anhydride	s.g.*	108-30-5	Merck
MAL	Maleic anhydride	99%	108-31-6	Sigma Aldrich
ITA	Itaconic anhydride	95%	2170-03-8	Sigma Aldrich
PHT	Phthalic anhydride	s.g.*	85-44-9	Sigma Aldrich

* synthesis-grade
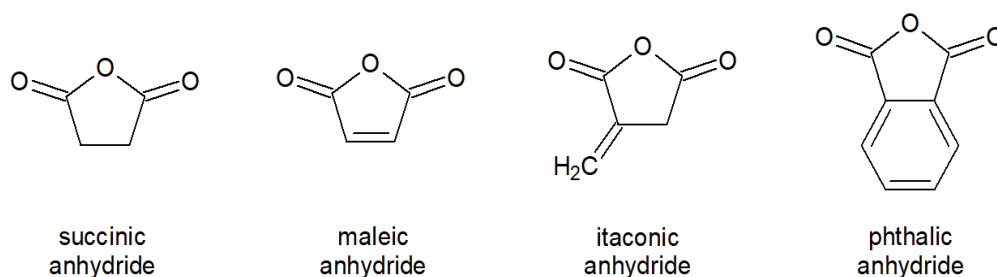
Figure 28 – Acid anhydrides used in the experimental work

3.1.4 Others

All the other chemicals needed in this experimental work which do not enter in anyone of the three previous main three material categories are reported in TABLE 23.

Table 23 – All the remaining chemicals required in the experimental work

Product	Conc.	CAS-Nr.	Producer	Use
Linseed oil	-	-	Huilerie Bio Occitane SASU**	Traditional alkyd resin synthesis
Sodium hydroxide	99.5%	1310-73-2	ChemSolute (Th. Geyer)	Catalyst for alcoholysis
Sulfuric acid	95%	7664-93-9	ChemSolute (Th. Geyer)	Catalyst for alcoholysis
Dicumyl peroxide	98%	80-43-3	Sigma Aldrich	Cross-linker
Di-tert-butyl peroxide	98%	110-05-4	Sigma Aldrich	Cross-linker

** linseed oil was merely purchased at a local REWE supermarket

3.2 Instruments

All the instruments have been utilized directly at the Fraunhofer IVV and they all belong to the Materials Development department. The distinction is based whether the instrument has been used for synthesis (TABLE 24) or characterization (TABLE 25). Further details on the procedure and on how to utilize the instruments are reported in SECTION 3.3 along with the descriptions of the methods used for this experimental work.

3.2.1 Synthesis and Film Production

Table 24 – All the instruments required for chemical synthesis in this work

Instrument	Model	Producer	Notes
Glass crucibles	65 mm ✕ 30 mm, 35 mL	Th. Geyer	
Weighing scale	1204 MP	Sartorius	
	MSA5	Sartorius	
Furnace	HeraTherm General Protocol Trockenschränke, 65 L	ThermoFisher Scientific	Natural convection
	ED-S 56, 62 L	Binder	Natural convection
Magnetic stirrer	RCT Basic	IKA	
	Monotherm	VarioMag	
Hot-press	Hydraulische Presse 25 tonnes	Perkin Elmer	Graseby Specac Temperature Controller
Thickness gauge	FT3	Hanatek	

3.2.2 Characterization

Table 25 – All the instruments required for material characterization in this work

Technique	Model	Producer	Software	Notes
DSC	DSC3+/400W/without Roboter/GC402	Mettler Toledo	STARe 15.00 a	Cooler: TC100+ CN2
FT-IR	Spotlight 400	Perkin Elmer	Spectrum 10	ATR: Specac's Golden Gate single reflection monolithic diamond
WVP	Klimaschrank KMF Series	Binder		

3.3 Methods

This section concerns in detail the reaction routes taken to synthesise both traditional and wax-based alkyd resins.

3.3.1 Synthesis

The reactive routes of interest mainly focus on ester and polyester chemistries, which are quite straightforward and well-known. It must be recalled that esters are organic compounds derived from the reaction of an acid and an alcohol. Here the oxygen of the alcoholic hydroxyl group *nucleophilically* attacks the positive carbonyl carbon of the carboxylic acid by means of catalyst activation (*e.g.*, H^+). This nucleophilic substitution (SN_2 mechanism) results in a bridging *alkoxy* group (-O-R) and release of water (H_2O) as a by-product (FIGURE 29).
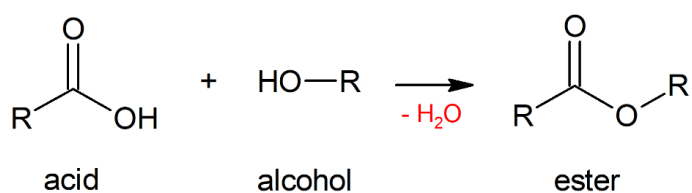
Figure 29 – Basic fundamentals of ester chemistry

Whether the starting material be a vegetable oil or a natural wax, the very first step in the synthesis of alkyds is the *transesterification* (or *alcoholysis*) of the existing esters. As the name suggests, transesterification consists in obtaining a different ester starting from a given ester. This is performed by simply substituting the alcohol constituting the ester with a different one, whereas the constituting acid remains the same. Typically, transesterification is used to produce biodiesel from vegetable oils, by substituting the glycerol constituting the triglycerides with methanol (CH_3OH) and thus obtaining *Fatty Acid Methyl Esters* (FAME). Transesterification is typically operated at elevated temperature under basic conditions. This will favour the deprotonation of the substituting alcohol and increase the likelihood of a nucleophilic attack on the partially positive charged carboxyl carbon atom of the acid species (FIGURE 30).

Acid catalysis is another less common and yet effective route, which has also been tested during this experimental work (FIGURE 31). Further details about reaction mechanisms and catalysis for transesterification can be found in literature [38].
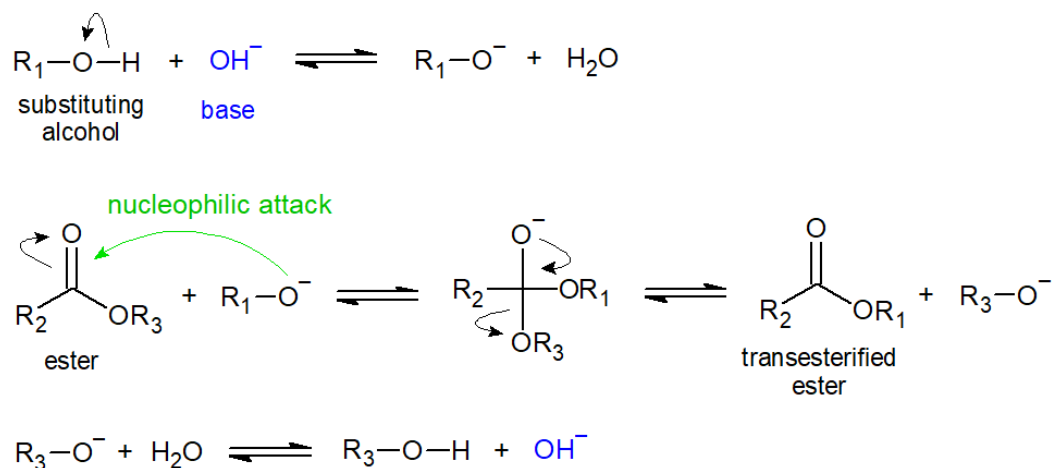
Figure 30 – Base-catalysed transesterification
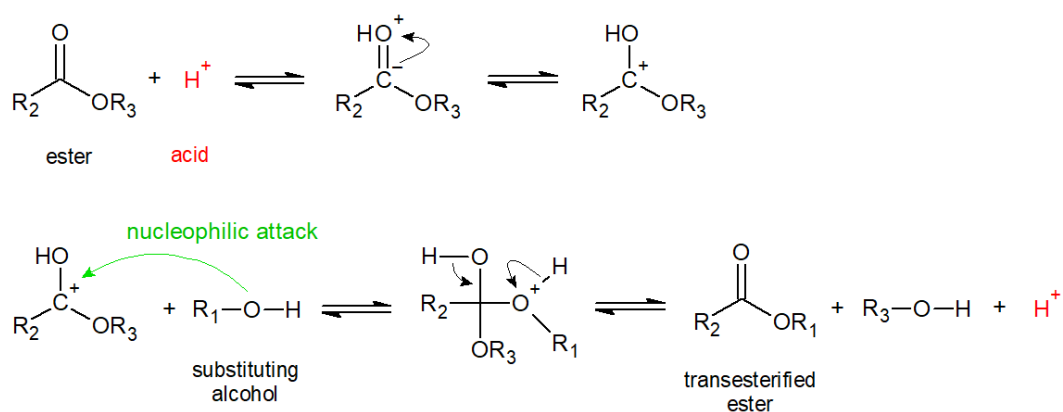
Figure 31 – Acid-catalysed transesterification

In our specific case, the substituent alcohol is one of the polyols reported in TABLE 21 and the esters to be transesterified are those already present in the natural waxes (see SECTION 1.4.1, TABLE 13). This procedure allows to obtain monoglycerides containing the fatty acid side of the wax esters, whereas the remaining fatty alcohols constituting the wax esters are free in the reaction medium (see SECTION 2.2.1, FIGURE 25).

The subsequent step is the actual polymerization of these transesterified monoglycerides with the given acid, which in our case has been selected as a carboxylic acid anhydride in order to mimic the traditional alkyd resin synthesis (FIGURE 32). The *polyesterification* is conducted at medium-to-high temperatures (i.e., at least 140 °C, and yet not higher than 200 °C to avoid the carbonization of organic matter) in absence of any catalysts to favour the polycondensation of the two residual hydroxyl groups present in the monoglycerides with the two carboxyl groups embedded in each molecule of acid anhydride.
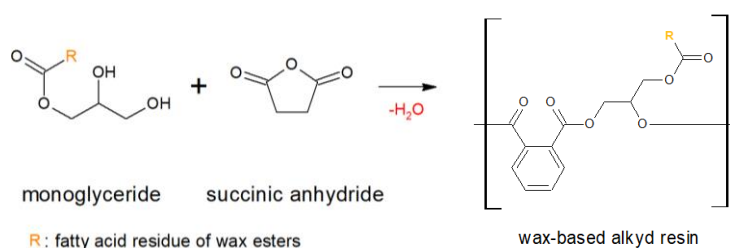
Figure 32 – Polyesterification of monoglycerides derived from wax esters and acid anhydrides (e.g., succinic anhydride)

The theoretical synthetic route is quite straightforward as it involves mainly a transesterification followed by a polymerization to obtain the polyester resin. However, on a practical basis, problems could easily arise due to factors which are reported in TABLE 26. They arose during different stages in the testing of different possible synthetic routes and several countermeasures were adopted in order to

Table 26 – Problems to deal with during the preparation of wax-based alkyds

Process step	Problems
Transesterification	• Being constituted by both long-chain fatty acids and fatty alcohols, wax esters have lower reactivity with glycerol than triglycerides in the traditional transesterification for biodiesel production.
Polyesterification	• If not properly removed from the reaction medium, H_2O generated during polyesterification can prevent the proper equilibrium shift towards the products. • Free fatty alcohols already present in the wax or produced by the transesterification of wax esters can terminate the polymerization by reacting with the acid anhydrides. • Increasing the temperature will favour faster reactivity at the expense of darkening of the medium due to beginning of carbonization of organic matter.

solve the encountered issues. The following section will concern the detailed protocols which were drafted to prepare the wax-based alkyd resins or to test the chemistry of traditional alkyds or to improve the reactivity and the synthesis.

3.3.2 Protocols

Several different synthetic routes were investigated in order to have a preliminary screening of the most interesting and promising formulations for the goals of the project. Each protocol is identified by an alphanumerical code to identify both the main selected reaction route and eventual variations in the procedure. As the samples were synthesised according to a given protocol, they were identified and chronologically classified with an increasing integer, starting from number #1.

3.3.2.1 R1.n

The very first protocol group to be drafted concerns the synthesis of alkyd resins and the understanding of its parameters. The identifying codes for each protocol in the group are reported in TABLE 27 along with a brief description and the samples produced according to the given protocol.

Table 27 – Code of identification, description and samples of R1.n protocols

Code	Description	Samples
R1.0	Synthesis and screening of traditional alkyd resins based on linseed oil, glycerol and four different acid anhydrides.	#1 – #36
R1.1	Synthesis and screening of alkyd resins based on seven different polyols, four different acid anhydrides and in absence of any vegetable oils.	#37 – #56 #101 – #110
R1.2	Synthesis and screening of alkyd resins based on two natural waxes, seven different polyols and two different acid anhydrides.	#57 – #100

R1.0 was derived by consulting different literature sources in order to have a basic understanding on how alkyd resins are synthesised [35], [37–43]. Several different compositions and formulations were tested. Hence, for each of the four different acid anhydrides reported in TABLE 22 (SECTION 3.1.3), a 3×3 matrix representing

the different molar ratios of each formulation was prepared to investigate how the final properties were affected by composition (TABLE 28). It was assumed to normalize glycerol at 1 mol. A total of 36 samples were prepared. Each sample resulted in 5 g of alkyd resin.

The actual procedure of synthesis is divided in a preliminary transesterification of triglycerides of linseed oil with glycerol to obtain monoglycerides to be further polyesterified with the given acid anhydrides. The transesterification was conducted in a convection oven at 230 °C and ambient pressure for 2 hours under basic conditions (NaOH, 0.2 wt. % of total resin mass) and intermitting stirring for 1-2 minutes every 30 minutes. After the transesterification, the samples were cooled down to ambient temperature, the given acid anhydride was added and polyesterification was initiated at 230 °C and ambient pressure for 3-4 hours. Once cooled down to ambient temperature again, the samples were stored with a parafilm lid or, if possible, in a desiccator to protect them from ambient moisture.

R1.1 involved the synthesis of alkyd resins in absence of any vegetable oil triglycerides to be transesterified. Thus, the reaction is essentially a polyesterification of polyols (SECTION 3.1.3, TABLE 21) with acid anhydrides (SECTION 3.1.3, TABLE 22). The resins were synthesised with a 1:1 molar ratio between polyol and acid anhydride. Only six resins (samples #40 – #42, #46 – #48) were synthesised with different molar ratios to test the effects of an excess of two different acid anhydrides (*i.e.*, succinic and maleic): 1:1.5 for both glycerol and

Table 28 – R1.0 molar ratio matrix.

	Acid anhydride (in deficit)	Acid anhydride (stoichiometric)	Acid anhydride (in excess)
Linseed oil (stoichiometric)	0.5 : 1 : 0.8	0.5 : 1 : 1	0.5 : 1 : 1.2
Linseed oil (glycerol in average excess)	0.3: 1: 0.8	0.3 : 1 : 1	0.3 : 1 : 1.2
Linseed oil (glycerol in large excess)	0.1 : 1 : 0.8	0.1 : 1 : 1	0.1 : 1 : 1.2

The molar ratios are reported as linseed oil : glycerol : acid anhydride

sorbitol, 1:2 for pentaerythritol. Each R1.1 sample consisted of 5 g of total resin. The reaction was conducted in a convection oven in the temperature range 190-200 °C and ambient pressure for 2 hours. The temperature was reduced with respect to R1.0 to avoid eventual carbonization of organic matter and to avoid evaporation of maleic anhydride in the vapour phase (boiling point at ambient pressure: 202 °C), as it is an irritating agent and its content required in the resin was higher than the previous protocol.

R1.2 concerns the first attempt to synthesise some wax-based alkyd resins and the *rationale* behind the drafting of the protocol was quite basic and unsophisticated. The waxes were directly compounded with the seven different polyols of TABLE 21 and the four different acid anhydrides of TABLE 22 at three distinct mass fractions (50 wt. %, 75 wt. % and 87.5 wt. % wax on the total resin mass, respectively). Each R1.2 sample consisted of 5 g of total resin. The reaction was conducted in a conductive furnace at 180-190 °C and ambient pressure for at least 2 hours. No catalyst was added to the reaction medium.

3.3.2.2   R2.n

The R2 protocol group is a refinement of the R1.2 protocol, since it involves a preliminary transesterification of wax esters to enhance reactivity and resin formation. The procedure is consistent with the very first protocol R1.0 to produce linseed oil-based alkyds, as the rationale is to obtain monoglycerides having long-chain alkyl residual groups by reacting wax esters with glycerol or other polyols. Such monoglycerides are to be polyesterified with acid anhydrides to produce the desired resin. However, reaction temperatures are reduced to avoid formation of carbonized matter. The code, description and correlated samples of each distinct protocol in the R2.n group are reported in TABLE 29. Each sample of each R2.n protocol consisted of 5 g of total synthesised resin.

R2.0 has been conducted exactly the same way as R1.0, by straightforwardly substituting linseed oil with carnauba wax. The main difference was that both transesterification and polyesterification were also performed at two different lower temperatures (*i.e.*, 160 °C and 120 °C).

Table 29 – Code of identification, description and samples of R2.n protocols

Code	Description	Samples
R2.0	Synthesis and screening of wax-based alkyd resins based on carnauba wax, glycerol and four different acid anhydrides. Three distinct temperatures have been tested. NaOH-catalysed transesterification.	#111 – #126
R2.1	Synthesis and screening of wax-based alkyd resins based on carnauba wax, glycerol and four different acid anhydrides. Two distinct temperatures have been tested. H_2SO_4-catalysed transesterification.	#127 – #134
R2.2	Synthesis and screening of wax-based alkyd resins based on carnauba wax, two distinct polyols and four different acid anhydrides. Both NaOH-catalysed and H_2SO_4-catalysed transesterification have been tested.	#145 – #152

Moreover, only two different molar ratios among wax esters and glycerol were tested at higher temperature (200-230 °C), respectively 0.5:1 and 0.1:1 (wax esters:glycerol), whereas only 0.5:1 (wax esters:glycerol) molar ratio was selected for the two lower temperature synthesis in order to have enough wax content to maintain its barrier to water. The stoichiometric ratio would be 1:1, but an excess of glycerol is designed to favour the transesterification of wax esters, by shifting the reaction equilibrium towards the products. In fact, the reaction is hindered by the tendency of wax and glycerol to mix homogeneously only at high temperatures and by the scarce reactivity of wax esters due to the spatial predominance of the alkyl residual chains. The wax ester content was calculated considering the ester value[6] provided by the wax supplier (TABLE 20).

For each temperature of synthesis, the transesterification of wax esters was performed under basic conditions (*i.e.*, NaOH as catalyst) and the given acid anhydride was added in 1:1.2 (glycerol : acid anhydride) molar ratio, which was selected as the most promising and interesting for resin formation from the results of R2.0 protocol. The molar ratios for each of the three different R1.0 synthesis are reported in TABLE 30.

---

[6] Ester value: mg of KOH (or NaOH, with the due correction for the molecular weight) required to hydrolyse all the esters contained in 1 g of wax.

Table 30 – R2.0 molar ratios at different temperatures of synthesis

	200–230 °C	160 °C	120 °C
Molar ratio (wax esters : glycerol : acid anhydride)	0.5 : 1 : 1.2	0.5 : 1 : 1.2	0.5 : 1 : 1.2
	0.1 : 1 : 1.2		

As for the higher temperature synthesis, the transesterification of wax esters was performed under basic conditions (NaOH as catalyst, 0.2 wt.% of total reactive mass) in a convection oven at 230 °C and ambient pressure for 2 hours. The polyesterification was performed in a convection oven at 200 °C at ambient pressure for 3 hours. The temperature was lowered with respect to R1.0 in order to reduce the carbonization of organic matter. On the other hand, the two lower temperature synthesis followed a different protocol. The synthesis at 160 °C consisted in the transesterification in a convection oven at ambient pressure for 3 hours and in the subsequent polyesterification for 4 h always at 160 °C. The synthesis at 120 °C consisted in the transesterification in a convection oven at ambient pressure for 4 hours, which was followed by the polyesterification for 4 hours always at 120 °C. All the polyesterified samples from both 160 °C and 120 °C were further esterified at 180 °C for 2 hours.

R2.1 is a very slight variation of R2.0, since the only difference is the use of H_2SO_4 as catalyst for transesterification in place of NaOH. The molar ratio is once again 0.5:1:1.2 (wax esters : glycerol : acid anhydride). For each sample, no more than two drops of a concentrated 95 wt.% aqueous solution of H_2SO_4 were added to the reactants for transesterification. The acid-catalysed transesterification was conducted in a convection oven at ambient pressure for 3 hours at 160 °C and for 4 hours at 120 °C, respectively. The subsequent polyesterification was performed at 200 °C for 3 hours for both 160 °C and 120 °C transesterified samples.

R2.2 is the iteration of both R2.0 and R2.1 by simply substituting glycerol as polyols with pentaerythritol and sorbitol, which are the two remaining selected branched-resin forming polyols (see SECTION 3.1.3). In spite of changing the given polyol, the molar ratio was not altered from the previously selected 0.5:1:1.2 (wax

esters : polyol : acid anhydride). Transesterification was performed under both acid and basic catalysis in a convection oven at ambient pressure at 140 °C for 3 h. Samples were then polyesterified at 180 °C for further 3 hours.

3.3.2.3 R3.n

R3.n is quite different from the previously reported protocol groups. In fact, this protocol focuses on the direct cross-linking of natural waxes by means of some peroxides as initiators. Waxes undergo cross-linking as received from the supplier. R2.0 consists in the cross-linking of five different waxes (SECTION 3.1.1, TABLE 20) by means of two different peroxides, namely dicumyl peroxide and di-tert-butyl peroxide (SECTION 3.1.4, TABLE 23). The procedure is straightforward as it requires to mix 5 g of wax with 5 wt.% of the given peroxide (*i.e.,* 0.25 g of peroxide). The cross-linking is performed in a convection oven at 130 °C and ambient pressure for 7.5 h. Only the two carnauba wax samples (#135 and #136) were first tested in the furnace at 110 °C for 3 h 45 min to check whether the peroxides would favour some exothermic phenomena with atmospheric oxygen. Assuring the safety of the system, both samples were then let cross-link with all the other samples at 130 °C for 7.5 h as well.

The description and the samples regarding R3.n protocol are reported in TABLE 31.

Table 31 – Code of identification, description and samples of R3.n protocols

Code	Description	Samples
R3.0	Cross-linking of five different natural waxes by means of two distinct peroxides as initiators.	#135 – #144

3.3.2.4 R4.n

R4.n is a further refinement of R2.n protocol group, since the rationale is to substitute the one-step transesterification of wax esters with a more sophisticated three-step process. This new procedure involves a preliminary saponification of both wax esters and free fatty acids present in the given wax, so that each single

esterifiable organic acid compound is valorised in the final resin. Description and samples from R4.n are reported in TABLE 32.

Table 32 – Code of identification, description and samples of R4.n protocols

Code	Description	Samples
R4.0	Synthesis and screening of wax-based alkyd resins based on carnauba wax, glycerol and four different acid anhydrides. Transesterification is substituted by a three-step process that involves saponification, esterification of fatty alcohols and esterification of fatty acids to form monoglyceride prepolymers.	#153 – #156
R4.1	Synthesis and screening of wax-based alkyd resins based on carnauba wax, two different polyols and two different acid anhydrides.	#157 – #160
R4.2	Synthesis and screening of wax-based alkyd resins based on carnauba wax, two different polyols and two different acid anhydrides.	#161 – #164

R4.0 involves the saponification of wax esters and free fatty acids as a first step. It occurs providing heat to the natural wax under basic condition by NaOH addition[7] and continuous stirring so that wax esters are hydrolysed in fatty alcohols and fatty acids. Free fatty acids and fatty acids obtained from hydrolysis of wax esters are saponified into sodium salt (*i.e.*, soap). Once saponification is performed, the soap is acidized by adding a strong acid (H_2SO_4) to protonate the acid anion and form the free fatty acids. Then the medium is washed with boiling water and neutralized with NaOH, the water phase is separated from the organic phase of interest by means of vacuum filtration and the recovered mass is dried overnight (110 °C in convection oven) to remove all excess water. Then, it is important to esterify the remaining fatty alcohols by adding an acid anhydride to prevent those alcohols from terminating polymer chains in the final polyesterification stage for forming the actual resin. Fatty alcohols and acid anhydrides react and form diesters which remain in solution without affecting the reactivity of further steps. Acid anhydrides are added in slight excess to favour the actual esterification of fatty alcohols. A

---

[7] NaOH is added according to the saponification value provided by the wax supplier (SECTION 3.1.1 TABLE 20). The maximum value in the range is selected to be sure saponification would occur at the largest extent.

washing with boiling water and a phase separation by vacuum filtration are then performed to purify the organic phase and the residual mass is then dried overnight for moisture removal. The last step of this new procedure is then the H_2SO_4-catalysed esterification of the purified fatty acids with glycerol to obtain monoglycerides, which function as a prepolymer for the final polyesterification with acid anhydrides. H_2SO_4 is added in the amount of 4-5 drops per gram of reactive components of the processed wax (*i.e.*, fatty acids), which were roughly estimated to be 50% of the blend. Once the esterification of those fatty acids with glycerol is terminated, the medium is washed once again with boiling water, neutralized with NaOH until pH is 6-7, vacuum filtered to separate the aqueous phase and the recovered organic phase is dried overnight. The final step is the polyesterification of the monoglyceride prepolymers with the given acid anhydride of interest. Being the procedure much more refined and cumbersome than the previous ones, a detailed step-by-step bulleted list is reported for synthesis and clarification, along with the molar ratios involved in each reactive stage (TABLE 33). The saponification of carnauba wax was performed so that the saponified wax could be then split in four distinct fractions for each of the following activities in the protocol involving a different acid anhydride. The wax to be saponified was added in larger extent so that 30 g of final resin would be theoretically produced. This allowed to have enough material at the end of each step to obtain in the end 5 g of resin per each acid anhydride. In fact, the different purification and separation processes involved inevitably some material loss at each stage.

For a better understanding of the procedure, the reactions involved in each step are reported in FIGURE 33-36.

R4.1 is the exact same procedure described for R4.0. The only consistent difference is the use of two different polyols in place of glycerol, namely pentaerythritol and sorbitol. Moreover, only maleic and itaconic anhydride were selected due to the presence of unsaturated C=C bonds that may favour cross-linking. The detailed step-by-step protocol reported in TABLE 33 is equally valid for this further protocol as well, apart from the final polyesterification, which was held at 180 °C.

R4.2 follows tightly the R4.1 protocol with only a couple of variations: the two polyols are glycerol and pentaerythritol and the esterification of fatty acids with the

Table 33 – Detailed step-by-step procedure for R4.0

Saponification of wax esters

1. Addition of 40 wt.% NaOH aqueous solution to carnauba wax, 100 °C, 2h, continuous stirring, 1:1 (NaOH : wax esters)[8].
2. Acidification with 95 wt.% H_2SO_4 aqueous solution (pH 3-4), 90-95 °C.
3. Washing with distilled water, 90-95 °C, 10-15 minutes.
4. Neutralization with 40 wt.% NaOH aqueous solution (pH 6-7), 90-95 °C.
5. Cooling to room temperature in water bath.
6. Separation of water phase from organic phase by vacuum filtration.
7. Drying overnight in convection oven at 110 °C.

A. *Esterification of fatty alcohols with acid anhydrides to prevent undesired termination of polymer chains in final polyesterification step*

8. Splitting of the dried purified saponified wax in 4 distinct fractions in accord with each acid anhydride.
9. Addition of the given acid anhydride, 120 °C, 2 h, 1:1.2 (fatty alcohols : acid anhydride).
10. Washing with distilled water, 90-95 °C, 10-15 minutes (removal of excess acid anhydride).
11. Cooling to room temperature in water bath.
12. Separation of water phase from organic phase by vacuum filtration.
13. Drying overnight in convection oven, 110 °C.

B. *Esterification of fatty acids with glycerol (modified polyols)*

14. Addition of glycerol, H_2SO_4 as catalyst (4-5 drops per g of wax fatty acids), 120 °C, 2 h, 1:1 (wax fatty acids : glycerol).
15. Washing with distilled water, 90-95 °C, 10-15 minutes.
16. Neutralization with 40 wt.% NaOH aqueous solution (pH 6-7), 90-95 °C.
17. Cooling to room temperature in water bath.
18. Separation of water phase from organic phase by vacuum filtration.
19. Drying overnight in convection oven, 110 °C.

C. *Polyesterification with acid anhydride*

20. Addition of the given acid anhydride, 140 °C, at least 2h, 1:1:1.2 (wax fatty acids : glycerol : acid anhydride).
21. Cooling to room temperature.
22. Storing in a desiccator.

---

[8] The hydrolysis of 1 mol of wax esters involves the formation of 1 mol each of fatty alcohols and fatty acids.
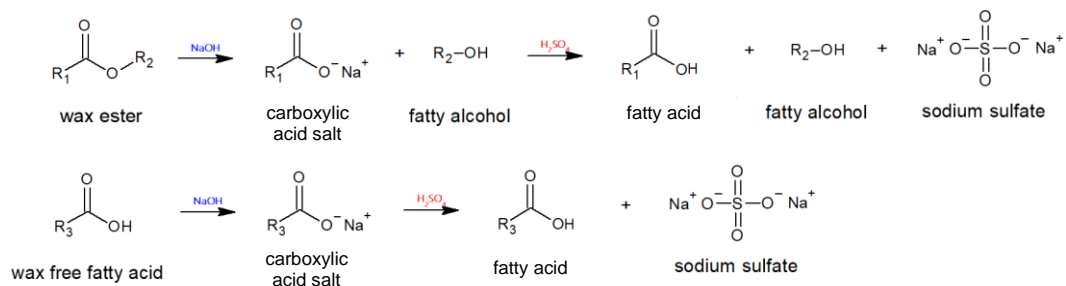
Figure 33 – Saponification of wax esters and wax free fatty acids and subsequent acidification of the formed salts
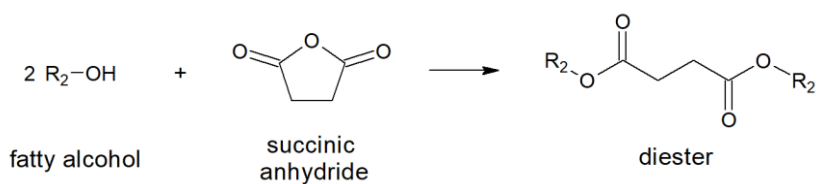
Figure 34– Esterification with acid anhydrides of free fatty alcohols from saponification of wax esters
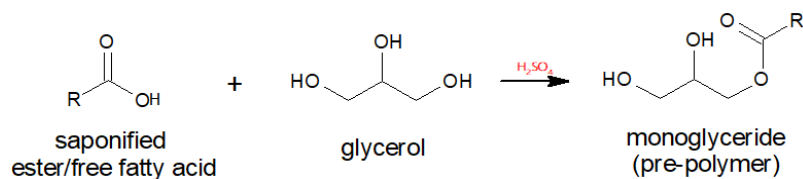
Figure 35 – Acid-catalysed esterification with glycerol of saponified esters and fatty acids
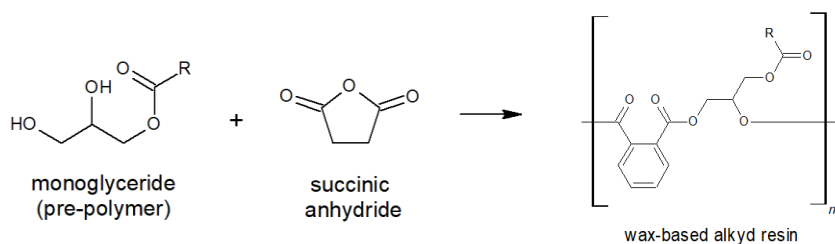
Figure 36 – Polyesterification with acid anhydrides to from the alkyd resin

given polyol (STEP C according to TABLE 33) is performed using NaOH as a catalyst. Moreover, the final weight of the resin is doubled to 10 g per each combination of polyol and acid anhydride so that enough material is produced to realize films for testing their barrier properties.

3.3.3 Film Production

In order to assess the water vapour permeability of the synthesised samples, films were required to be formed. The samples to undergo this procedure were taken only from the R4.2 protocol, which was specifically designed for this purpose. Hot-pressing was selected as the processing technique since it allowed the best control on temperature, pressure and homogeneity of thickness. Due to the peculiar composition of each sample, multiple process conditions have been tested to optimize the film formation and to obtain the most homogeneous morphology as possible. The set of process conditions are reported in TABLE 34 for each sample. The intrinsic brittleness of the materials involved initial difficulties in understanding how to operate the process and set the right parameters in order to obtain flat, easy to handle and pore-free films. After being hot-pressed, samples underwent a very quick ageing at 70 °C in the convection oven for at least 2 hours in order to release eventual thermal stress that were induced during the hot-pressing and slightly increase the ductility for an easier handling. At least four films per synthesised material were produced in order to have meaningful results from the WVP test. Films of pure carnauba wax were produced as well to have a reference. The thickness of each film has been assessed by means of a precision thickness gauge. The samples could be measured only before the WVP test, because films

Table 34 – Hot-pressing parameters for film production

Sample	Temperature (°C)	Pressure (t)[9]	Time (s)	Cooling	Ageing
161	168	1	90	Ambient[10] temperature	✓
162	206	1	90	"	✓
163	172	1	90	"	✓
164	132	1	90	"	✓
CRB	86	1	90	"	✗

[9] 25 t correspond to 312 bar and thus the area of the pressing plates is roughly 78 cm^2.
[10] Films were produced in the in-house pilot plant T_{amb} ranged between 10-20 °C on average.

swelled due to water absorption after the test had been performed. Swollen films were tacky, prone to break and not flat so that they provided unreliable data in terms of thickness. Five measurements per film were performed in order to have a more homogeneous and statistically significant evaluation.

3.3.4   Characterization

3.3.4.1   Differential Scanning Calorimetry

In order to analyse the thermal properties of synthesised resins, *Differential Scanning Calorimetry* (DSC) was used. DSC is a technique consisting in subjecting the given sample to one or multiple thermal cycles to assess the thermal parameters of interest (*e.g.*, glass transition temperature, melting temperature, crystallization temperature, chemical reactions such as oxidation, decomposition and curing and the corresponding enthalpy involved in all those thermodynamic transitions). The particular interest of our analysis was to assess whether the resins displayed a statistically relevant increase in melting point with respect to the corresponding natural wax as received and whether a glass transition was present due to the formation of the cross-linked resin.

The basic principle of DSC is to heat and subsequently cool at a set constant pace according to a given heating programme two aluminium pans at the same time: the one is the reference pan and it is empty, the other is the pan containing the sample of interest. The absorbed (endothermic transition) or released (exothermic transition) heat of the sample in relation to the reference causes a heat flux between the two pans. This allows to obtain a heat diagram which provides all the thermal relevant information about the sample under analysis. Being melting an endothermic transition, a sharp peak can be observed in the heat flux diagram. The area under the peak corresponds to the melting enthalpy. However, unlike melting, the change from glassy to rubbery state during the glass transition is not a 1st order transition[11], showing here an endothermic an *S*-shape step in the heat flux diagram.

---

[11] The order of a phase transition corresponds to the lowest derivative of the Gibbs free energy at constant P and T (or Helmholtz free energy at constant V and T) which is discontinuous at the transition. In more practical terms, a 1st order transition will display a *latent heat* (*i.e.*, the system

The selected heat programme was called -80°C–250°C/2x/10K$_{MIN}^{-1}$/5$_{ISO}$/N$_2$ and the thermal cycle is displayed in FIGURE 37 and it is described in TABLE 35.

Table 35 – Detailed thermal cycle for DSC characterization

DSC Thermal Cycle
1. **Heating** from -80 °C to 250 °C at a constant 10 K/min heating rate
2. **Cooling** from 250 °C to -80 °C at a constant 10 K/min cooling rate
3. **Isothermal** holding at -80 °C for 5 minutes
4. **Heating** from -80 °C to 250 °C at a constant 10 K/min heating rate
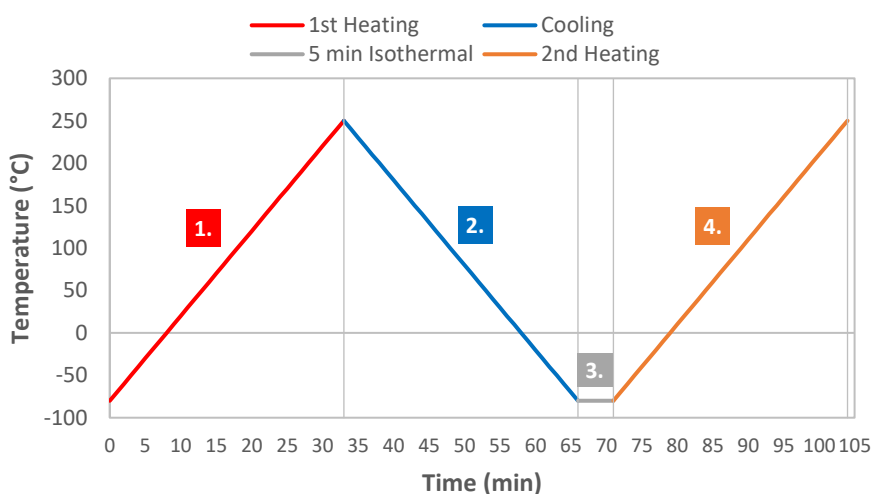
Figure 37 – DSC thermal cycle

All thermal cycles were performed in N$_2$ inert atmosphere to prevent undesired oxidative phenomena. The first heating is performed to analyse the sample as synthesised. At the end of the first heating, the thermal history of the sample (*i.e.*, thermal stresses potentially arisen during synthesis or post-processing) is cancelled and eventual residual by-products are evaporated away. A controlled cooling allows to lower the temperature down to -80 °C without subjecting the sample to further thermal stresses. A second heating is then performed to analyse once more the thermal properties of the sample and assess eventual differences with respect to the first heating. Only the two heating curves are of relevance in our experimental work.

---

absorbs or release energy at constant temperature throughout the whole transition), whereas a 2nd order transition is will not display latent heat and it is said to be *continuous*. Glass transition is a *sui generis* transition in-between 1st and 2nd order, indeed.

Sample preparation is quite important for obtaining good and meaningful results. Samples to be analysed with DSC were prepared by cutting thin and flat slabs of material to be placed inside a 40 μL lid-sealed aluminium pan. It is of utmost relevance to obtain the flattest samples as possible, in order to allow a most homogeneous heat conduction between the aluminium surface and the sample surface itself. In case of bent or not properly flat sample surfaces, the heat flux is not homogeneously absorbed by the sample and the heat flux diagram is negatively affected. The weight of a sample typically ranged between 4 mg and 10 mg. Each empty crucible was weighted as well before setting the corresponding slab of sample inside of it, so that the sample mass loss could be gauged after DSC. Heat flux diagram have been recorded, edited and analysed by means of Mettler Toledo *STARe* software.

3.3.4.2 Fourier Transfer Infrared Spectroscopy

The second technique to be employed for sample characterization is *Fourier Transfer Infrared Spectroscopy* (FTIR). Infrared spectroscopy allows to characterize the functional groups present in the sample upon their capacity to absorb IR radiation. In fact, IR radiation triggers stretching or bending vibrational movements of the chemical bonds. The possible vibrational configurations are energetically quantized. Hence, only the IR radiation carrying the exact amount of energy at a given wavelength will favour the transition to higher energy states which correspond to a given vibrational configuration. Since every functional group displays its own characteristic vibrational energy configuration, it is possible to distinguish each and one of them and acknowledge the chemical nature of the sample.

In IR spectroscopy, the radiation is typically described in terms of *wavenumber*, which is the spatial frequency of a given wave (*i.e.*, how many wavelengths per unit distance). The unit of measure of the wavenumber is cm^{-1}. The physical quantity to be measured in FTIR is the *transmittance* (or, analogously, its inverse *absorbance*), which is the ratio of the intensity of the radiation transmitted throughout the sample and the intensity the incident radiation.

The analysis has always been performed in *Attenuated Total Reflection* (ATR) mode. This involves that the infrared radiation passes through an ATR crystal having a higher refractive index than the sample being in contact with the crystal itself. Being the sample less optically dense than the ATR crystal, the IR wave will be refracted back multiple times into the crystal at a certain angle. This refraction will develop a so-called *evanescent wave* throughout the very surficial layer of the sample in contact with the crystal. The depth of penetration of the evanescent wave is in order of few µm and this allows only a surficial characterization of the given sample. For this reason, a refined sample preparation is not fundamental. However, it is important to create a blank absorption spectrum[12] to subtract the underlying background from the spectrogram of the sample of interest. In this experimental work both solid and liquid samples have been characterised with FTIR in ATR mode. IR spectra have been recorded, edited and analysed by means of PerkinElmer *Spectrum* software.

3.3.4.3   Water Vapour Permeability

The hot-pressed films were tested in terms of water vapour permeability, which is a pivotal parameter with regard to MAP packaging materials for fresh foodstuffs (see SECTION 1.2). The test is performed gravimetrically by measuring the mass water uptake over time at fixed ambient conditions (23 °C, 85→0 RH%).

The most important activity to obtain significant results has been the sample preparation. The first step consisted in the masking of the film by means of two layers of aluminium adhesive foils. The film was to be inserted in-between the two foils and kept in place by the adhesive sides of the foils. Before adding the films, a 5 cm^2 hole was punched in the middle of these aluminium foils and that was the area of the film to be exposed to the testing atmosphere at a given water vapour concentration. The whole procedure required extreme care due to the high brittleness of the samples. Once the films had been masked, they could be inserted

---

[12] The *spectrum* (or *spectrogram*) is the diagram displaying the transmittance (or absorbance, equivalently) as a function of the wavenumber. The experimental spectrum can be compared either with those of known substances present in commercial databases or with reference spectra that display the range of wavenumbers corresponding to a given functional group vibrational stretching or bending.

in the gravimetric chamber and sealed to be placed further placed in the conditioning cabinet at 23°C and 85% relative humidity. One side of the film was directly exposed to the atmosphere at set humidity, whereas the other side was exposed to the inner part of the gravimetric chamber, which had been previously filled with silica gel granulates to maintain a theoretical 0% relative humidity. The testing has been running for seven days and the films have been weighted in order to monitor the water uptake with respect to the starting dry conditions. Due to the slow-paced water uptake, films have been weighted before starting, then at day zero, one, three and seven. Pure carnauba wax and #161 films were weighted twice on day zero to assess whether they would break during the test. The films embedded in the aluminium foils and prepared for the WVP test are reported in TABLE 36.

Table 36 – Films for WVP test from synthesised samples (after the test)

#161   #162   #163   #164

Once the mass of water uptake has been measured over time, only the data that can be fit by a linear interpolation are considered for the evaluation of water vapour permeability. Data are linearly regressed to have information on this linear trend which corresponds to the steady state flux of water vapour throughout the film. The test was performed according to EN ISO 15106-1:2005 [46], which states that the water uptake Δm per unit area A of the film in a given time range Δt corresponds to the mass of water that has permeated through the film per unit area and time. This value is termed *water vapour transmission rate* (WVTR). Once the thickness of the film is known, WVP can be calculated by simply multiplying WVTR by the thickness. The values are normalised on an arbitrary thickness of 100 μm. The films which had broken during the test were not considered in the evaluation. Moreover,

the statistical Inter-Quartile Range (IQR) method of outlier detection was used to discard the thickness values of films that did not lie inside the following range reported in TABLE 37.

Table 37 – IQR method of outlier detector for thickness of films

Lower bound:	Q1 – 1.5·IQR
Upper bound:	Q3 + 1.5·IQR

Q1: first *quartile* (*i.e.*, 25% of data lie below this value); Q3: third *quartile* (*i.e.*, 75% of data lie below this value)IQR = Q3 – Q1

The path to evaluate the WVP of films starting from the linearly regressed experimental data is reported in EQUATIONS 3.3.4.3-1 and 2.

$$WVTR = \frac{1}{A_{film}} \frac{\Delta m_{H_2O,linear}}{\Delta t} \qquad (3.3.4.3\text{-}1)$$

$$WVP = \frac{WVTR \cdot \bar{\delta}_{film}}{100 \ \mu m} \qquad (3.3.4.3\text{-}2)$$

4. Results and Discussions

This chapter will display the main relevant results obtained from the experimental work along with detailed analysis and comments of the most interesting investigated and observed aspects. The results will be reported following the classification operated in MATERIALS AND METHODS. A detailed roadmap for all the protocols is reported in FIGURE 38 and the colours refer to the key code in FIGURE 62 (ANNEX II). This will help have a visual and quick recap while discussing the results.

4.1 Synthesis and Film Production

The synthesised samples differed very much one from each other due to a variety of studied compositions. Each protocol presents its own characteristic features, which are reported in TABLE 38 . However, it is likely to find differences within the very same protocol. For a clear visualization of the properties and the appearance, all the characterised samples are collected in TABLE 66 in ANNEX II along with a short comment of the most relevant features.

Table 38 – Most relevant properties per each operated protocol

Protocol	Main features
R1.0	Amber, resinous, and springy
R1.1	Highly dependent on composition (see ANNEX II for further detail)
R1.2	Hard, brittle, and mainly waxy
R2.0	Hard, brittle, mainly waxy, with some visible resin content
R2.1	Hard, brittle, mainly carbonized
R2.2	Hard, brittle, mainly waxy, with some visible resin content
R3.0	Waxy, with flashier colouration than supplied waxes
R4.0	Hard and brittle
R4.1	Hard and brittle
R4.2	Hard and brittle
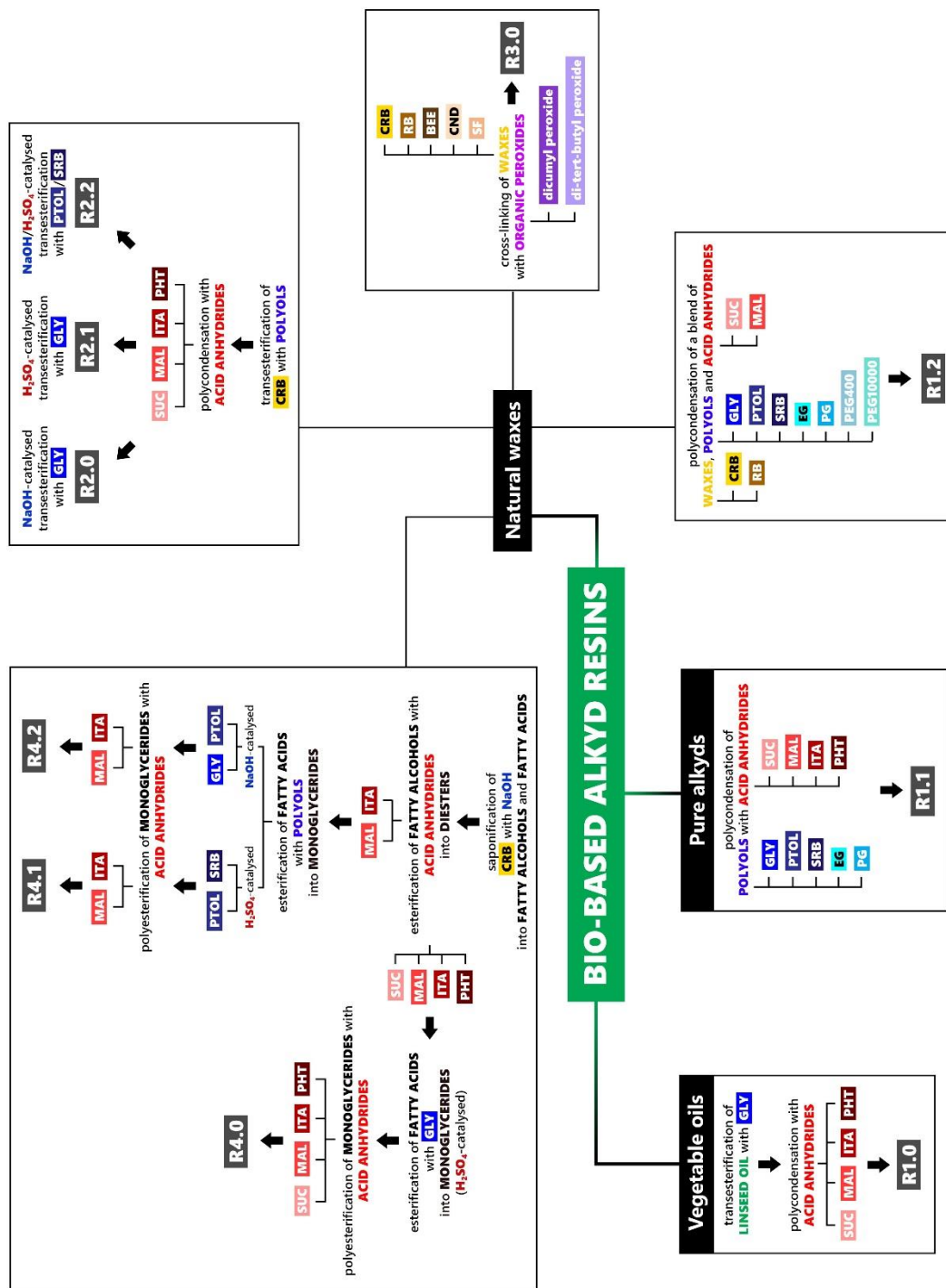
Figure 38 – Roadmap for all the protocols of this work

Due to the great number of produced samples and their large variety of properties, a more detailed discussion will be focused only on the samples belonging to R4.2 protocol, as they were the only ones to be further processed into films and analysed in terms of water vapour permeability. R4.2 samples were synthesised to be hot-pressed in films in light of the *know-how* acquired by all the previously synthesised samples, which functioned as a broad screening.

As already explained in SECTION 3.3.2.4, R4.2 consisted in a four-step synthesis. The first step of saponification allowed to obtain a light beige and smooth cream upon water addition (*i.e.*, wax-derived soap). The continuous stirring provided a homogeneous consistency, but it stirring speed had to be increased from 500 rpm up to 1000 rpm to guarantee a proper mixing due to increased viscosity of the medium. Then, the acidification of the soap by means of H_2SO_4 made the soap turn slightly darker in colouration. Once washed and filtrated, the creamy medium has been spread as thinly as possible in crystallisers. Each crystalliser had been previously covered with a silicon-paper sheet, to favour the detachment once the saponified wax had been dried overnight in the convection oven. Dried saponified wax looked like large sand-based biscuits and it was divided in two distinct batches for STEP A (see SECTION 3.3.2.4, TABLE 33). At this stage, the saponified wax was mixed with the two distinct anhydrides at 120 °C in the convection oven and its melting resulted not as fast as expected, since after 30 minutes most of the mixture had not been melting. This step was designed to neutralize the reactivity of the fatty alcohols derived from saponification of wax esters. In fact, they could have reacted with the given acid anhydride in the final polyesterification (STEP C, TABLE 33) and have reduced the polycondensation yield with modified polyols obtained at STEP B (TABLE 33). The addition of the given anhydride in slight excess and the subsequent formation of fatty alcohols diesters reduce the likelihood of their interfering with the desired reaction route. Thus, the two mixtures have been transferred on two distinct magnetic stirrers for 30 minutes to see if continuous stirring would have helped. However, the exact temperature was difficult to control and thus the two batches were transferred back in the convection oven. Once the reaction was terminated and distilled water had been added for the washing, the vacuum filtration step was not performed because both samples were too creamy and emulsified to

achieve an effective separation of the aqueous phase from the organic phase. The maleic anhydride batch (#161/#163) was rougher in consistency than the itaconic anhydride batch (#162/#164), displaying even some solid chunks. Then, both batches were directly dried in the convection oven overnight, once spread on crystallizers using the same technique previously discussed for saponification. Then, each of the two batches was further split in two distinct batches, one per each selected polyol in order to obtain four batches overall (#161, #162, #163, and #164). The esterification with polyols was NaOH-catalysed. Considering that 1 mol of the given polyol was correspondingly catalysed by 1 mol of NaOH, the mass fraction of NaOH ranged between 5-6% of the overall mixture. The four batches displayed a dark amber-brown colouration with a resinous resemblance and some foamy appearance due to the evaporation of residual water at 120 °C in the convection oven. The peculiarity of this step was the inability to quickly melt each batch of mixture at temperatures up to 140 °C. The mixture started to look like highly viscous caramel after 5-10 minutes of heating upon magnetic stirring but no consistent and homogeneous melting could be observed. This feature was never observed in the previously performed R4.0 and R4.1 protocols. The main cause could be attributed to the NaOH catalysis, which was the only significant difference with respect to the previous protocols. NaOH could be more effective than H_2SO_4 in catalysing the esterification of wax-derived fatty acids with the given polyol. Further insight is given in SECTION 4.3 where FTIR spectra of the synthesised samples are discussed. The impossibility of melting the mixture – short of reaching higher temperature that could trigger some unwanted decomposition phenomena – involved complications in the washing step. Samples were simply rinsed with distilled water and set in the convection oven to favour drying overnight without any further refined separation process. Any attempted filtration or separation would have involved consistent loss of material because the removal of the samples from the crucible involved very minute or even powdered particles that would have easily got washed away. The process was probably less effective than any other STEP B (see SECTION 3.3.2.4, TABLE 33) in both R4.0 and R4.1 due to a higher residual water content from the washing. In fact, some residual surficial moisture could be noted after the overnight drying. Then, each of the four batches was mixed with the

70

corresponding acid anhydride for the final polyesterification process at 180 °C . The itaconic anhydride batches (#162 and #164) resulted more liquid and bubbling than the maleic anhydride batches (#161 and #163) and it is not clear whether the phenomenon is due to chemical nature or residual water content, or even a blend of the two reasons. #161 and #163 were mostly solid with a caramel-like consistency. The weighing for each step of the synthesis is reported in ANNEX III, TABLE 67. It is clear to note that at each step the quantities are theoretically calculated in excess than actually required for the following step. This is because at each washing, filtration and drying, some material was necessarily lost. In fact, it has been observed from the analysis of R4.0 and R4.1 that a theoretical 5 g of resin corresponded in reality to roughly 2.5 g, thus involving an estimated 50% loss of material overall. Therefore, theoretical 20 g of final resin would be required to obtain 10 g of final resin. Considering 4 distinct batches, the reported starting 82.49 g are obtained. Another critical step was to assure the final mass of 10 g. That is why an average 15% mass loss was estimated from the previous protocols before adding the polyols (STEP B, TABLE 33). The same was done for the final polyesterification step, since before adding the given acid anhydride an average 22% mass loss was estimated (STEP C, TABLE 33).

Once these four batches had been synthesised, the subsequent step involved their processing into films. The actual production of films was somewhat complicated by the unique composition of each sample and each batch involved a *trial-and-error* investigation of the proper combination of temperature, pressure and time. Multiple trials per each batch have been attempted before obtaining acceptable results to be further tested. Another consistent limitation was the intrinsic brittleness of the samples, which was to be related to the wax itself. The selected processing temperatures ranged between 132 °C and 206 °C (see SECTION 3.3.4, TABLE 34) and thus a large thermal gradient existed with respect to ambient temperature. Therefore, the cooling was quite fast and not homogenous and it favoured the formation and propagation of cracks that would irreversibly compromise the film stability. Moreover, the lack of homogeneity upon cooling involved that the film would present some bending and some part of the film were still liquid while the rest was already solidified. Hence, upon removal of the silicon-coated paper sheets

utilised to favour an easier detachment of the film, some tiny liquid droplets were removed along with the sheet and some pores were formed in the film. The phenomenon compromised obviously the testability to water vapour permeability. A more controlled cooling was obtained by placing an aluminium weight at ambient temperature on top of the formed film as soon as it was removed from the hot-press. This solution allowed the films to be flat, to have a smoother temperature decrease and to reduce consistently the pore formation and propagation of cracks. After this step, films were to be placed in the convection oven at 70 °C for at least 2 hours to undergo a short physical ageing. The films were laid in-between two silicon-coated paper sheets and an aluminium weight was placed on top to keep them flat. This process would favour the release of thermal stresses that could have arisen during the hot-pressing. The temperature was set at 70 °C for precaution, because higher temperatures could have favoured the wax-based resin to partially melt and to flow without control. Photos of the produced films are reported in TABLE 39.

Table 39 – Images of each hot-pressed film
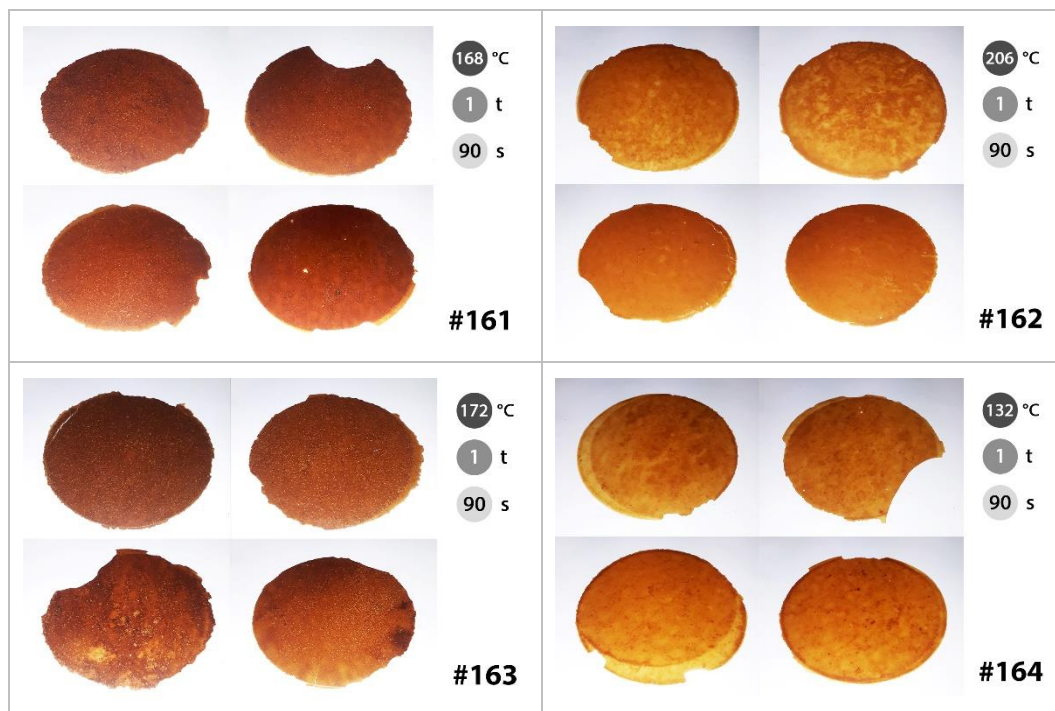
4.2   Differential Scanning Calorimetry

DSC was performed to assess the thermal properties of the synthesised samples. The most detailed and relevant results will focus on R4.n protocols (*i.e.*, R4.0, R4.1 and specially R4.2) not to weigh the argument of this thesis down. However, DSC results will be reported and commented for each attempted protocol in the form of column graphs to display how melting and glass transition – when assessed and significant – have been affected by different compositions and reagents and to have a synthetic and comparative overview on the entire screening as well.

Before starting to present and comment the thermal properties observed by means of DSC, a couple of clarifications are required. First, the results refer only to the minute sample obtained from the overall final batches, which were not likely to be completely homogenous. A statistically meaningful analysis would have required multiple testing of multiple areas of the synthesised materials. However, such refined procedure would have gone beyond the scope of this work of preliminary screening. Secondly, when it was possible for clarity's sake, the colours used to represent data are consistent with the colour code reported in ANNEX II to unequivocally identify each sample at a glance (see FIGURE 62 as a key for the colour code). Moreover, DSC results refer only to the second heating of the pre-set thermal cycle (see SECTION 3.3.4.1, TABLE 35 and FIGURE 37) for a leaner treatise of the subject. The second heating has been selected, since it reports the thermal properties *per* se, independently of the thermal history, which had been erased after the first heating.

All the reported graphs and plots use abbreviations for the given starting materials that have been utilised. Each abbreviation refers to SECTION 3.1.1, TABLE 20 for waxes, to SECTION 3.1.2, TABLE 21 for polyols and SECTION 3.1.3, TABLE 22 for acid anhydrides. The same coding is used for reporting IR and WVP results as well.

The thermal properties of linseed oil-based alkyd resins from R1.0 protocol are reported in FIGURE 39 and TABLE 40. The samples never underwent melting, but they only displayed a glass transition in quite a different range of temperatures. It must be reported that the first two values – which are related to samples #7 and #9 (*i.e.*, maleic anhydride and two distinct linseed oil:glycerol molar ratios) – are not referred to proper glass transitions. In fact, the DSC heat diagram displayed an
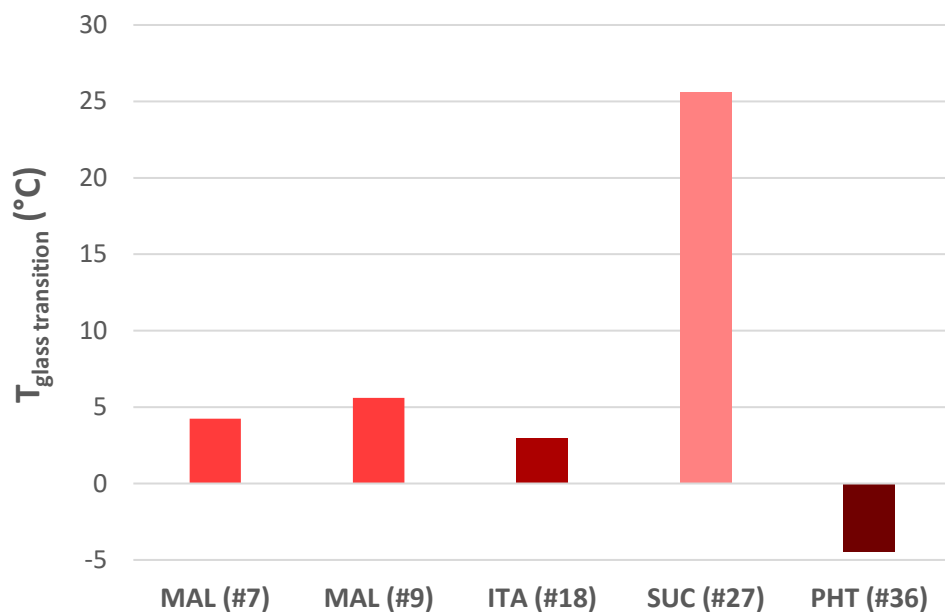
Figure 39 – R1.0 glass transition temperatures

Table 40 – R1.0 glass transition temperature values (°C)

MAL (#7)	MAL (#9)	ITA (#18)	SUC (#27)	PHT (#36)
4.24	4.60	3.00	25.62	-4.50

exothermic crest (*i.e.*, release of energy as heat) rather than the endothermic transition which is to be expected in a glass transition. The phenomenon is probably due to a relaxation of the coiled chains and it corresponds to the release of potential elastic energy. This would also explain the springy and elastomeric behaviour of the two samples (see TABLE 66, ANNEX II). The remaining three samples of the R1.0 protocol (#18, #27, and #36) display a proper glass transition, instead. #18 and #36 have T_g well below ambient temperature (3 °C and -4.5 °C, respectively), which should display a rubbery behaviour and deformability. However, the itaconic anhydride displays a C=C double bond that may favour further cross-linking in #18, while the aryl ring of phthalic anhydride provides a stiffening of the network of polymer chains in #36 (see SECTION 3.1.3, FIGURE 28 to have a glance at chemical structure of the used acid anhydrides). These two distinct rationales may be the reasons why #18 and #36 are harder and glassier than expected from DSC alone. On the other hand, #27 has a higher T_g (25.62 °C), which is roughly comparable to

an ambient temperature of 25 °C. This explains why the sample was rubbery and deformable without incurring in fragile fracture, since the material is right in the transition from glassy to rubbery at ambient temperature. Moreover, the presence of succinic anhydride involves a lower degree of cross-linking due to the absence of C=C double bonds, favouring even more a rubbery and ductile tendency.
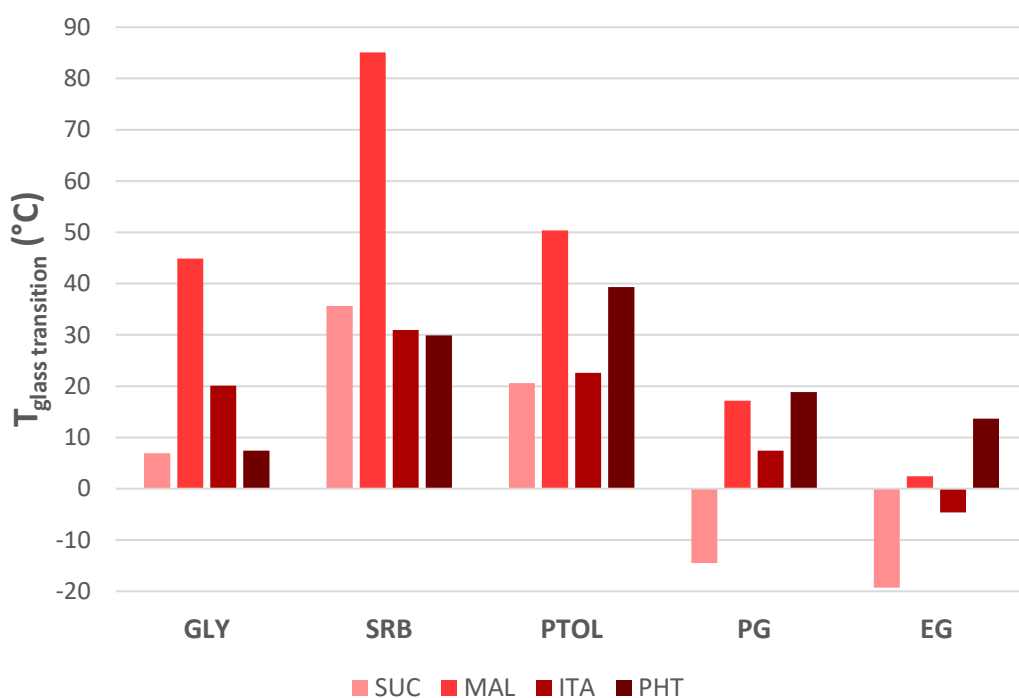
Figure 40 – R1.1 glass transition temperatures

Table 41 – R1.1 glass transition temperature values (°C)

	GLY	SRB	PTOL	PG	EG
SUC	6.90	35.61	20.58	-14.48	-19.32
MAL	44.88	85.09	50.38	17.18	2.42
ITA	20.11	30.95	22.57	7.45	-4.60
PHT	7.45	29.87	39.35	18.84	13.64

The thermal properties of basic polyol-acid anhydride alkyd resins from R1.1 are reported in FIGURE 40 and TABLE 41. The samples underwent only a glass transition, thus showcasing the proper formation of thermoset polymers via cross-linking. Here a distinction between branched resin-forming polyols (*i.e.*, 3 or more reacting

hydroxyl groups such as in glycerol, pentaerythritol, and sorbitol, see SECTION 3.1.2, FIGURE 27) and linear resin-forming polyols (*i.e.*, 2 reacting hydroxyl groups such as in ethylene glycol and propylene glycol, see SECTION 3.1.2, FIGURE 27) is necessary. As a rule of thumb, branched resins display higher glass transition temperatures than linear resins and this is due to the higher likelihood of esterification, which triggers the formation of a more highly 3D connected resin network. However, once a given polyol is selected, each different anhydride imparts quite different thermal properties due to their different chemical structure and ability to favour cross-linking (*i.e.*, presence and reactivity of C=C double bonds). As previously discussed in FIGURE 38, succinic anhydride is the least prone acid anhydride to favour cross-linking and thus it displays the lowest T_g for each selected polyol, apart from sorbitol. This corresponds to a rubbery behaviour or even a viscous liquid. As for branched resins, the highest T_g are related to maleic anhydride, whose C=C double bond triggers cross-linking among distinct polymer chains. This forms and stabilizes the network of polymer chains and it explains its considerably higher glass transition temperatures (*e.g.*, ranging from 44.88 °C with glycerol up to 85.09 °C when sorbitol is selected as polyol). This reflects the solid, harder and glassier nature of the corresponding resins. In regards with branched resins, those who displayed T_g higher than 20-25 °C (*i.e.*, an average ambient temperature) were thermoformable by means of hot-pressing and transparent, flexible films were obtained. This behaviour was triggered by the heat provided through hot-pressing, which activates the movement of polymer chains and favours a properly formed film. On the other hand, when considering linear resins, the T_g are consistently lower than branched resins instead, as previously said. This is due to a lower number of reacting hydroxyl groups and the presence of smaller molecular size of the selected polyols. In fact, when unreacted, both ethylene glycol and propylene glycol function as plasticisers, thus reducing the glass transition temperature. The same effect is to be considered in glycerol as well, even though at a lower extent due to the presence of three hydroxyl groups that increase the reactivity. This plasticising effect is observed in the values of T_g, which range from -19.32 °C to 18.84 °C and thus below an average ambient temperature range of 20-25 °C. This involves the viscous liquid appearance of the synthesised samples.

However, in this case the less plasticised resins (*i.e.*, higher T_g) result those with phthalic anhydride, whose presence could stiffen the linear network of polymer chains due to its aryl ring and reduce the likelihood of chain mobility.

An interesting outcome is that these R1.1 resins were among the first samples to be synthesised and after months of storage at ambient atmosphere, a further curing (or so-called *drying*) was observed. This was due to the exposure to atmospheric oxygen that favoured autoxidation phenomena (see SECTION 2.2, TABLE 19) and an increase in cross-linking degree. By touching the surface of the dried resins with a wooden stick, the consistency resulted hardened, as if a stiffer surficial film were formed over time.
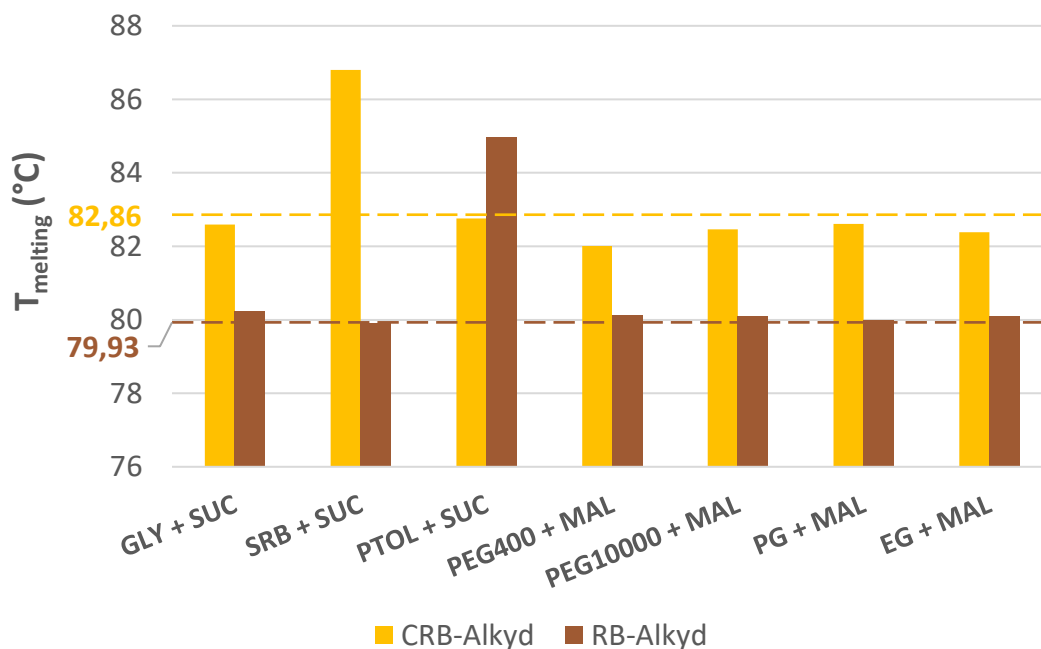
Figure 41 – R1.2 melting temperatures

Table 42 – R1.2 melting temperature values (°C)

	GLY+SUC	SRB+SUC	PTOL+SUC	PEG400+MAL	PEG10000+MAL	PG+MAL	EG+MAL
CRB	82.59	86.80	82.76	82.01	82.46	82.61	82.38
RB	80.23	79.90	84.96	80.12	80.10	80.00	80.09

The thermal properties of R1.2 samples are reported in FIGURE 41 and TABLE 42. These were the first attempted resins that contained natural waxes. The *rationale* behind the synthetic route was quite *naïf*, since it involved simply to blend the wax

with a given polyol and a given acid anhydride and to esterify them at high temperature. This resulted in quite heterogeneous samples, which displayed a prevalence of wax properties with minor dispersed resin content. The melting peak from DSC for carnauba wax (yellow dotted line in FIGURE 40) and rice bran wax (brown dotted line in FIGURE 41) as received from KahlWax are reported as references, so that it is easier to compare the thermal performance of the synthesised samples. As previously stated for R1.1, the first three polyols refer to branched resins, whereas the remaining four refer to linear resins. Only succinic and maleic anhydrides were selected because they both display very similar molecular structures, and yet maleic present a C=C double bonding that would favour cross-linking at a larger extent. This could have allowed us to have an assessment on how the degree of cross-linking could affect the thermal properties. Succinic anhydride was used only with branch resin-forming polyols, whereas maleic anhydride was used only with linear-forming polyols. This decision was based on the DSC results of R1.1 to avoid obtaining too glassy and brittle resins that could affect any further thermoformability. As FIGURE 40 displays, the minor and heterogeneous resin formation did not influence much the thermal properties with respect to pure natural waxes. T_m percentage variations are reported in TABLE 43 with respect to FIGURE 41. From the reported percentage variation, it is clear that the only relevant results are those related to *carnauba/sorbitol/succinic anhydride* (*i.e.*, #62, +6.29%) and *rice bran/pentaerythritol/succinic anhydride* (*i.e.,* #74, +4.76%). The larger increase could be related to the higher number of reacting hydroxyl groups in both

Table 43 – Melting temperature percentage change of R1.2 samples from pure waxes

Sample	$\Delta T_{m,CRB}$ (%)	$\Delta T_{m,RB}$ (%)
GLY + SUC	-0.33	+0.38
SRB + SUC	+4.76	-0.04
PTOL + SUC	-0.12	+6.29
PEG400 + MAL	-1.03	+0.24
PEG10000 + MAL	-0.48	+0.21
EG + MAL	-0.30	+0.09
PG + MAL	-0.58	+0.20

pentaerythritol (4 OH groups) and sorbitol (6 OH groups), that increases the likelihood of a polymeric network to be formed and to stiffen the overall structure of the blend. This means that the several distinct wax molecules (mainly wax esters) are not quite likely to be chemically bound to the resin network, but the small resin content would somehow function as a stabilising matrix that reduces the wax chain movements. This would require higher energy to activate their free motion under melting, which translates to a higher melting temperature.

Melting temperatures of R2.0 samples are reported in FIGURE 42 AND TABLE 44. Here the colours are selected to highlight the difference in temperature of synthesis (*i.e.*, from the lower temperature in pale yellow to the higher temperature in crimson).

The *rationale* of the protocol was to trace the R1.0 synthesis of linseed-oil alkyd resins, by using carnauba wax instead (see SECTION 3.3.2.2). Four different anhydrides and three distinct temperatures have been investigated as reported in the FIGURE 42. It is evident in all cases that the melting temperature slightly decreases
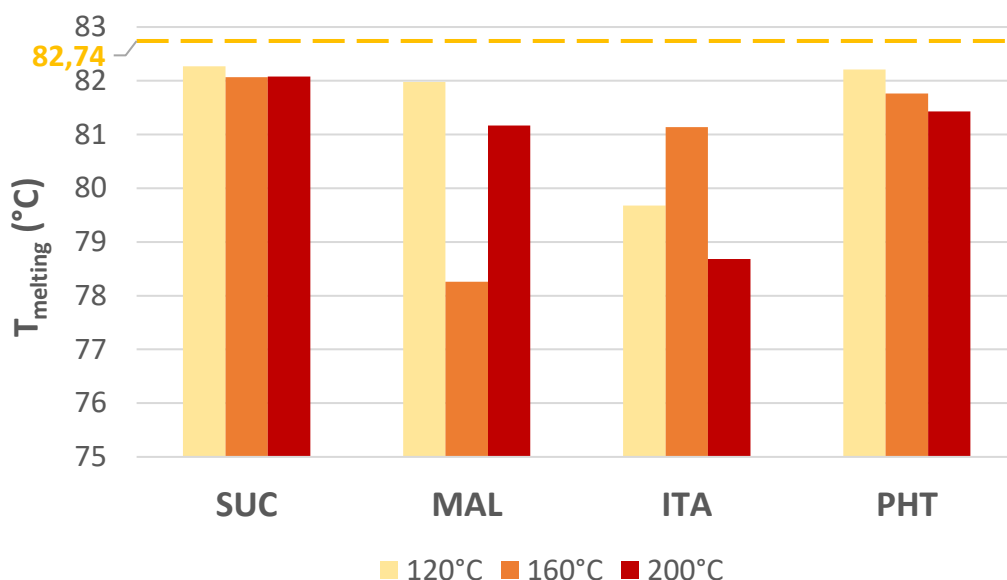
Figure 42 – R2.0 melting temperatures

Table 44 – R2.0 melting temperature values (°C)

	SUC	MAL	ITA	PHT
120 °C	82.27	81.98	79.68	82.21
160 °C	82.07	78.26	81.14	81.76
200 °C	82.08	81.17	78.68	81.43

with respect to the pure wax. Apart from itaconic anhydride, the samples synthesised at 120 °C displayed the highest T_m and it could be due to a not high enough temperature to favour further cross-linking of the C=C double bond of itaconic anhydride that could thermally stabilise the sample. On the other hand, the samples synthesised at 200 °C displayed the lowest T_m. This effect could be related to the onset of degradation phenomena at rising temperature that could favour a reduction of molecular weight of the polymer chains and thus the formation of shorter molecules which are more prone to move under absorption of heat.

Table 45 – Melting temperature percentage change of R2.0 samples from pure waxes

Acid anhydride used in sample	$\Delta T_{m,120\ °C}$ (%)	$\Delta T_{m,160\ °C}$ (%)	$\Delta T_{m,200\ °C}$ (%)
SUC	-0.57	-0.82	-0.80
MAL	-0.92	-5.41	-1.90
ITA	-3.70	-1.93	-4.91
PHT	-0.64	-1.18	-1.58

However, percentage changes from the melting point of pure carnauba wax were quite restrained and they are reported in TABLE 45. Itaconic anhydride is the anhydride that consistently displays the most affected thermal properties, for the reasons just discussed. Since R2.0 is somehow a variation of R1.0 protocol, it is interesting to assess whether each sample was able to display a glass transition. T_g values for those R2.0 samples displaying the given transition are reported in FIGURE 43 and TABLE 46. It is clear that only the samples containing succinic and itaconic anhydride were able to undergo a glass transition. The very few data available show that increasing the synthesis temperature involves a reduction in T_g and this may be related to the already discussed reduction of molecular weight of polymer chains that could facilitate their mobility. Plus, while the T_g value of the samples containing itaconic anhydride have no resemblance with the corresponding R1.0 sample, the T_g of succinic anhydride sample varies in a range of temperatures (from
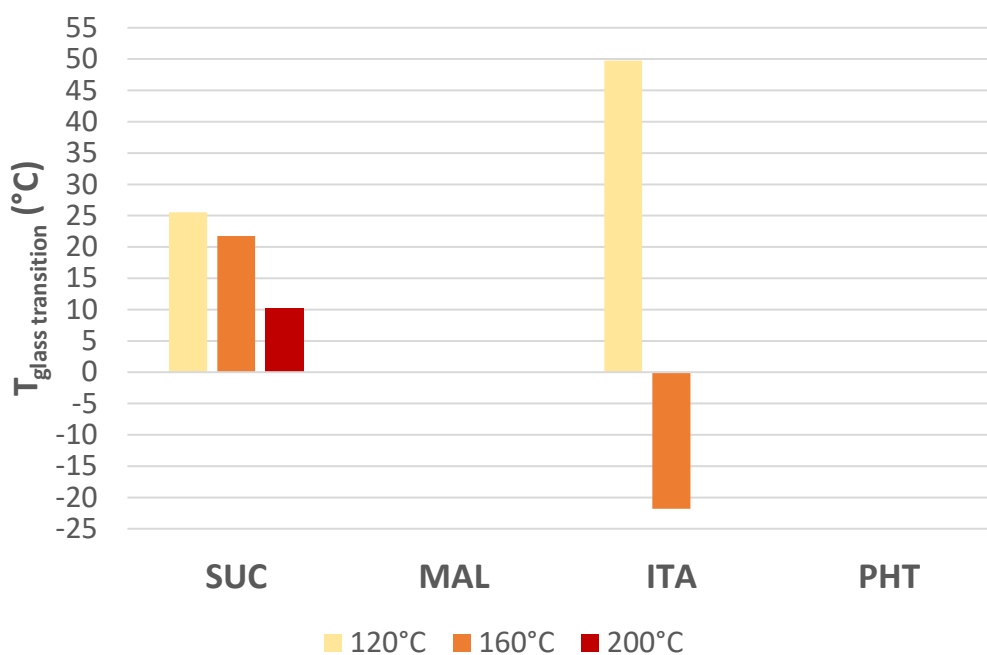
Figure 43 – R2.0 glass transition temperatures

Table 46 – R2.0 glass transition temperature values (°C)

	SUC	MAL	ITA	PHT
120 °C	25.54	-	49.76	-
160 °C	21.74	-	-21.79	-
200 °C	10.12	-	-	-

10.12 °C at 200 °C up to 25.54 at 120 °C) that is more consistent with the value observed for the corresponding #27 R1.0 sample (*i.e.*, 25.62 °C). The reason why samples containing maleic and phthalic anhydrides do not display any glass transition could be related to the fact that the network has a higher cross-linking degree (*i.e.*, polymer chains are stabilised in a network and their movement is hindered) and the steric hindrance of the aryl group, respectively. However, it could also be related to a lower tendency to successfully react and form the resin for both acid anhydrides.

Melting temperatures for R2.1 samples are reported in FIGURE 44 and TABLE 47. This protocol follows tightly the previous R2.0 with the only exception of using H_2SO_4
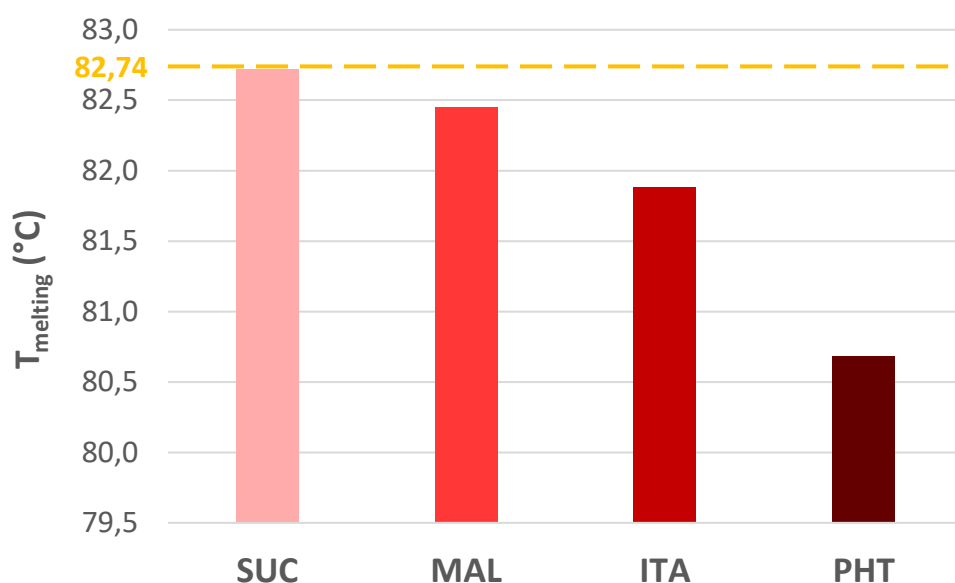
Figure 44 – R2.1 melting temperatures

Table 47 – R2.1 melting temperature values (°C)

	SUC	MAL	ITA	PHT
120 °C	82.72	82.45	81.88	80.68

as a catalyst for transesterification in place of NaOH (see SECTION 3.3.2.2). Although two distinct temperatures have been investigated (i.e., 120 °C and 160 °C), in light of the previous discussion of slightly higher melting temperatures at lower temperature, only data at 120 °C are reported. R2.1 samples displayed only melting points and any glass transition could be noted. A clear trend can be observed, as the melting temperature decreases from succinic to phthalic anhydride. In comparison with R2.0 at 120 °C, the trend is consistent apart from the phthalic anhydride. This could be due to a higher content of carbonised matter, that could reduce the thermal properties of the material (see TABLE 66, ANNEX II). Percentage changes from the melting point of carnauba wax as received are reported in TABLE 48.

Melting temperatures of R2.2 samples are reported in FIGURE 45 and TABLE 49. In this protocol glycerol has been substituted with both pentaerythritol and sorbitol to assess whether an increase in reacting hydroxyl group would favour a higher yield of resin.

Table 48 – Melting temperature percentage change of R2.1 samples from pure waxes

Sample	$\Delta T_{m,120\ °C}$ (%)
SUC	-0.02
MAL	-0.35
ITA	-1.04
PHT	-2.49
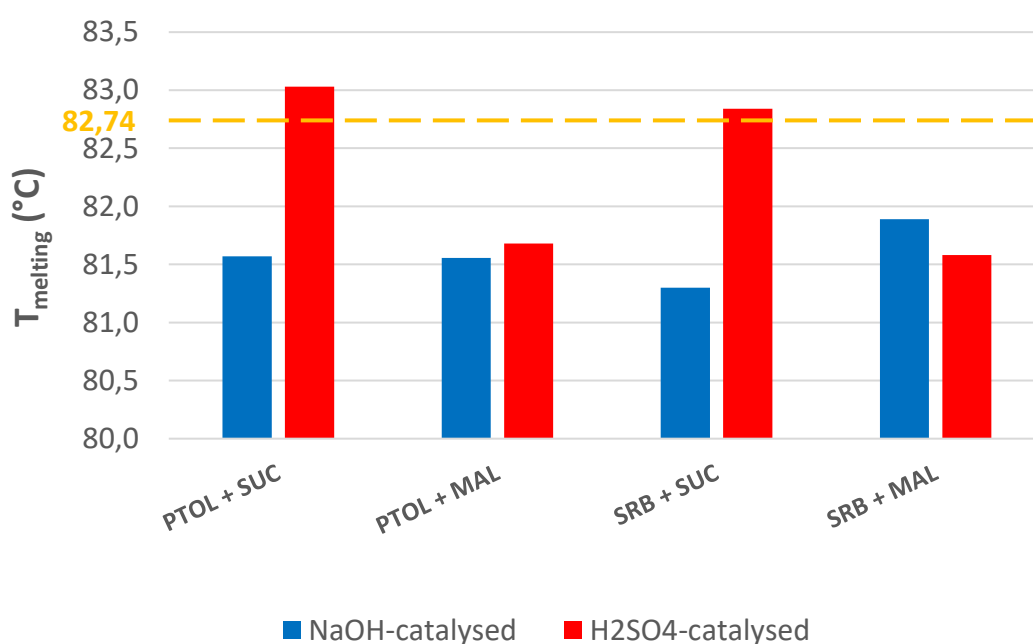
Figure 45 – R2.2 melting temperatures

Table 49 – R2.2 melting temperature values (°C)

	PTOL+SUC	PTOL+MAL	SRB+SUC	SRB+MAL
NaOH	81.57	81.56	81.30	81.89
H_2SO_4	83.03	81.68	82.84	81.58

Here we can see at a glance the difference between the base-catalysed transesterification and the acid-catalysed transesterification. As a general trend, H_2SO_4-catalysed samples result in higher T_m, which could be derived from a more effective nucleophilic attack on the carboxyl carbon atom of wax esters by the

polyol hydroxyl groups during the preliminary transesterification step. Percentage change from pure carnauba wax is reported in TABLE 50 for each sample.

Table 50 – Melting temperature percentage change of R2.2 samples from pure waxes

Sample	$\Delta T_{m,NaOH}$ (%)	$\Delta T_{m,H2SO4}$ (%)
PTOL + SUC	-1.41	+0.35
PTOL + MAL	-1.43	-1.28
SRB + SUC	-1.74	+0.12
SRB + MAL	-1.03	-1.40

For both H_2SO_4-catalysed samples which contain succinic anhydride, T_m is even higher than the corresponding value of pure carnauba wax, despite the deviation is very minute. On the other hand, H_2SO_4-catalysed samples which contain maleic anhydride display a T_m value which is lower than that of the pure wax and much closer to the corresponding NaOH-catalysed counterparts. All NaOH-catalysed samples display a T_m value lower than the pure natural wax and the discrepancy between each sample is more restrained with respect to H_2SO_4-catalysed samples. By simple analysis of thermal properties via DSC it is still not clear whether one catalyst is more efficient than the other. This kind of issue will be investigated via FTIR in SECTION 4.3. The melting temperatures of R3.0 are reported in FIGURE 46 and TABLE 51. As it appears immediately at first sight, no relevant variation is to be observed from the cross-linking of natural waxes by means of two distinct organic peroxides (see TABLE 52). This does not imply that the cross-linking had not occurred, but the treatment has not probably impacted the thermal properties as much as desired. On the other hand, other properties could have been impacted, such as mechanical properties [47]. However, this route has not been further explored since it did not provide significant results for the scope of this thesis. In any case, it is interesting to assess that the best thermally performing natural waxes (i.e., higher T_m) are those with the highest ester content (see SECTION 1.4.1, TABLE 13): carnauba, rice bran and sunflower waxes.
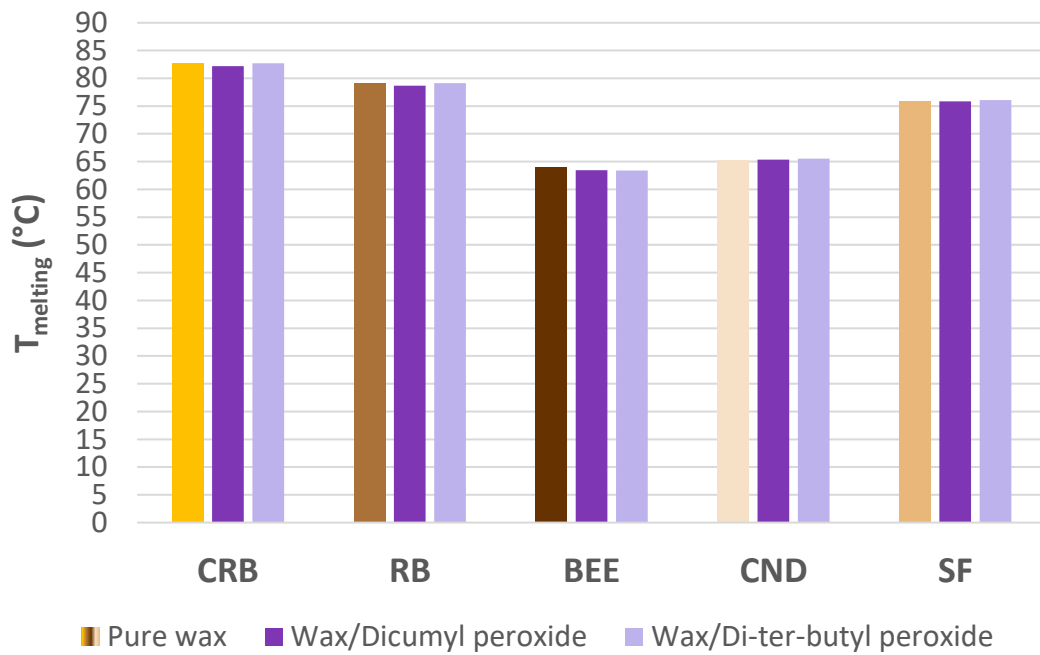
Figure 46 – R3.0 melting temperatures

Table 51 – R3.0 melting temperature values (°C)

	CRB	RB	BEE	CND	SF
Pure wax	82.74	79.10	63.94	65.30	75.91
Dicumyl peroxide	82.16	78.70	63.45	65.36	75.82
Di-ter-butyl peroxide	82.72	79.11	63.39	65.51	76.09

Table 52 – Melting temperature percentage change of R3.0 samples from pure waxes

Sample	$\Delta T_{m,\text{dicumyl peroxide}}$ (%)	$\Delta T_{m,\text{di-tert-butyl peroxide}}$ (%)
CRB	-0.70	-0.02
RB	-0.51	+0.01
BEE	-0.77	-0.86
CND	+0.09	+0.32
SF	-0.12	+0.24

Finally, the discussion of the most interesting protocol group (*i.e.*, R4.n) for the goal of this experimental work. Before presenting the data, it is necessary to display a key for full comprehension of the following plots. Since the protocol involved four subsequent synthetic steps (see Section 3.3.2.4), the graphs will report on the x-axis a corresponding *step-timeline*, in which each point corresponds to a given step. The legend of this timeline is reported in Table 53 and it is valid for each and every one of the three R4.n protocols (*i.e.*, R4.0, R4.1 and R4.2). The colours do not correspond to the colour key in Figure 62 (Annex II), they are provided in order to have a much clearer visualization among the plotted lines. In each of the following graphs, the horizontal dotted line corresponds to the melting temperature of pure carnauba wax to have a comparative reference.

Table 53 – Key to x-axis representation of the 4-step synthesis from R4.n protocols

Timeline point	Synthetic step
0	Pure wax as received
1	Saponification of wax esters and fatty acids
2	Esterification of fatty alcohols with acid anhydride
3	Esterification of fatty acids with polyol (modified polyol)
4	Polyesterification of modified polyol with acid anhydride

R4.0 results are reported in Figure 47. It is recalled that R4.0 involves the selection of glycerol as polyol and four different anhydrides (see Section 3.3.2.4). Here, the thermal behaviour of each sample at each step is provided. The saponification was in common for all the four given samples and it involved a decrease in melting temperature. This is to be attributed to the breaking of ester bonds into fatty alcohols and fatty acids that reduces the length of wax esters and thus facilitates the movement of previously longer chains upon heat absorption.

The subsequent step of esterification of free fatty alcohols in diesters by means of a given acid anhydride corresponded in an increase of thermal properties for each of the four anhydrides.
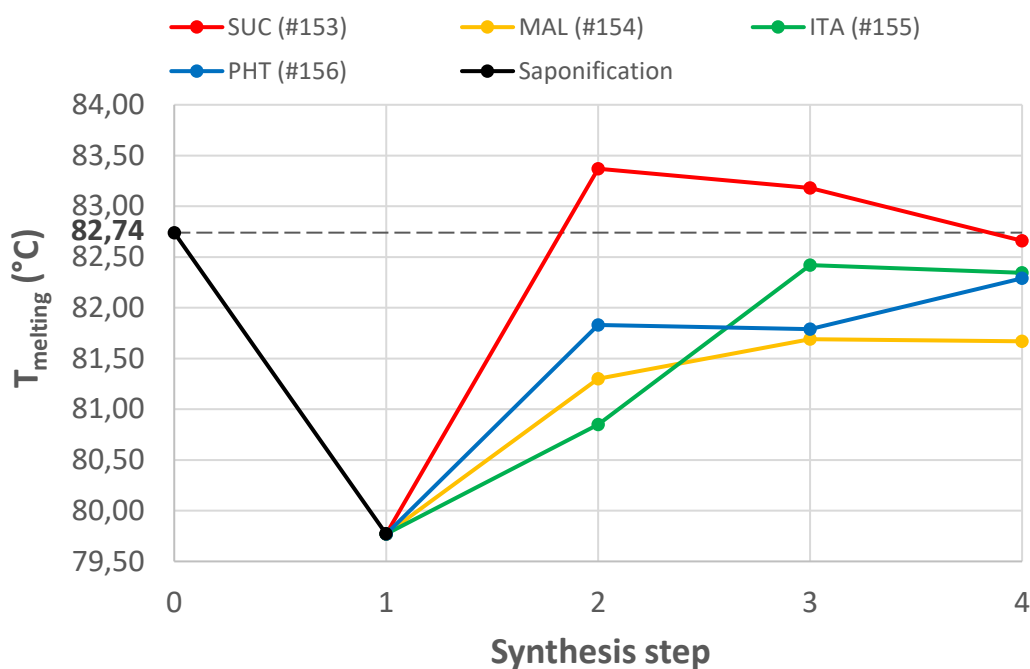
Figure 47 – R4.0 melting point for each of the 4-step synthetic route

In fact, the formation of diesters presenting long chain fatty alcohol residues at each sides of their molecules involves a further spatial hindrance with respect to free fatty alcohols, which are then further stabilised by this step. Moreover, the formed diesters further impede the movement of free fatty acids obtained from the saponification step. Free fatty acids are esterified with the selected added acid anhydride as well, even if in minor content and this involves the same phenomenon just discussed for esterified fatty alcohols. Unlike the other acid anhydrides, succinic anhydride-esterified fatty alcohols impart a T_m which is even higher than pure carnauba. This could be due a higher symmetry and lower spatial hindrance of the molecule (see SECTION 3.1.3, FIGURE 28) that favours a better packing of the long chain molecules into a more crystalline conformation that involves higher energy absorption to have looser chains and thus a molten state. The trend is consistent with the other acid anhydrides. In fact, it can be noted that: phthalic anhydride displays the second highest T_m and it is as symmetric as succinic and the aryl group stabilises the structure, but its spatial hindrance reduces the close-packing likelihood; maleic is the following and the C=C double bond adds some spatial asymmetry on the overall molecule due to the *p*-orbitals which are perpendicular to the longitudinal *s*-orbitals; itaconic anhydride has the least symmetric structure

which corresponds to the lowest T_m. The further step is the esterification of fatty acids with glycerol. Here it can be observed that the blends containing acid anhydrides with C=C double bonds (*i.e.*, maleic and itaconic) displayed an increase in T_m, while the opposite was to be noted for the remaining acid anhydrides. This could be explained by supposing that minor cross-linking could have already occurred at this stage, thermally stabilising the whole structure. Moreover, the thus formed modified polyols are sufficiently large molecules to display a reduced mobility (see SECTION 3.3.2.4, FIGURE 35, recalling that **R** is a long alkyl chain). The final step consists in the final polyesterification of the modified polyols and here the thermal performance are curious. In fact, the increase in molecular weight due to polycondensation and the subsequent cross-linking should involve an increase in T_m. However, such an increase is not to be observed. In fact, apart from phthalic anhydride, all other samples display a melting point that either slightly reduces in value or *plateaus*. The phenomenon may be due to a low polycondensation yield that could be hindered by the following reasons reported in TABLE 54.

Table 54 – Reasons why the final polyesterification could not occur as desired

• Low diffusivity of the given acid anhydride throughout the medium due to the long residual alkyl chains (i.e., **R**)
• Lower reactivity of secondary hydroxyl groups of glycerol molecules embedded in the modified polyol
• Low temperature to initiate the polycondensation and sustain the chain propagation

The sample esterified with succinic anhydride displayed the highest – and the closest to pure carnauba – T_m value. Percentage variation of melting temperatures per each step of the synthesis are reported in TABLE 55. It can be seen that apart from the first saponification step, the discrepancies with the pure wax are restrained.

R4.1 results are reported in FIGURE 48. Here it is important to recall that protocol involved the use of two selected anhydrides (*i.e.*, maleic and itaconic) and two selected polyols (*i.e.*, pentaerythritol and sorbitol) (see SECTION 3.3.2.4).

Table 55 – Melting temperature percentage change of R4.0 samples from pure waxes

Sample	$\Delta T_{m,1}$ (%)	$\Delta T_{m,2}$ (%)	$\Delta T_{m,3}$ (%)	$\Delta T_{m,4}$ (%)
SUC	-3.59	+0.76	+0.53	-0.10
MAL	-3.59	-1.74	-1.27	-1.29
ITA	-3.59	-2.28	-0.39	-0.48
PHT	-3.59	-1.10	-1.15	-0.54
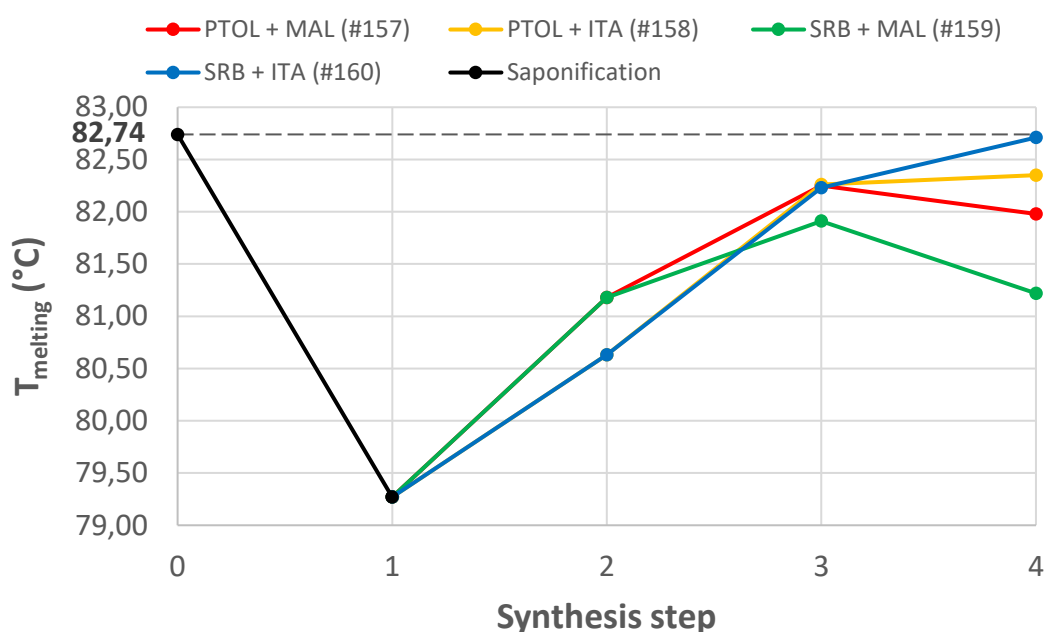
Figure 48 – R4.1 melting point for each of the 4-step synthetic route

The acid anhydrides were chosen due to the presence of the C=C double bond that could have favoured the cross-linking, whereas the polyol were chosen because they displayed the highest number of reacting hydroxyl group, so that the likelihood of esterification – and thus resin formation – could be potentially increased. As for both steps 1 (*i.e.*, saponification of wax) and 2 (*i.e.*, esterification of free fatty alcohols with acid anhydrides to diesters), the trend is identical to the previously discussed R4.0 results in FIGURE 47, since the procedure is exactly identical. The *rationale* is the same and thus the same discussion just proposed is still valid. It is to be reminded that step 2 is performed in one single batch per acid anhydride and each of them is subsequently subdivided in two further batches per given polyol.

Data for both step 1 and step 2 are consistent with the values obtained in R4.0 protocol.

A further increase in T_m can be observed at step 3 and the trend is clearer with respect to R4.0, in which only the acid anhydrides displaying a C=C double bond would display such tendency. Here the phenomenon is to be connected to the increased number of reacting hydroxyl groups in the given polyol which is added at this stage. This has increased the chance that the free fatty alcohols in the blend would react with the polyol to form the modified polyol. Despite two lacking hydroxyl groups with respect to sorbitol, pentaerythritol seems more effective and this could be probably due to the presence of four primary -OH groups that are more reactive than secondary -OH groups. In fact, sorbitol displays only two primary, but also four secondary hydroxyl groups, and the overall molecule is larger and it would diffuse at a lower extent in the reaction medium (see SECTION 3.1.2, FIGURE 27).

As for the final step of polyesterification, different trends can be noted. The addition of itaconic anhydride to the sorbitol-esterified pre-polymer involves an increase in T_m to a value very close to the pure wax. This may be due to larger number of available free hydroxyl groups that are able to react with the acid anhydride and involve a higher molecular weight of the final polymer. The addition of itaconic anhydride to the pentaerythritol-esterified pre-polymer involves an increase as well, in spite of a lower extent. On the other hand, the addition of maleic anhydride to both sorbitol- and pentaerythritol-esterified pre-polymers entails a reduction in T_m. The trend is different from what has been assessed in R4.0, in which the T_m would *plateau*. An explanation could be referred to the increased polycondensation temperature for step 4. Temperature was raised from 140 °C in R4.0 up to 180 °C in R4.1. This could have implied that parts of the mixture underwent some degradation phenomena that involved a reduction in the average molecular weight, thus contrasting the polycondensation itself and negatively influencing the thermal properties. Anyway, the final T_m values are consistently close to the pure wax value even for samples polyesterified with maleic anhydride. The actual percentage change per each step are reported in TABLE 56.

90

Table 56 – Melting temperature percentage change of R4.1 samples from pure waxes

Sample	$\Delta T_{m,1}$ (%)	$\Delta T_{m,2}$ (%)	$\Delta T_{m,3}$ (%)	$\Delta T_{m,4}$ (%)
PTOL + MAL	-4.19	-1.89	-0.59	-0.92
PTOL + ITA	-4.19	-2.55	-0.58	-0.47
SRB + MAL	-4.19	-1.89	-1.00	-1.84
SRB + ITA	-4.19	-2.55	-0.62	-0.04

DSC results for R4.2 are reported in FIGURE 49. Here a somewhat different trend from the previously discussed protocols can be observed. It must be recalled that R4.2 replicates R4.1 with glycerol in substitution of sorbitol and with a base-catalysed esterification of polyols and fatty acids at STEP B.
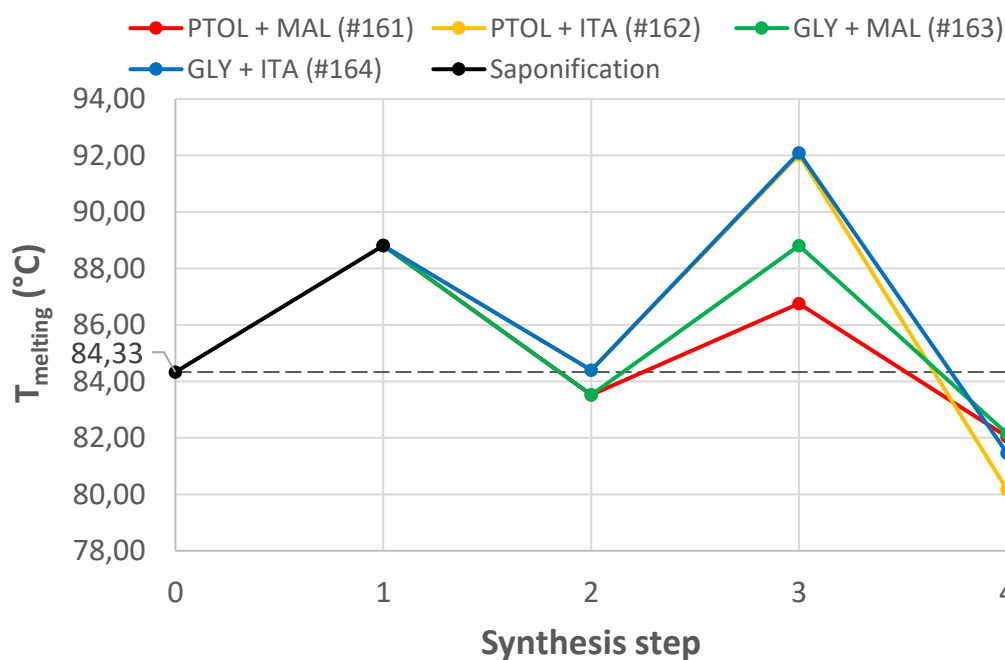
Figure 49 – R4.2 melting point for each of the 4-step synthetic route

The first remarkable difference is the significant increase in T_m after the saponification has occurred. In the previous protocols an opposite trend was observed, because the wax esters – and thus mainly the wax structure – had been hydrolysed in their constitutive fatty acids and fatty alcohols. Here the increase of melting temperature does not imply that the saponification did not happen, but it is rather more likely that a consistent amount of sodium carboxylate salt is still present

before Step A. This could be related to the fact that a quadruple amount of wax had been used in R4.2 with respect to both R4.0 and R4.1. This involved the acidification of the carboxylates to re-protonate them to carboxylic acids had not been sufficient enough for the entire saponified mass. Those residual carboxylate salts were stabilised by the ionic interactions between cations (i.e., Na^+) and anions (i.e., $RCOO^-$) and thus the melting point of the heterogeneous blend increased after the saponification.

The subsequent step 2 involved a decrease in T_m to a value closer to the value of pure carnauba wax for both maleic anhydride (*i.e.*, #161 and #163) and itaconic anhydride (*i.e.*, #162 and #164). This trend is a mixed effect of the residual carboxylate salts and the esterified fatty alcohols. The two contributions balance out one another, since the former would promote a melting point increase, while the latter would reduce (see step 2 in FIGURES 46 and 47 for comparison). Itaconic anhydride imparts a slightly higher T_m, which is essentially in line with the natural wax value.

Another interesting variation with the previous protocols can be noted at step 3. This stage involves the esterification of the added polyol with the fatty acids from saponification. However, here the reaction is catalysed by NaOH in place of H_2SO_4. The base catalysis involved a further relevant increase in T_m and the reason may be the same proposed for the saponification. NaOH strongly triggers the hydrolysis of ester bonds, whether they are wax esters or diesters from fatty alcohols and acid anhydrides. This favours the formation of further sodium salts that tend to further increase the melting point due to a more stabilised crystalline structure. It is to be observed that the presence of itaconic anhydride involves a higher T_m which is roughly 92 °C, independently of the polyol. This may induce that the polyol is only mildly incorporated in the desired monoglycerides and affects in minor part the thermal properties. The presence of maleic anhydride leads to a lower melting point (*i.e.*, T_m ranges roughly between 87 °C and 89 °C). Glycerol imparts slightly better performance, which is somehow unexpected. In fact, the presence of the extra hydroxyl group of pentaerythritol would suppose that it better stabilises the polymer network. The observed trend could be potentially explained by taking into consideration ionic repulsion among hydroxyl groups of the given polyol and the

92

carboxylate ions. Repulsions could be more frequent and intense in presence of pentaerythritol and they could involve a larger free volume available for chain mobility.

The final esterification step is interesting since a consistent drop in melting temperature is recorded, which was not observed in the previous protocols. The trend is probably due to the esterification of the carboxylates with the acid anhydrides, thus reducing the beneficial effect of the salts on thermal properties. A more detailed discussion on these phenomena at molecular level is possible in light of analysis of IR spectra in the following section. In conclusion to this DSC section, percentage change from the pure wax for each sample at each step of the synthesis are reported in TABLE 57.

Table 57 – Melting temperature percentage change of R4.2 samples from pure waxes

Sample	$\Delta T_{m,1}$ (%)	$\Delta T_{m,2}$ (%)	$\Delta T_{m,3}$ (%)	$\Delta T_{m,4}$ (%)
PTOL + MAL	+3.09	-2.36	+0.86	-5.40
PTOL + ITA	+3.09	-2.47	+2.09	-3.28
GLY + MAL	+3.09	-2.36	+1.28	-2.47
GLY + ITA	+3.09	-2.47	+1.92	-4.86

4.3 Fourier Transfer Infrared Spectroscopy

The IR spectroscopy results will be centred only on the R4.n protocol group. In fact, this technique is useful to clearly represent the 4-step timeline reported in FIGURES 47-49 and to follow the route of synthesis. The spectra per each step are stacked one on top of each other to assess the variation at a glance. The spectra of each used reagent are reported as well to merely visually estimate how much the conversion to products was efficient. As described in SECTION 3.3.4.2, FTIR is very interesting in order to chemically characterise the produced sample. However, it allows only a qualitative analysis, since the technique does not provide information on the relative content of each functional group. Nonetheless, we can monitor the reactions of interest by observing the variations of the intensity of the incident radiation throughout the sample. In fact, if we consider the given functional group which is

involved in the given reaction, we can observe how the increase or reduction of intensity qualitatively corresponds to whether a successfully reaction was performed or not.

R4.0 and R4.1 spectra are reported for each of the eight samples (*i.e.*, #153 – #156 and #157 – #160, respectively) in FIGURES 63-66 and FIGURES 67-70 in ANNEX III. Only R4.2 spectra are reported in this section to highlight the most important feature of the synthesised samples for film production (FIGURES 50-53). Generally speaking, the main observations related to R4.2 are also valid for R4.0 and R4.1, since the *rationale* of each protocol was always the same. Each spectrum also reports the range of wavenumbers (see SECTION 3.3.4.2) corresponding to the given functional groups that are involved in the reactions of the 4-step synthesis (SECTION 3.3.2.4, FIGURES 33-36). The abbreviations for shortly describing the reagents correspond to those already proposed in TABLES 20-22 (SECTIONS 3.1.1, 3.1.2 and 3.1.3, respectively).
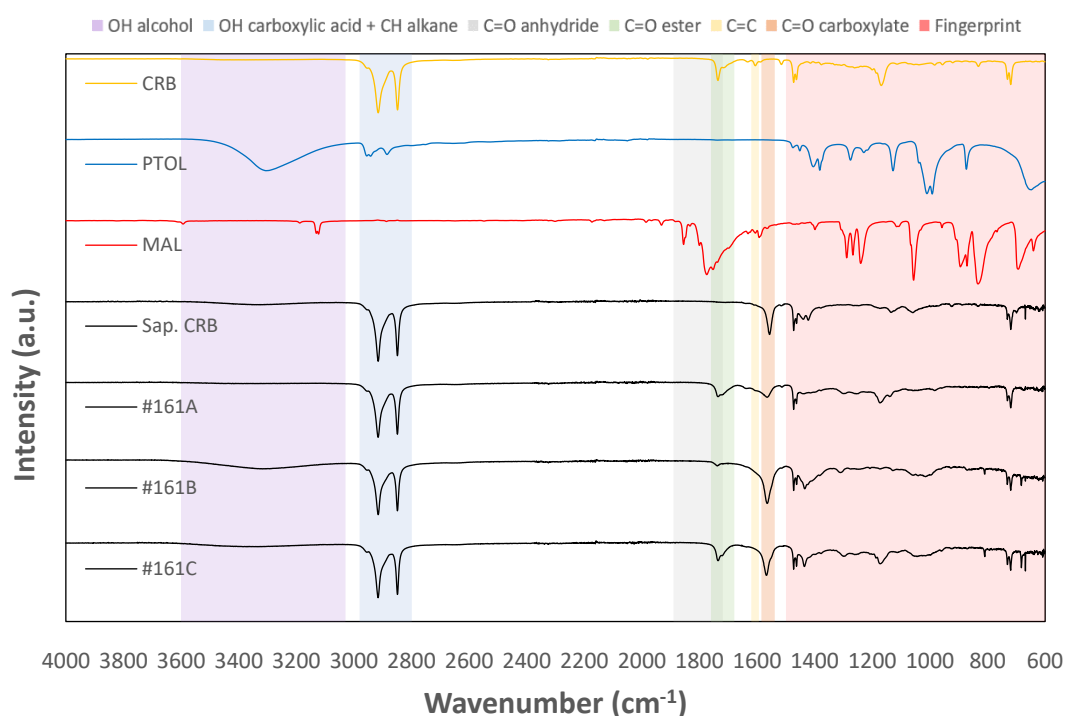
Figure 50 – #161 FTIR spectra
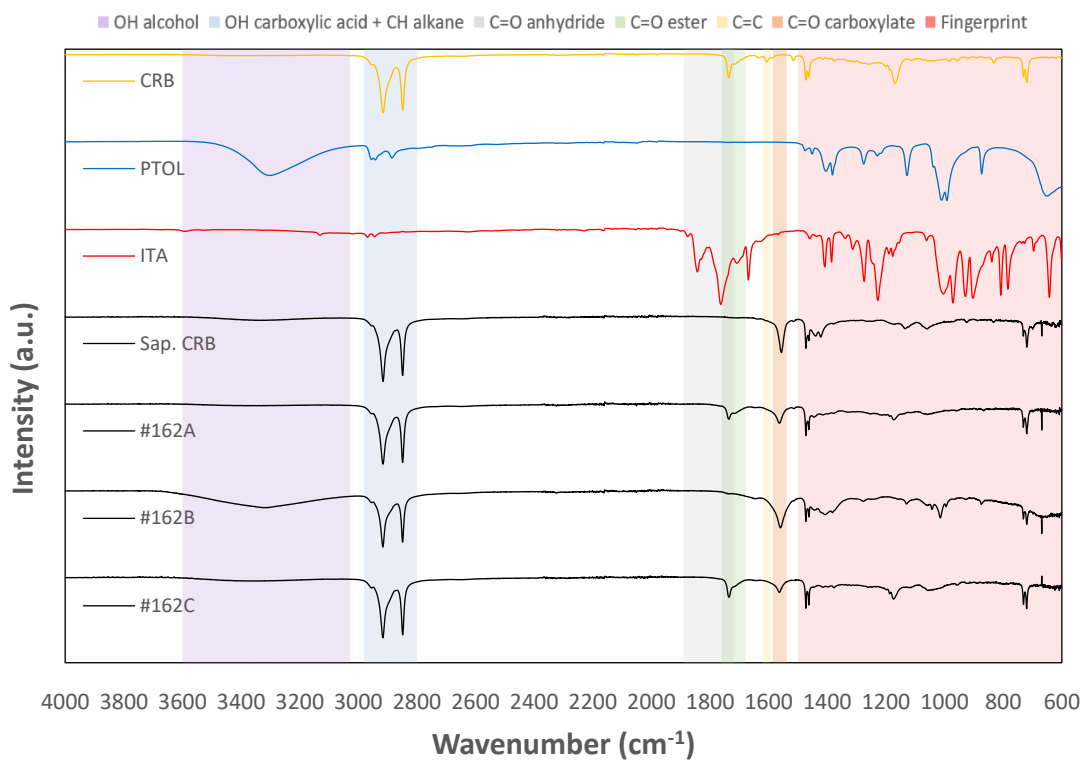
Figure 51 – #162 FTIR spectra
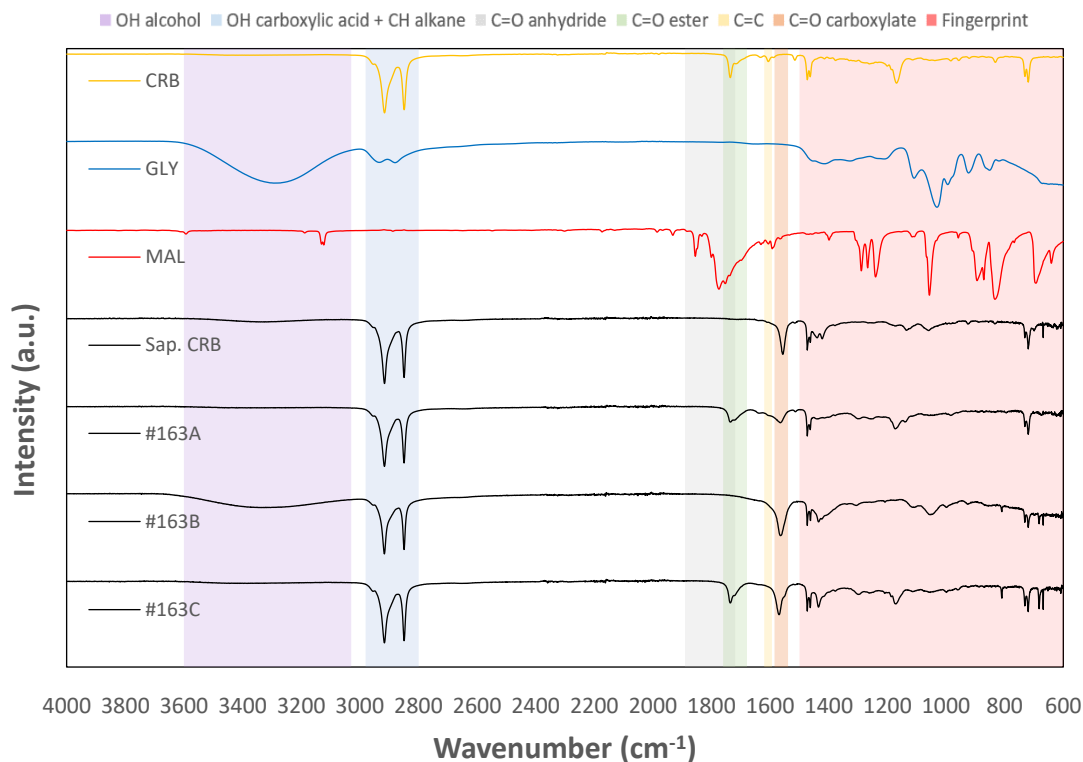
Figure 52 – #163 FTIR spectra
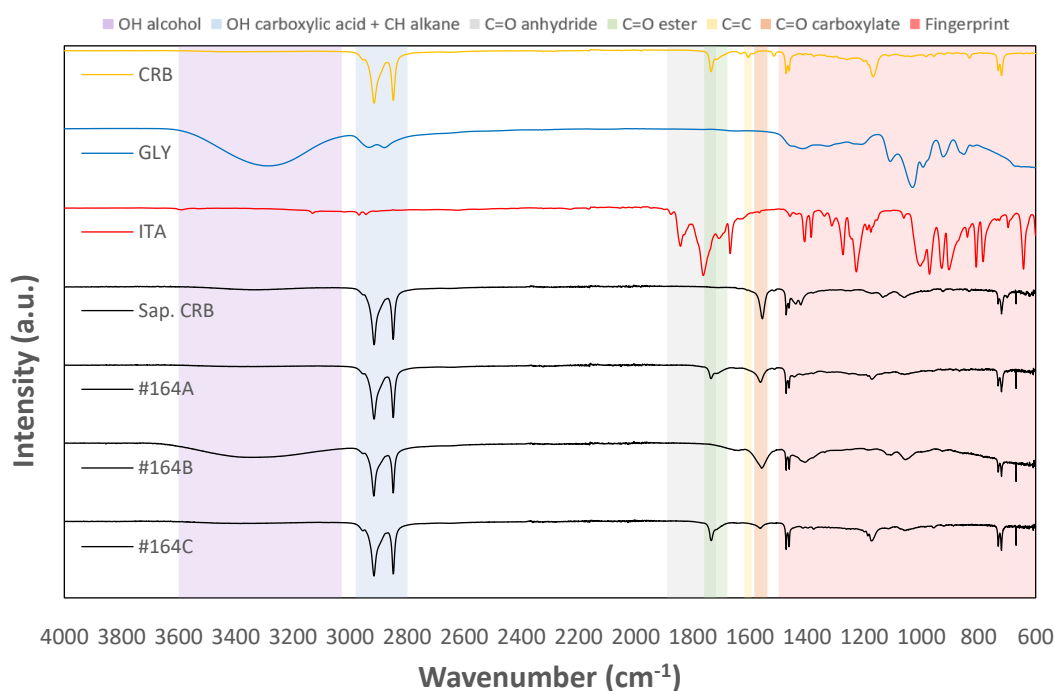
Figure 53 – #164 FTIR spectra

As for each of the four FTIR stacked spectra reported just above, the first three spectra refer to the main reagents (*i.e.*, wax in yellow, polyol in blue and acid anhydride in red). The subsequent four black spectra refer in a top-bottom cascade to each step of the four-step synthesis. The letter added to each sample number (i.e., A, B or C) corresponds to the given step of the synthesis according to SECTION 3.3.2, TABLE 33.

The most evident feature for the whole four reported samples is that the spectrum corresponding to the final esterification (STEP C) could be perfectly overlapped for the most part on the starting carnauba wax spectrum. This means that despite some undisputed chemical change had occurred, the main chemical structure is to be referred to the natural wax. This can be observed in the two high-intensity peaks mainly related to the stretching of the C-H alkane groups (blue area, 2800–3000 cm^{-1}), which are identically recurring in each of the four steps. The trend is somehow desired, since the natural wax imparts desirable water vapour barrier to the material. However, a finer analysis brings to light some interesting results. First and foremost, the saponification step was effective four all the samples. In fact, the peak in the spectrum which corresponds to the stretching of C=O in both ester and carboxylic acid groups (green area, 1680–1760 cm^{-1}) cannot be observed after the

saponification has been performed. This means that all the saponifiable functional groups were actually saponified. The countercheck is the intense peak which corresponds to the stretching of C=O in carboxylate groups (orange area, 1540–1585 cm^{-1}) and which was not to be observed in the natural wax as received. This means that after the saponification, all carboxylic acids were present as their corresponding sodium salts. Moreover, it implies that the acidification of the saponified wax was not completely effective. The reason could be the increased viscosity of the saponified wax which did not allow a vigorous stirring and thus a homogeneous reduction of pH and protonation of carboxylates to carboxylic acids. The following step involved the esterification of free fatty alcohols from saponification with an acid anhydride (STEP A). The reaction was effective, since a peak which corresponds to the C=O ester group (green area) can be spotted. However, the esterification was not probably efficient, because a decrease in intensity in the C=O carboxylate group is simultaneously recorded. By simple FTIR analysis, the efficiency of the reaction cannot be evaluated.

The further step is the esterification of the given polyol (*i.e.*, either pentaerythritol or glycerol) with the free fatty alcohols from saponification. The reaction was base-catalysed with NaOH. This is an important difference with respect to the R4.0 and R4.1 protocols, because the same STEP B was acid-catalysed with H$_2$SO$_4$ there. On the one hand, both an evident reduction to practically zero intensity in the C=O ester group peak and a corresponding increase in the C=O carboxylate group peak can be observed in FIGURES 49-52 from R4.2. On the other hand, the intensity of the C=O ester group peak somewhat increases from the previous STEP A, whereas the C=O carboxylate group peak is either not present or very feeble in FIGURES 63-70 (ANNEX III) from both R4.0 and R4.1. This trend suggests that NaOH is more effective than H$_2$SO$_4$ in hydrolysing ester bonds by dissociating them in the constitutive alcohols and acids. Whereas this trend is favourable in the first saponification step, it is undesirable in STEP B. In fact, the hydrolysis of ester bonds is detrimental for the two reasons reported in TABLE 58.

Proceeding towards the final polyesterification with the acid anhydride at STEP C, an increase in intensity of the C=O ester group peak and a reduction in the C=O carboxylate group peak can be once more noted. However, at this stage we do not

Table 58 – Reasons why the final polyesterification could not occur as desired

• The pre-polymer is not formed correctly and its subsequent polycondensation will be hindered
• The diesters formed at STEP A are hydrolysed and fatty alcohols are once more free and able to block the correct polycondensation

have any knowledge of whether the ester peak corresponds to polyester structure or simply to the successful reactions of either the acid anhydrides with both fatty alcohols and the selected polyol or the latter with the free fatty acids and acidified carboxylates. What is surely acknowledged is that the intensity of the C=O ester group peak in R4.2 is lower with respect to both the same group peak in R4.0 and R4.1 (see ANNEX III). This involves that in those protocols the promotion of esterification was facilitated and the polycondensation of the monoglyceride pre-polymers into a polyester alkyd resin could be more likely.

As for the differences among the four different polyol-acid anhydride combination in R4.2, the comparison could be partly compromised by the potential ineffectiveness encountered at STEP B and previously discussed. However, it can be noted that for samples presenting maleic anhydride (*i.e.*, #161 and #163), the final material displays a slightly broader and yet equally intense C=O ester group peak and a remarkably more intense C=O carboxylate group peak than samples presenting itaconic anhydride (*i.e.*, #162 and #164). The lack of any characteristic peak of the given acid anhydride after STEP A and C means that either the reactivity was successful or the cleansing with distilled water was effective enough to wash away any eventual residue. As for the polyols, their addition at STEP B is evident by the broad band which corresponds to the stretching of the OH alcohol group (purple area, 3050–3600 cm^{-1}). If we compare the Step B from R4.2 with those from R4.0 and R4.1, the reduced likelihood of such a clear broad band in the latter protocols is to be noted. It could mean that the polyols were more prone to be incorporated into monoglyceride pre-polymers with respect to R4.2. However, it is to be recalled that unbound polyol molecules could function as plasticisers and favour an easier formability in further processing stages. Apart from this trend, major differences

between pentaerythritol (*i.e.*, #161 and #162) and glycerol (*i.e.*, #163 and #164) are not to be observed.

4.4   Water Vapour Permeability

The most interesting results for the scope of this thesis are finally reported and discussed here. As already stated, only R4.2 samples have been processed in films to be further tested in terms of their water vapour permeability. A comparison with the water vapour barrier performance of natural wax is essential to understand how the selected route influences the properties of the synthesised materials.

The first results to be reported are the isothermal water uptake curves (23 °C, 85%→0% RH) in FIGURES 54-58, in which the mass increase is plotted versus the time and normalised on a thickness of 100 μm for data comparison. Each plot refers to a given synthesised material, while each curve refers to one of the multiple films produced per synthesised sample (see SECTION 4.1, TABLE 39). The flux of water vapour throughout the films approached on average a steady state roughly after three days under exposure at the selected test conditions. This can be assessed by observing that the water uptake turns linear with time. The only exception is CRB S1, which displays a peculiar trend that dampens in an oscillating fashion until it
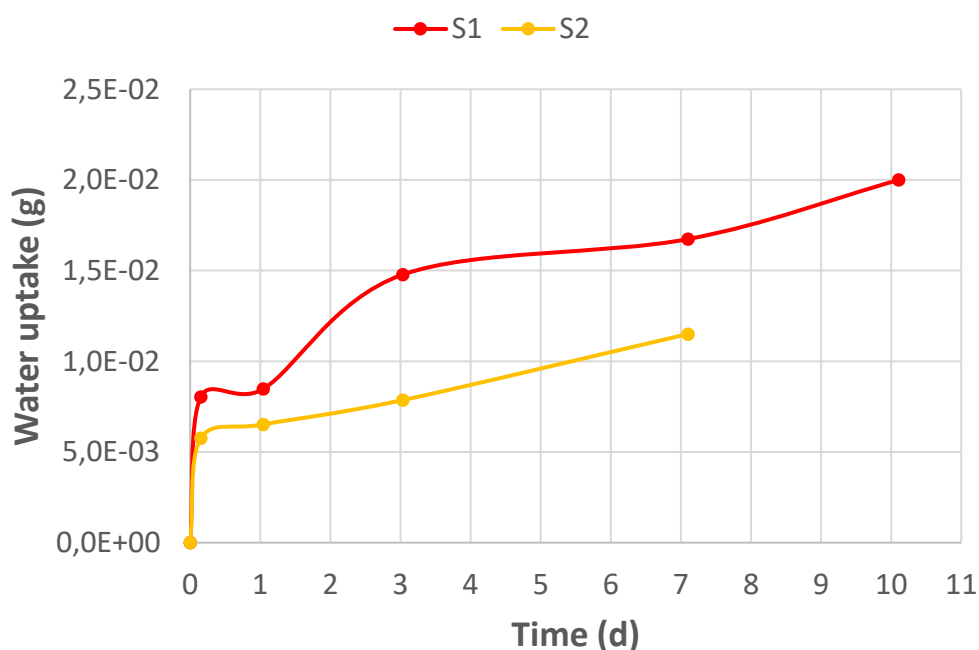
Figure 54 – CRB water uptake curve
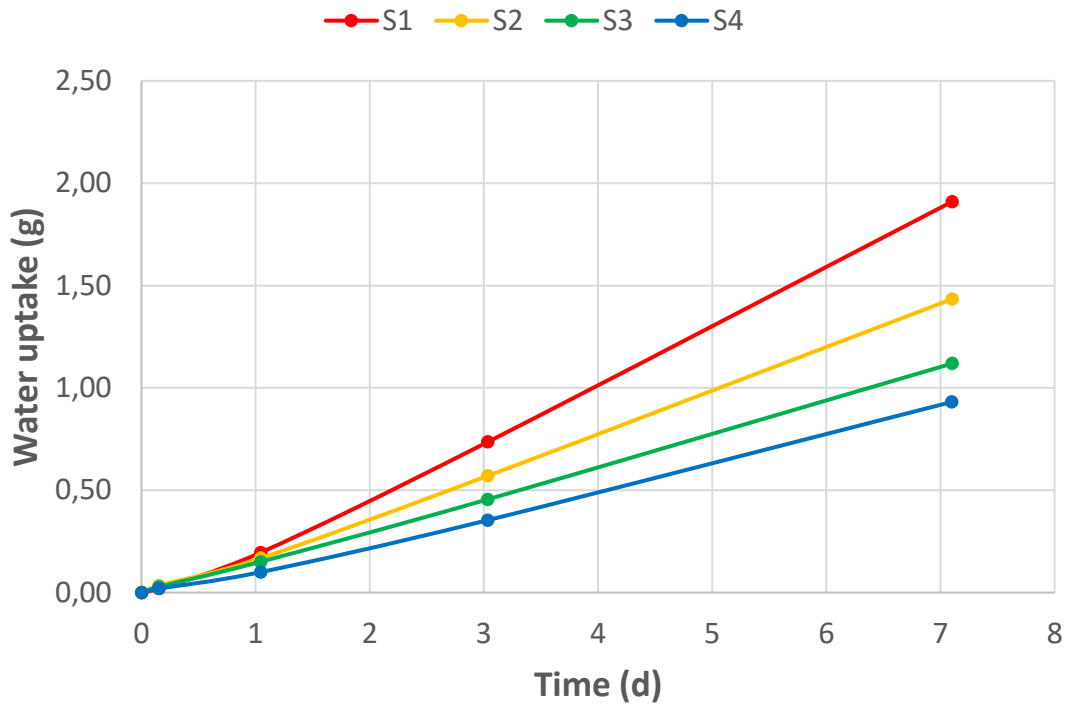
Figure 55 – #161 water uptake curve
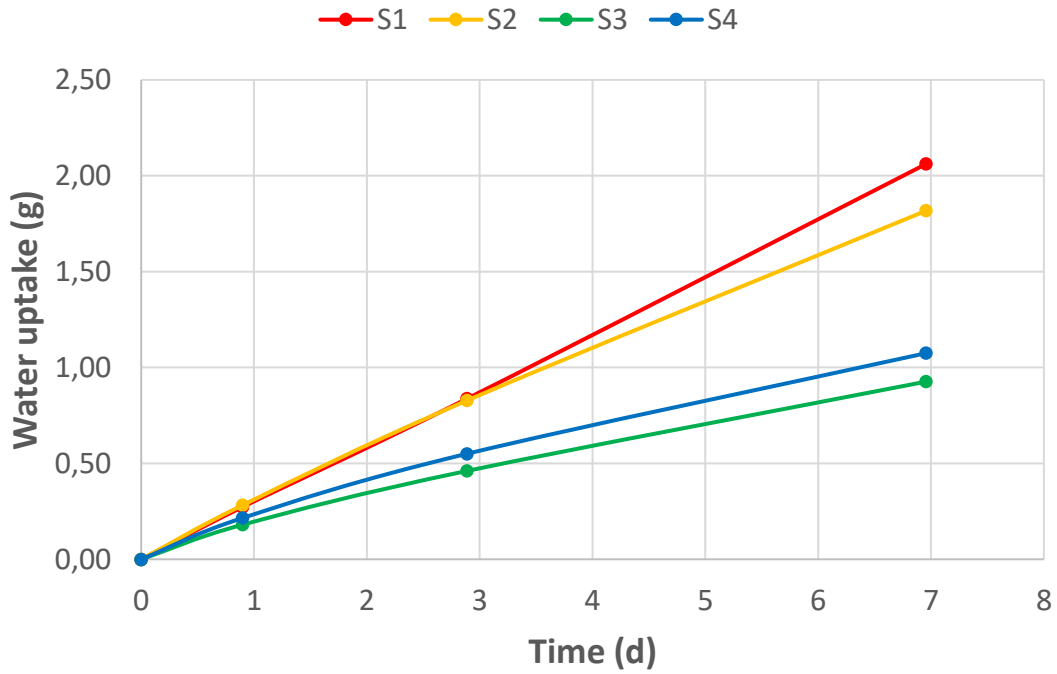
Figure 56 – #162 water uptake curve
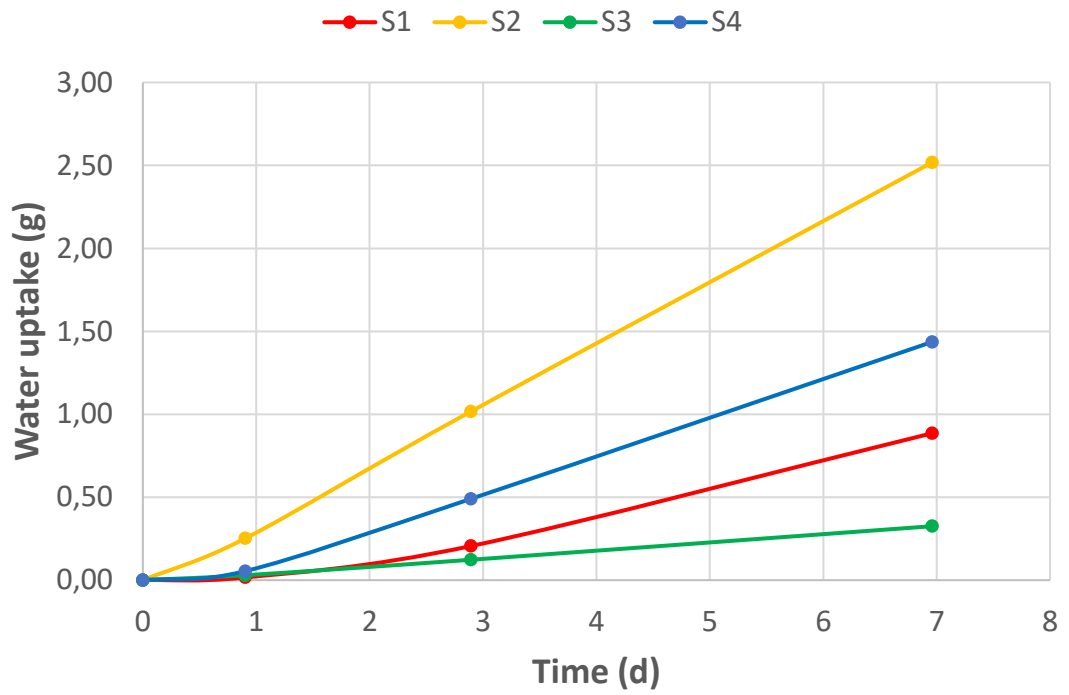
Figure 57 – #163 water uptake curve
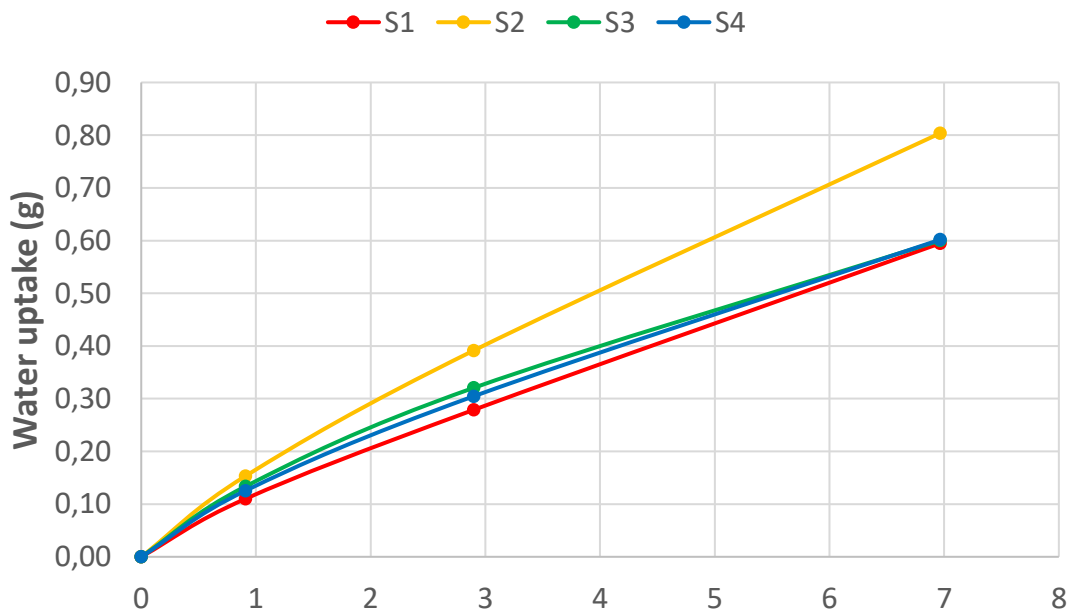
Figure 58 – #164 water uptake curve

somewhat linearise after ten days. For this reason, CRB S1 was the only sample to be held in the conditioning cabinet more than seven days to assess whether it would eventually stabilise towards a steady state.

The first observation is that for each distinct sample composition, the curves do not superimpose one another and this may be due to the heterogeneity of the synthesised materials. Samples #161 and #163 have the same absorption kinetics, which is slower than the kinetics of #162 and #164. This is interesting because the FTIR analysis in the previous SECTION 4.3 highlighted that #161 and #163 display a larger carboxylate salts content than #162 and #164. This could suggest that the sample would be more hydrophilic due to the presence of partially charged ions and thus the water absorption would be more favoured. However, it should also be considered that these carboxylate salts are mainly constituted by long aliphatic chains (C16-C24 or higher, see SECTION 1.4.1, TABLE 13), which are most likely predominating in the overall structure. Nonetheless, as already discussed, the ionic stabilisation probably allows a more organized and packed chain configuration in #161 and #163 that reduces the kinetics of water absorption. Since #162 and #164 display a lower carboxylate content, this trend is reduced and the absorption is faster.

As already presented in SECTION 3.3.4.3, the linear regression of water uptake data allows to evaluate the WVTR of the films. The combination of WVTR with the average thickness of the films gives the value of the WVP (see SECTION 3.3.4.3, EQUATION 3.3.4.3-2 and ANNEX I, SECTION 7.1, EQUATION 7.1-17). The thicknesses of each tested film are reported in TABLE 68 (ANNEX III) and it is also specified with a check mark whether they are complying with the IQR method of outlier detection. The reported mean value is calculated excluding the outliers. The calculated WVP values for each film are reported in TABLE 59. The mean WVP values for each synthesised sample (*i.e.*, CRB, #161, #162, #163, and #164) are evaluated only taking into consideration the films that were still intact after the test. Any crack or fracture in a given film would compromise the meaningfulness of the water vapour permeability result. The mean WVP values are also reported in FIGURE 59 to have a better visualisation and comparison of water vapour barrier performance of the synthesised material with respect to pure carnauba wax.

Table 59 – WVP values of produced films

Sample	WVP$_{S1}$ (kg·m/m²·s·Pa)	WVP$_{S2}$ (kg·m/m²·s·Pa)	WVP$_{S3}$ (kg·m/m²·s·Pa)	WVP$_{S4}$ (kg·m/m²·s·Pa)	WVP$_{mean}$ (kg·m/m²·s·Pa)
CRB	1.65 E-17	1.92 E-17	-	-	1.79 E-17
#161	*	4.79 E-15	3.66 E-15	3.16 E-15	3.87 E-15
#162	*	*	*	3.20 E-15	3.20 E-15
#163	3.36 E-15	*	1.12 E-15	*	2.24 E-15
#164	1.82 E-15	2.43 E-15	1.73 E-15	1.78 E-15	1.93 E-15

- : the film was not produced; * : the film broke during the test
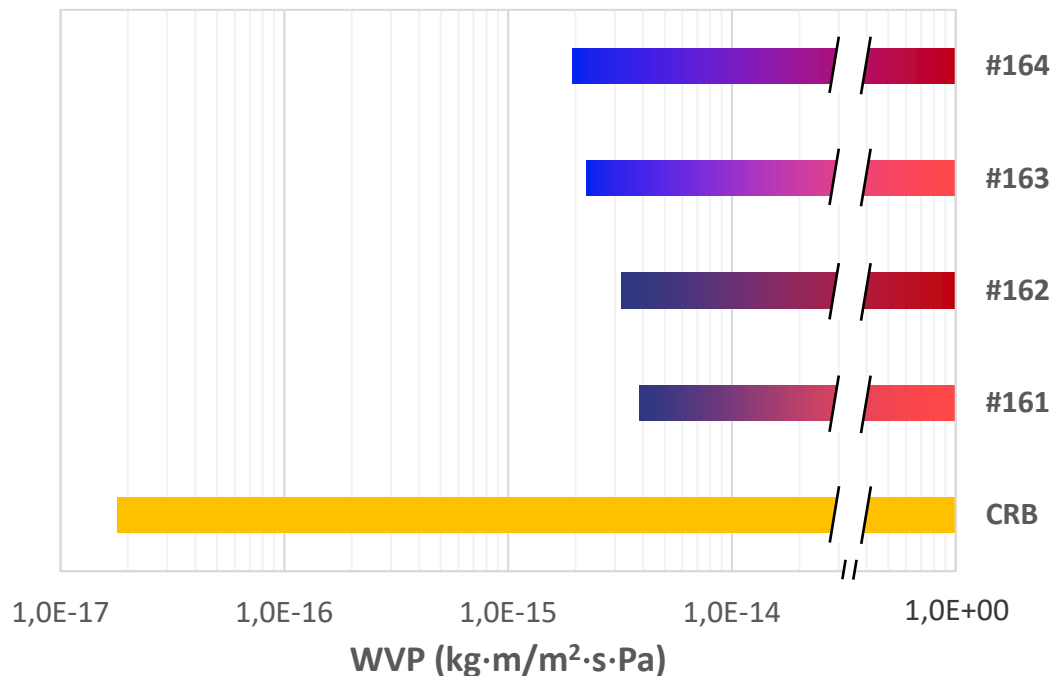
Figure 59 – Water vapour permeability of the hot-pressed films from R4.2 in comparison with carnauba wax as received

The first evidence from TABLE 59 is probably the relevant percentage of broken films during the test (*i.e.*, one out of three samples). This is obviously detrimental for an eventual application as thin coating, but it is also an intrinsic feature which is due to the crystallinity of carnauba wax itself. As for the pure carnauba films, only two films were tested.

FIGURE 59 is strikingly clear in displaying a consistent water vapour barrier reduction of the synthesised samples with respect to pure carnauba wax. In fact, the

order of magnitude of WVP for #161, #162, #163 and #164 is 10^{-15} (kg·m)/(m^2·s·Pa), whereas the value of the natural wax lies two order of magnitude lower at 10^{-17} (kg·m)/(m^2·s·Pa). This is undoubtedly an undesired outcome for the scope of this experimental work, because the most interesting properties of a given natural wax are mainly lost. However, it must be observed that the WVP are still more performing than PLA, which would be the actual substrate of the coating (SECTION 1.3.2, TABLE 10). In fact, WVP of PLA is one order of magnitude larger (*i.e.*, 10^{-14} (kg·m)/(m^2·s·Pa)) than the wax-based alkyds and the value refers to an even lower relative humidity – and thus lower driving force for permeation (*i.e.*, 50% RH). Nonetheless, the performance displayed by the synthesised wax-based alkyds are still not sufficient to guarantee a proper functional barrier in MAP packaging of fresh foods (see SECTION 2.1, TABLE 18, GOAL G2). A minor reduction of water vapour barrier properties was expected *a priori*, since the four-step synthesis compromised the original strongly alkyl structure of wax esters to theoretically obtain a cross-linked resinous structure which should increase the thermal resistance. Moreover, the addition of polar compounds such as the polyols and the acid anhydrides – which are necessary for the proper alkyd formation – are also inducing a reduction in water vapour barrier.

As for the synthesised films, #164 displays the highest barrier (or the lower WVP value, equivalently), whereas #161 displays the lowest barrier. The general trend is that samples containing glycerol are best performing than those containing sorbitol. This may be due to the more intense plasticising effect given by the glycerol. A more flexible film is then produced and it probably has a more homogenous and less porous microstructure. Itaconic anhydride seems to provide better resistance than maleic anhydride to the permeation of water molecules. This trend may be due to the methylene group that could be more prone to cross-link or to provide a non-polar obstacle in the diffusion path of polar water molecules.

5. Conclusions

The broad screening performed in this experimental work provided interesting insight in the potential application of natural waxes as water vapour barrier coatings for packaging.

The DSC analysis of the synthesised wax-based alkyds disclosed that the thermal properties are not much likely to be improved significantly for the purpose of thermoforming. Nonetheless, it was observed that the chemical functionalisation did not compromise the original thermal performance of the natural waxes. Especially carnauba wax-based alkyds have a melting point that could be already high enough for potential technical applications. For future research, it would be interesting to have a more exhaustive understanding of the cross-linking and to check whether a higher degree thereof could increase the thermal performance, particularly the melting point.

The FTIR analysis displayed detailed molecular-level information about the effectiveness of the four-step synthesis which has been adopted for the entire R4.n protocols. The possibility to monitor the reaction route at each step has given fundamental comprehension on what the bottlenecks of the synthesis could be. For future research, it would be suggested to maintain the more effective NaOH-catalysed saponification and to switch to the H_2SO_4-catalysed esterification of polyols and wax-derived fatty acids. This could induce a higher yield of the monoglyceride pre-polymers, which could polymerise at a consistent larger extent. Two interesting points of development are reported in TABLE 60.

The WVP test allowed to understand that the barrier properties of the synthesised alkyds were consistently compromised partly by the slightly more polar chemical nature of the novel materials and in major part probably by both an ineffective

Table 60 – Outlook of strategies of synthesis

• Start the synthesis from pure long-chain fatty acids (13≤C≤22) or even very-long chain fatty acids (C≥22) and directly esterify them with polyols to form the monoglyceride pre-polymers
• Select a proper non-polar solvent to favour the solvent extraction of the fatty alcohols from the mixture of saponification of the wax

polycondensation and by the difficulty to produce flexible and thoroughly pore-free films. Future improvements should be focused on increasing the efficiency of polycondensation and on having a finer control on the film production. The addition of additives to plasticisers (*e.g.*, glycerol itself) could favour more flexible films.

In conclusion, this thesis highlighted that wax-based alkyds could be an interesting bio-based solution for coating applications for food packaging. The results displayed in this work are yet to be ripe for any applications on a PLA substrate. However, the outcomes are interesting enough to allow for further consideration about how to develop these novel materials and to troubleshoot the arisen problems.

6. Bibliography

[1]   FAO, "Global Food Losses and Food Waste", 2011.

[2]   FAO, "The State of Food and Agriculture", 2019.

[3]   UN, "World Population Prospects 2019: Highlights", 2019.

[4]   J. Han, "Food Packaging : A Comprehensive Review and Future Trends", 2018.

[5]   PlasticsEurope, "Plastics: The Facts", 2019.

[6]   European Parliament, "EU 2019/904 - Directive on the reduction of the impact of certain plastics products on the environment", 2019.

[7]   Eurostat, "Packaging waste by waste management operations and waste flow", 2020.

[8]   Ellen MacArthur Foundation, "The New Plastics Economy: Catalysing Action", 2017.

[9]   M. Van Den Oever, K. Molenveld, M. Van Der Zee, and H. Bos, "Bio-based and biodegradable plastics – Facts and Figures Focus on food packaging in the Netherlands", no. July 2018. 2017.

[10]   European Bioplastics, "What are bioplastics?", 2018.

[11]   European Bioplastics, "2019 Market Data Report", 2019.

[12]   Sustainable Packagin Coalition, "Definition of Sustainable Packaging," 2011.

[13]   The European Parliament and Council of the European Union, "Regulation (EU) 1169/2011", 2011.

[14]   M. A. Tørngren, M. Darré, A. Gunvig, and A. Bardenshtein, "Case studies of packaging and processing solutions to improve meat quality and safety", *Meat Sci.*, vol. 144, no. February, pp. 149–158, 2018.

[15]   K. W. Mcmillin, "Where is MAP Going ? A review and future potential of modified atmosphere packaging for meat", vol. 80, pp. 43–65, 2008.

[16]   K. V. Kendra, "LWT - Food Science and Technology Modified atmosphere packaging of fresh produce : Current status and future needs", *LWT - Food Sci. Technol.*, vol. 43, no. 3, pp. 381–392, 2010.

[17]   J. Rhim, H. Park, and C. Ha, "Progress in Polymer Science Bio-

nanocomposites for food packaging applications", *Prog. Polym. Sci.*, vol. 38, no. 10–11, pp. 1629–1652, 2013.

[18] D. Garlotta, "A Literature Review of Poly (Lactic Acid)", vol. 9, no. 2, 2002.

[19] P. Skoczinski *et al.*, "Bio-based Building Blocks and Polymers – Global Capacities, Production and Trends 2019 – 2024", 2020.

[20] R. Auras, B. Harte, and S. Selke, "An Overview of Polylactides as Packaging Materials", pp. 835–864, 2004.

[21] L. Lim, R. Auras, and M. Rubino, "Progress in Polymer Science Processing technologies for poly (lactic acid)", vol. 33, pp. 820–852, 2008.

[22] S. Farah, D. G. Anderson, and R. Langer, "Physical and mechanical properties of PLA , and their functions in widespread applications — A comprehensive review", *Adv. Drug Deliv. Rev.*, vol. 107, pp. 367–392, 2016.

[23] E. Krendlinger *et al.*, "Waxes", in *Ullmann's Encyclopedia of Industrial Chemistry*, p. 63, 2005.

[24] R. A. Moreau *et al.*, "Analysis of wax esters in seven commercial waxes using C30 reverse phase HPLC Analysis of wax esters in seven commercial waxes using C30 reverse phase HPLC", *J. Liq. Chromatogr. Relat. Technol.*, vol. 41, no. 10, pp. 604–611, 2018.

[25] A. P. Tulloch, "The Composition of Beeswax and Other Waxes Secreted by Insects", 1954.

[26] J. F. Toro-vazquez, E. Dibildox-alvarado, and M. Charo, "Thermal and Textural Properties of Organogels Developed by Candelilla Wax in Safflower Oil Thermal and Textural Properties of Organogels Developed by Candelilla Wax in Safflower Oil", no. May 2014, 2007.

[27] N. Peelman *et al.*, "Application of bioplastics for food packaging", *Trends Food Sci. Technol.*, vol. 32, no. 2, pp. 128–141, 2013.

[28] E. A. Wilder and S. C. Johnson, "The Structural Constituents of Carnauba Wax", no. 3, pp. 514–518, 1970.

[29] F. Science, N. Sugimoto, and H. Akiyama, "Method for the determination of natural ester-type gum bases used as food additives via direct analysis of their constituent wax esters using high- temperature GC / MS Method for the

determination of natural ester-type gum bases used as food additives via direct analysis of their constituent wax esters using high-temperature GC / MS", no. July, 2014.

[30] S. Ramjan, Y. Ju, T. Narayana, B. Kaimal, and Y. Chern, "A Process for the Preparation of Food-Grade Rice Bran Wax and the Determination of Its Composition", vol. 82, no. 1, pp. 11–13, 2005.

[31] I. G. D. I and O. Fennema, "Water Vapor and Oxygen Permeability of Wax Films", vol. 70, no. 9, pp. 867–873, 1993.

[32] M. Schmid *et al.*, "Properties of Whey-Protein-Coated Films and Laminates as Novel Recyclable Food Packaging Materials with Excellent Barrier Properties", vol. 2012, pp. 5–7, 2012.

[33] R. G. Craig, J. D. Eick, F. A. Peyton, and K. Green, "Strength Properties of Waxes at Various Temperatures and Their Practical Application", pp. 300–305, 1967.

[34] KahlWax, "Technical Data Sheet – KahlWax 8109 Yellow Food Beeswax", 2020.

[35] KahlWax, "Technical Data Sheet – KahlWax 2442 Carnauba", 2020.

[36] Fraunhofer IVV, "PLA4MAP", 2020. [Online]. Available: https://www.ivv.fraunhofer.de/en/packaging/biopolymers/pla4map.html.

[37] F. N. Jones, "Alkyd Resins", in *Ullmann's Encyclopedia of Industrial Chemistry*, 2003.

[38] M. K. Lam, K. T. Lee, and A. R. Mohamed, "Homogeneous , heterogeneous and enzymatic catalysis for transesteri fi cation of high free fatty acid oil (waste cooking oil) to biodiesel : A review", *Biotechnol. Adv.*, vol. 28, no. 4, pp. 500–518, 2010.

[39] C. Koning *et al.*, "Novel renewable alkyd resins based on imide structure", *J. Coatings Technol. Res.*, vol. 14, no. 4, pp. 783–789, 2017.

[40] A. Jahandideh, N. Esmaeili, and K. Muthukumarappan, "Synthesis and Characterization of Novel Star-Shaped Itaconic Acid Based Thermosetting Resins", *J. Polym. Environ.*, vol. 26, no. 5, pp. 2072–2085, 2018.

[41] J. La Nasa, I. Degano, F. Modugno, and M. P. Colombini, "Industrial alkyd resins : characterization of pentaerythritol and phthalic acid esters using

integrated mass spectrometry", 2014.

[42] V. B. Nikolic and P. M. Spasojevic, "Simple One-Pot Synthesis of Fully Biobased Unsaturated Polyester Resins Based on Itaconic Acid", 2017.

[43] A. Jahandideh, N. Esmaeili, and K. Muthukumarappan, "Facile synthesis and characterization of activated star-shaped itaconic acid based thermosetting resins", *Polym. Degrad. Stab.*, vol. 153, pp. 201–209, 2018.

[44] Q. Methods and M. H. Swann, "Determination of Dibasic Acids in Alkyd Resins", pp. 1448–1453, 1949.

[45] W. T. Elliott, "ALKYD RESINS", 1993.

[46] EN ISO, "Plastics — Film and sheeting — Determination of water vapour transmission rate", vol. 3. 2005.

[47] A. Brink and F. Dressler, "Wax Crosslinking with Dicumyl Peroxide", *Br. Polym. J.*, vol. 1, 1969.

7. Annex I

7.1   Principles of Mass Transfer Phenomena for Packaging Applications

Packaging performance is highly dependent on the barrier efficiency to specific gases and vapours, whether it is desired a certain permeation in and out or a complete block. A packaging system can be modelled satisfactorily as a *membrane* which separates two distinct phases: the surrounding environment and the packaged product (FIGURE 60).
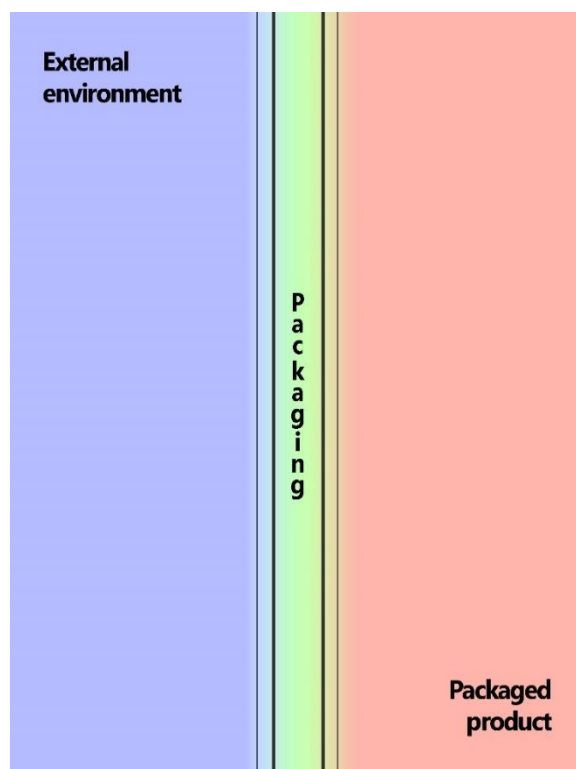
Figure 60 – Packaging as a membrane system

The basics of membrane functioning are fundamental to understand how packaging works and which design parameters are of utmost relevance. As just stated, membranes separate two distinct phases and selectively allow mass transfer throughout themselves. This involves that molecules may or may not be able to permeate the membrane and move from one phase to the other depending on their size, chemistry and interactions with the membrane. The *driving force* of this whole phenomenon is a *chemical potential gradient* $\nabla \mu$ between the two distinct phases

and across the membrane. Being the chemical potential μ a thermodynamical quantity[13], it involves difficulties to use it in practical applications. That is why a *concentration gradient* is typically reported as a simplified driving force for the mass transfer of the species of interest. The concentration gradient can be expressed in the terms reported in TABLE 61, depending on the necessity and convenience of the modelling.

Table 61 – Different expressions for the concentration gradient

Species concentration	Symbol	Units of measure
Mass concentration	ρ_i	kg/m³
Molar concentration	c_i	mol/m³
Mass fraction	ω_i	dimensionless
Molar fraction	x_i	dimensionless
Partial pressure	p_i	Pa

Mass transfer can be classified in two distinct types, which are reported in TABLE 62. It is important to note that they are not mutually exclusive, as even in presence of a convective motion, molecules can still diffuse throughout the medium due to microscopic motions which are triggered by concentration gradients present in the medium itself.

Table 62 – The two possible types of mass transfer

Mass transfer type	Description
Diffusive	The motion of molecules is exclusively due to microscopical vibrations and impacts of particles themselves
Convective	The motion of molecules is associated with a macroscopical external overall motion field of a given fluid which is generated by pressure gradients or gravity

---

[13] For a more detailed treatment of chemical potential and its thermodynamics meaning, see S.I. Sandler, *Chemical, Biochemical and Engineering Thermodynamics*, 4th Ed., John Wiley and Sons, 2006.

In the most generic scenario, the molar flux $\mathbf{N}_i$ of the species of interest i represents the number of moles per unit time crossing a surface of unit area[14]. The corresponding flux in mass terms is $\mathbf{n}_i = M_i \mathbf{N}_i$, where M_i is the molar mass of species i. The part of the species flux which is due to convective bulk flow and the part which is due to diffusion depend on the definition of the mixture velocity. Many different average velocities can be computed for a given mixture, depending on how the velocities of the individual species are weighted. If a fixed coordinate system is selected, the velocity $\mathbf{v}_i$ of species i is defined as reported in EQUATION. 7.1-1.

$$\mathbf{v}_i = \frac{\mathbf{N}_i}{c_i} = \frac{\mathbf{n}_i}{\rho_i} \tag{7.1-1}$$

where c_i and ρ_i are the concentrations of species i as already reported in TABLE 61. Two useful reference frames are the *mass-average* velocity, $\mathbf{v}$, and the *molar-average* velocity, $\mathbf{v}^{(M)}$, which are defined as reported in EQUATION 7.1-2.

$$\mathbf{v}_i \equiv \sum_{i=1}^{n} \omega_i \mathbf{v}_i, \quad \mathbf{v}^{(M)} \equiv \sum_{i=1}^{n} x_i \mathbf{v}_i \tag{7.1-2}$$

where ω_i and x_i are the mass fraction and mole fraction of species i, respectively (see TABLE 61), and n is the total number of chemical species in the mixture.

The various diffusional fluxes which are defined using $\mathbf{v}$ or $\mathbf{v}^{(M)}$ are reported in TABLE 63.

In the case of interest of packaging application, the only relevant contribution to the total flux $\mathbf{N}_i$ of the generic species i will be only the diffusive term as reported in EQUATION 7.1-3 for both molar and mass fluxes.

$$\mathbf{N}_i = \mathbf{J}_i, \quad \mathbf{n}_i = \mathbf{j}_i \tag{7.1-3}$$

---

[14] It is to be noted that the molar flux of a given species i is a *vectorial* quantity. All vectors in this work are reported in bold.

Table 63 – Definition of diffusional fluxes depending on the reference velocity of the system

Reference velocity	Molar units	Mass units
$\mathbf{0}$	$\mathbf{N}_i$	$\mathbf{n}_i$
$\mathbf{v}$	$\mathbf{J}_i$	$\mathbf{j}_i$
$\mathbf{v}^{(M)}$	$\mathbf{J}_i^{(M)}$	$\mathbf{j}_i^{(M)}$
$\mathbf{N}_i = c_i\mathbf{v} + \mathbf{J}_i = c_i\mathbf{v}^{(M)} + \mathbf{J}_i^{(M)}$	$\sum_{i=1}^{n} \mathbf{N}_i = c\mathbf{v}^{(M)}$	$\sum_{i=1}^{n} \mathbf{J}_i = 0$
$\mathbf{n}_i = \rho_i\mathbf{v} + \mathbf{j}_i = \rho_i\mathbf{v}^{(M)} + \mathbf{j}_i^{(M)}$	$\sum_{i=1}^{n} \mathbf{n}_i = \rho\mathbf{v}^{(M)}$	$\sum_{i=1}^{n} \mathbf{j}_i = 0$

Now it would be quite interesting to correlate the diffusive flux to both the material properties of species i and the system properties (temperature, pressure, composition). Adolph Fick proposed such a constitutive equation for describing diffusion in a binary mixture constituted by components A and B, the so-called *Fick's first law*. The law is reported in four different equivalent expressions in TABLE 64 and each one of them depends on the reference velocity and whether molar or mass units are considered.

Table 64 – Fick's first law of binary diffusion

Reference velocity	Molar units	Mass units
$\mathbf{v}$	$\mathbf{J}_A = -\dfrac{\rho D_{AB}}{M_A}\nabla\omega_A$	$\mathbf{j}_A = -\rho D_{AB}\nabla\omega_A$
$\mathbf{v}^{(M)}$	$\mathbf{J}_A^{(M)} = -cD_{AB}\nabla x_A$	$\mathbf{j}_i^{(M)} = -cM_A D_{AB}\nabla x_A$

The negative sign always recurring in Fick's first law means that the mass transfer occurs from regions at higher concentrations of species A towards regions at lower concentrations. Moreover, the flux is proportional to the driving force of the phenomenon ($\nabla\omega_A$ when considering mass-averaged reference velocity $\mathbf{v}$ or $\nabla\omega_A$ when considering molar-averaged reference velocity $\mathbf{v}^{(M)}$) and the proportionality constant is the so-called *diffusion coefficient* (or *diffusivity*). D_{AB} depends both on system properties such as temperature and the binary combination of components

A and *B*. It can be demonstrated mathematically that $D_{AB} = D_{BA}$. However, Fick's first law is valid only in *steady-state* conditions, which involve systems that are not evolving towards a new state in absence of external inputs. Whenever this requirement is not met, a time dependence must be introduced and the phenomenon is described by Fick's second law, which is merely a mass balance over a control volume consisting in the system of interest (TABLE 65).

Table 65 – Fick's second law of binary diffusion

Reference velocity	Molar units	Mass units
$\mathbf{v}$	$\dfrac{\rho}{M_A}\dfrac{\partial \omega_A}{\partial t} + \mathbf{\nabla} \cdot \mathbf{J} = 0$	$\rho \dfrac{\partial \omega_A}{\partial t} + \mathbf{\nabla} \cdot \mathbf{j} = 0$
$\mathbf{v}^{(M)}$	$c \dfrac{\partial x_A}{\partial t} + \mathbf{\nabla} \cdot \mathbf{J}^{(M)} = 0$	$cM_A \dfrac{\partial x_A}{\partial t} + \mathbf{\nabla} \cdot \mathbf{j}^{(M)} = 0$

If the Fick's first and second law are combined together for describing a time-dependent diffusing system, the so-called *Fick's diffusion law* is obtained (EQ. 7.1-4, 5). Let us consider only the case in which we select molar units and the molar-average velocity as reference for simplicity's sake and we substitute $\mathbf{J}^{(M)}$ with the corresponding result from Fick's first law (see TABLE 64).

$$c \frac{\partial x_A}{\partial t} + \mathbf{\nabla} \cdot (-cD_{AB}\mathbf{\nabla}x_A) = 0 \tag{7.1-4}$$

$$\frac{\partial x_A}{\partial t} = \mathbf{\nabla} \cdot (D_{AB}\mathbf{\nabla}x_A) \tag{7.1-5}$$

So far, the description of the problem has been set up in three-dimensional space considering 3D vectorial quantities. However, the representation can be considerably simplified considering that a packaging system can be modelled as a flat-surface membrane and the flux of matter is crossing the membrane only in the orthogonal direction to the surface. Hence, we reduced the problem to a much straightforward mono-dimensional one. We will define the direction of the mass transfer as direction *z*. EQ. 7.1-5 now becomes as follows (EQ. 7.1-6).

$$\frac{\partial x_A}{\partial t} = \frac{d}{dz} \cdot \left(D_{AB} \frac{dx_A}{dz} \right) \tag{7.1-6}$$

In this case, species *A* refers to the species of interest being transferred throughout the packaging membrane, whose polymer molecules constitute the species *B*. Assuming that the diffusivity D_{AB} is not varying with the spatial coordinate z, the previous equation can be rewritten as follows (EQ. 7.1-7).

$$\frac{\partial x_A}{\partial t} = D_{AB} \frac{d^2 x_A}{dz^2}$$

(7.1-7)

Having obtained the formula dynamically modelling the system over time and space, we need both initial (*time-related*) and boundary (*space-related*) conditions in order to solve the problem. However, our real interest is to evaluate the system at steady state after the system has stabilised and the flux has become constant. Then, we can drop the time-dependence and consider only what is occurring over
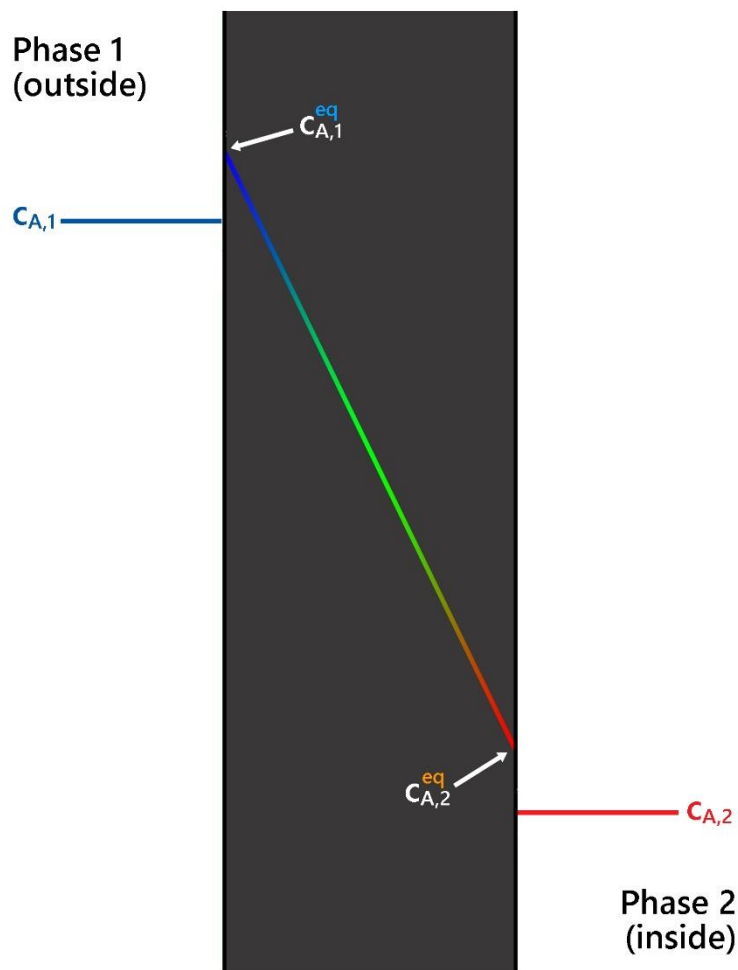
Figure 61 – Concentration profile of a generic species A diffusing through a membrane (linear at steady-state)

the spatial coordinate z. For an easier treatment, we will now consider molar concentrations of species A, rather than molar fractions (recall that $c_A = x_a c$, where c is the molar concentration of the overall mixture, EQUATION 7.1-8). At steady state, a linear concentration profile is being established as reported in FIGURE 61.

$$\frac{\partial c_A}{\partial t} = D_{AB} \frac{d^2 c_A}{dz^2} \qquad (7.1\text{-}8)$$

It can be assumed that the molar concentration of species A in both phase 1 and phase 2 are spatially homogeneous. However, the molar concentration at the very interfaces between each phase and the packaging display different values than the bulk-phase values. In fact, it is assumed that at both interfaces the molar concentration of species A is the corresponding thermodynamic equilibrium value for the given phase and the packaging membrane. The thermodynamic equilibrium molar concentration can be described as a function of the bulk molar concentration in the corresponding phase (EQUATION 7.1-9, 10).

$$c_{A,1}^{eq} = f(c_{A,1}) \qquad (7.1\text{-}9)$$

$$c_{A,2}^{eq} = g(c_{A,2}) \qquad (7.1\text{-}10)$$

$f(c_{A,1})$ and $g(c_{A,2})$ are two generic functions. However, in an ideal scenario, the equilibrium value is directly proportional to the bulk-phase value. The dimensionless proportionality constant is called *partition coefficient* of species A among the membrane and the given phase, $K_{A,1}$ and $K_{A,2}$. In the most straightforward case, the two partition coefficients for the two distinct phases are coincident (EQUATION 7.1-11, 12).

$$c_{A,1}^{eq} = K_A c_{A,1} \qquad (7.1\text{-}11)$$

$$c_{A,2}^{eq} = K_A c_{A,2} \qquad (7.1\text{-}12)$$

The mass transfer throughout the membrane is dictated by the equilibrium concentration difference existing at its interfaces. This driving force is reported in EQUATION 7.1-13.

$$\Delta c_A^{membrane} = c_{A,1}^{eq} - c_{A,2}^{eq} \tag{7.1-13}$$

For the reasonings just cited above, this gradient can be expressed in terms of bulk-phase molar concentration, which are strikingly easier to evaluate by measurement than the thermodynamical equilibrium values (EQUATION 7.1-14).

$$\Delta c_A^{membrane} = K_A\left(c_{A,1} - c_{A,2}\right) \tag{7.1-14}$$

The species of interest A will display a given diffusivity D_{AB} throughout the membrane, whose thickness is defined as δ. Hence, the steady-state molar flux of species A can be described as follows (EQUATION 7.1-15).

$$J_A^{(M)} = -D_{AB}\frac{dc_A}{dz} = D_{AB}\frac{\Delta c_A^{membrane}}{\delta} = \frac{D_{AB}K_A}{\delta}\left(c_{A,1} - c_{A,2}\right) \tag{7.1-15}$$

Two fundamental packaging parameters can be obtained from this very last equation. The first one is the so-called *transmission rate TR* of species A (EQUATION 7.1-16), whereas the second one is called *permeability P* of the membrane to species A (EQUATION 7.1-17).

$$TR_A = \frac{D_{AB}K_A}{\delta} = \frac{J_A^{(M)}}{c_{A,1} - c_{A,2}} \tag{7.1-16}$$

$$P_A = \frac{J_A^{(M)}\delta}{c_{A,1} - c_{A,2}} = TR_A \cdot \delta = D_{AB}K_A \tag{7.1-17}$$

TR is expressed in $\frac{mol \cdot m}{m^3 \cdot s \cdot Pa}$ in the SI, while P is expressed in $\frac{mol \cdot m^2}{m^3 \cdot s \cdot Pa}$ in the SI. The results are exactly equivalent when mass units are considered instead of molar units, by simply multiplying the molar results by the molar mass of the species of interest. Since in packaging applications the most interesting diffusing species consist of vapours or gases such as H_2O or O_2, typically the driving force through the membrane is reported in terms of bulk partial pressure of the species of interest in the given phase. The equilibrium relation between the molar concentration c_A of species A within the membrane material and the corresponding external bulk-phase vapour pressure p_A is described by the following *Henry's law* (EQUATION 7.1-18).

$$p_A = S_A c_A \qquad\qquad (7.1\text{-}18)$$

S_A is the solubility of species A in the membrane material and it is expressed in $\frac{mol}{m^3 Pa}$. Thus, the flux and permeability of species A can now be reported as follows (EQUATION 7.1-19, 20).

$$J_A^{(M)} = \frac{D_{AB} S_A}{\delta}(p_{A,1} - p_{A,2}) \qquad\qquad (7.1\text{-}19)$$

$$P_A = D_{AB} S_A \qquad\qquad (7.1\text{-}20)$$

EQUATION 7.1-20 is quite interesting because it reveals that the permeability of a given species throughout a membrane consists of two contributions. On the one hand, it depends on the *diffusivity*, which is a kinetic parameter related to the molecular motion inside the system due to a concentration gradient. On the other hand, it depends on *solubility*, which is a thermodynamic parameter representing the equilibrium concentration of the penetrant species at a given pressure throughout the membrane when it is in contact with a given environment. Hence, the permeability is an *intensive* property which depends exclusively on the physical-chemical characteristics of both penetrant species and the membrane matrix. It provides important information on which material and which thermodynamic conditions should be selected in order to obtain the desired barrier effect for the given application. Unlike TR, P displays no geometrical dependence on the thickness of the membrane.

8. Annex II

Table 66 – Images of each synthesised and characterised sample. The colour coding is for chemical identification[15]

R1.0 #7	**R1.0** #9	**R1.0** #18	**R1.0** #27
Yellow-orange, springy, rubbery, foamy	Orange-amber, springy, rubbery, foamy	Dark brown-amber, tacky, hard, brittle	Orange-amber, rubbery, hard
R1.0 #36	**R1.1** #37	**R1.1** #38	**R1.1** #39
Brown-amber, glassy, hard, brittle, tacky	Partly transparent, plastic, tacky, thermoformable	Transparent, glassy, tacky, hard, brittle, thermoformable	Partly transparent, glassy, tacky, hard, brittle, thermoformable
R1.1 #43	**R1.1** #44	**R1.1** #45	**R1.1** #51
Transparent, gluey, viscous, tacky	Partly transparent, tacky, hard, plastic, thermoformable	Off-white, gluey, highly tacky, rubbery, thermoformable	White, gluey, viscous, tacky, spreadable

---

[15] The numbers in the coloured circles refer typically to molar ratios and only to mass fractions when *wt%* is reported.

R1.1	R1.1	R1.1	R1.2
#52	#55	#56	#59
White, opaque, viscous, gluey, tacky	*White, opaque, viscous, gluey, tacky*	*White, soft, gluey, tacky, plastic*	*Ochre, hard, brittle*
R1.2	R1.2	R1.2	R1.2
#62	#65	#68	#71
Ochre, hard, brittle	*Ochre, hard, brittle*	*Dark brown, hard, brittle, minor gluey residue*	*Dark brown, hard, brittle*
R1.2	R1.2	R1.2	R1.2
#74	#77	#80	#83
Dark brown, hard, brittle	*Ochre, hard, brittle, minor tacky residue*	*Ochre, hard, brittle*	*Ochre, hard, brittle, minor tacky residue*
R1.2	R1.2	R1.2	R1.2
#86	#91	#94	#97
Ochre, hard, brittle, minor tacky residue	*Dark brown, hard, brittle*	*Dark brown, hard, brittle, white hard residue*	*Dark brown, hard, brittle, ochre softer residue*

R1.2 #100	**R1.1** #101	**R1.1** #102	**R1.1** #103
Dark brown, hard, brittle	Bright yellow, highly tacky, springy, gelatinous	Yellow, glassy, hard, tacky, partly plastic	Yellow, glassy, hard, tacky, partly plastic
R1.1 #104	**R1.1** #105	**R1.1** #106	**R1.1** #107
Bright yellow, tacky, springy, gelatinous	Bright yellow, tacky, springy, gelatinous	Mostly transparent, glassy, tacky	Partly transparent, tacky, plastic
R1.1 #108	**R1.1** #109	**R1.1** #110	**R2.0** #111
Partly transparent, glassy, hard, brittle	Mostly transparent, tacky, viscous, plastic	White, opaque, gluey, tacky, viscous	**Wax**: dark brown, hard, brittle, top **Resin**: black-brown, hard, brittle, carbonised, bottom
R2.0 #113	**R2.0** #114	**R2.0** #115	**R2.0** #117
Wax: light brown, hard, brittle, top **Resin**: light brown, hard, brittle, bottom	Red-amber, glassy, hard, brittle	Dark brown, hard, brittle	Dark brown, hard, brittle, minor tackiness
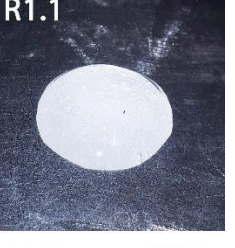
R2.0 #119 0.5 1 1.2	R2.0 #120 0.5 1 1.2	R2.0 #121 0.5 1 1.2	R2.0 #122 0.5 1 1.2
Wax: dark brown, hard, brittle, top *Resin: brown, soft, malleable, tacky, bottom*	*Wax: dark brown, hard, brittle, top* *Resin: dark brown, soft, malleable, tacky, bottom*	*Light brown, hard, brittle*	*Dark brown, hard, brittle*
R2.0 #123 0.5 1 1.2	R2.0 #124 0.5 1 1.2	R2.0 #125 0.5 1 1.2	R2.0 #126 0.5 1 1.2
Wax: brown, hard, brittle, top *Resin: red-amber, glassy, hard, brittle, bottom*	*Top: wax, dark brown, hard, brittle* *Bottom: resin, dark red-amber, glassy, hard, brittle*	*Brown, hard, brittle*	*Dark brown, hard, brittle*
R2.1 #127 0.5 1 1.2	R2.1 #129 0.5 1 1.2	R2.1 #131 0.5 1 1.2	R2.1 #133 0.5 1 1.2
Black, hard, brittle, carbonised	*Black, glassy, brittle, carbonised*	*Black, brittle, fragile, minor ochre residue*	*Black brittle, fragile, carbonised*
R3.0 #135 95 wt% 5 wt%	R3.0 #136 95 wt% 5 wt%	R3.0 #137 95 wt% 5 wt%	R3.0 #138 95 wt% 5 wt%
Bright yellow-orange, hard, brittle	*Bright yellow-orange, hard, brittle*	*Bright white-yellow, hard, brittle*	*Bright white-yellow, hard, brittle*

R3.0 #139 (95 wt%, 5 wt%)	R3.0 #140 (95 wt%, 5 wt%)	R3.0 #141 (95 wt%, 5 wt%)	R3.0 #142 (95 wt%, 5 wt%)
Bright off-white, malleable, ductile, soft	*Bright off-white, malleable, ductile, soft*	*Bright yellow-orange, hard, brittle*	*Bright yellow-orange, hard, brittle*
R3.0 #143 (95 wt%, 5 wt%)	R3.0 #144 (95 wt%, 5 wt%)	R2.2 #145 (0.5, 1, 1.2)	R2.2 #146 (0.5, 1, 1.2)
Bright white-yellow, hard, brittle	*Bright white-yellow, hard, brittle*	**Wax**: *dark brown, hard, brittle* **Resin**: *partly transparent, plastic, hard*	*Dark brown, hard, brittle*
R2.2 #147 (0.5, 1, 1.2)	R2.2 #148 (0.5, 1, 1.2)	R2.2 #149 (0.5, 1, 1.2)	R2.2 #150 (0.5, 1, 1.2)
Wax: *dark brown, hard, brittle* **Resin**: *partly transparent, ochre, glassy, brittle*	*Dark brown, hard, brittle*	*Dark brown, hard, brittle*	*Black-brown, hard, brittle, fragile*
R2.2 #151 (0.5, 1, 1.2)	R2.2 #152 (0.5, 1, 1.2)	R4.0 #153 (1, 1, 2.4)	R4.0 #154 (1, 1, 2.4)
Dark brown, hard, brittle, minor tacky ochre residue	*Dark brown, hard, brittle, minor glassy and fragile black residue*	*Dark brown, hard, brittle*	*Dark brown, hard, brittle*

R4.0 #155 🟡1 🔵1 🔴2.4	**R4.0** #156 🟡1 🔵1 🔴2.4	**R4.1** #157 🟡1 🔵1 🔴2.4	**R4.1** #158 🟡1 🔵1 🔴2.4
Dark brown, hard, brittle	*Brown, hard, brittle, minor crystalline fibrils*	*Brown, hard, brittle*	*Brown, hard, brittle*
R4.1 #159 🟡1 🔵1 🔴2.4	**R4.1** #160 🟡1 🔵1 🔴2.4	**R4.2** #161 🟡1 🔵1 🔴2.4	**R4.2** #162 🟡1 🔵1 🔴2.4
Black-brown, hard, brittle	*Black-brown, hard, brittle, minor ochre residue*	*Light brown, hard, brittle*	*Light brown, hard, brittle*
R4.2 #163 🟡1 🔵1 🔴2.4	**R4.2** #164 🟡1 🔵1 🔴2.4	**KahlWax** Beeswax 100 wt%	**KahlWax** Candelilla wax 100 wt%
Light brown, hard, brittle	*Light brown, hard, brittle*	*Yellow, shiny, malleable, soft, ductile*	*Orange, shiny, hard, brittle*
KahlWax Carnauba wax 100 wt%	**KahlWax** Rice bran wax 100 wt%	**KahlWax** Sunflower wax 100 wt%	
Yellow, shiny, hard, brittle	*White-yellow, shiny, hard, brittle*	*Off-white, shiny, hard, brittle*	
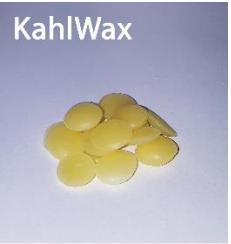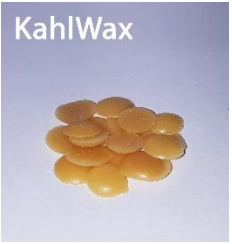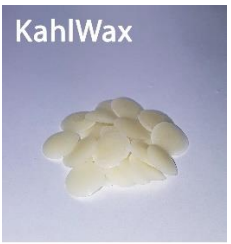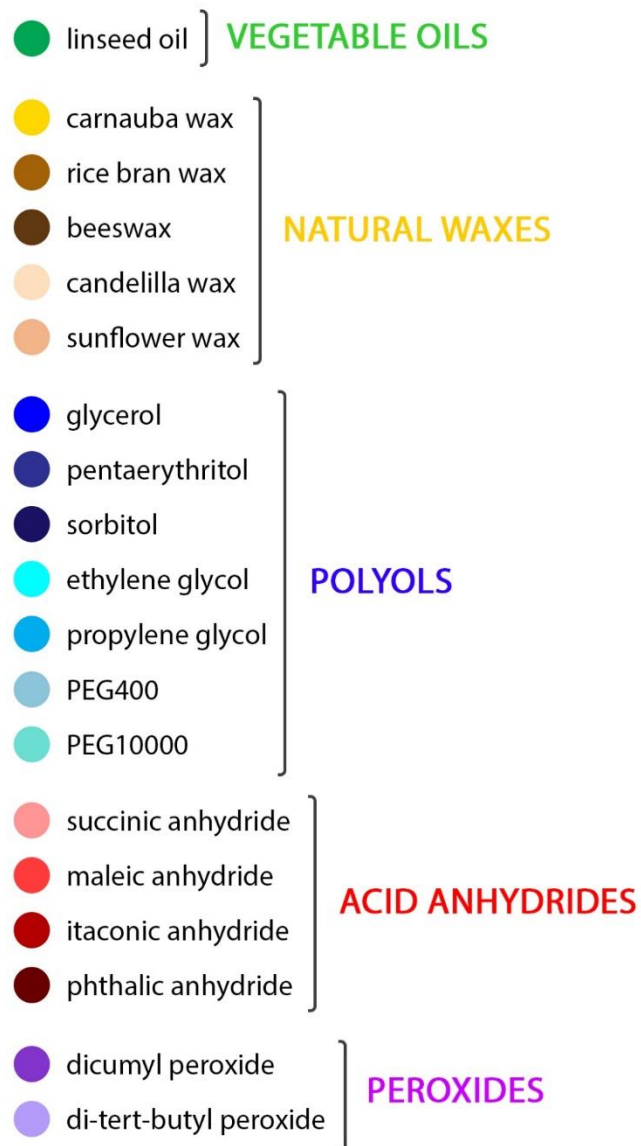
Figure 62 – Colour coding key

9. Annex III

Table 67 – R4.2 weighing

Saponification *(to be split in 2 batches for reaction with different anhydrides)*		
Sap. CRB	**Theoretical (g)**	**Measured (g)**
NaOH 40 wt.% aqueous solution	*27.93*	***27.96***
Carnauba wax	*82.49*	***82.50***
Fatty alcohol + Acid anhydride → Diester (to be split in 4 batches → 2 polyols × 2 anhydrides)		
#161/#163	**Theoretical (g)**	**Measured (g)**
Saponified carnauba wax	*28.25*	***26.84***
Maleic anhydride	*2.67*	***2.69***
#162/#164	**Theoretical (g)**	**Measured (g)**
Saponified carnauba wax	*26.08*	***26.10***
Itaconic anhydride	*2.97*	***2.99***
Polyol esterification		
#161	**Theoretical (g)**	**Measured (g)**
Saponified carnauba wax (esterified fatty alcohols)	*11.12*	***11.12***
Pentaerythritol	*2.56*	***2.56***
NaOH 40 wt.% aqueous solution	*1.88*	***1.88***
#162	**Theoretical (g)**	**Measured (g)**
Saponified carnauba wax (esterified fatty alcohols)	*10.81*	***10.82***
Pentaerythritol	*2.49*	***2.50***
NaOH 40 wt.% aqueous solution	*1.83*	***1.88***
#163	**Theoretical (g)**	**Measured (g)**
Saponified carnauba wax (esterified fatty alcohols)	*11.68*	***11.69***
Glycerol	*1.82*	***1.83***
NaOH 40 wt.% aqueous solution	*1.98*	***2.01***
#164	**Theoretical (g)**	**Measured (g)**
Saponified carnauba wax (esterified fatty alcohols)	*11.35*	***11.35***
Glycerol	*1.77*	***1.78***
NaOH 40 wt.% aqueous solution	*1.92*	***1.95***
Polyesterification		
#161	**Theoretical (g)**	**Measured (g)**
Pentaerythritol-wax prepolymer	*8.70*	***8.70***
Maleic anhydride	*1.30*	***1.31***
#162	**Theoretical (g)**	**Measured (g)**
Pentaerythritol-wax prepolymer	*8.55*	***8.56***
Itaconic anhydride	*1.45*	***1.45***
#163	**Theoretical (g)**	**Measured (g)**
Glycerol-wax prepolymer	*8.63*	***8.63***
Maleic anhydride	*1.37*	***1.38***
#164	**Theoretical (g)**	**Measured (g)**
Glycerol-wax prepolymer	*8.48*	***8.49***
Itaconic anhydride	*1.52*	***1.53***
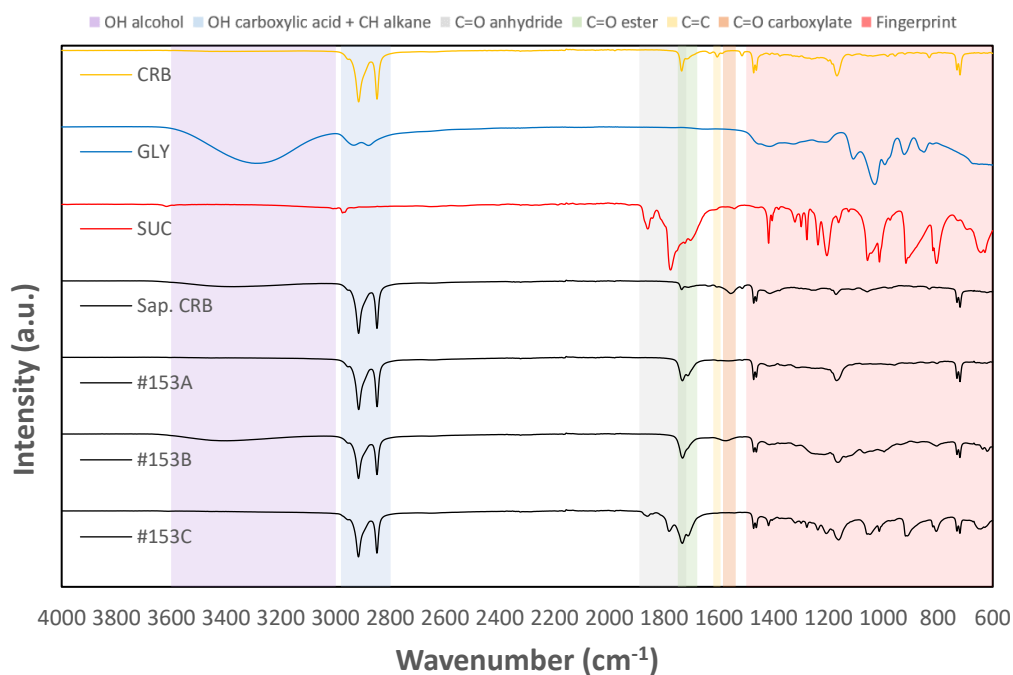
Figure 63 - #153 FTIR spectra (R4.0)
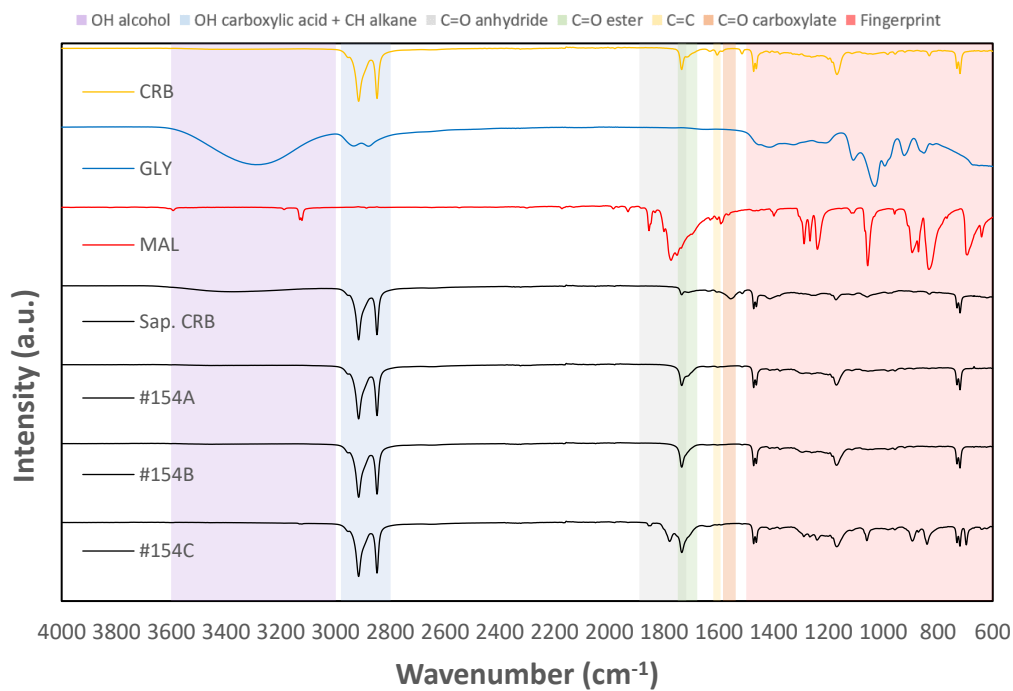
Figure 64 - #154 FTIR spectra (R4.0)
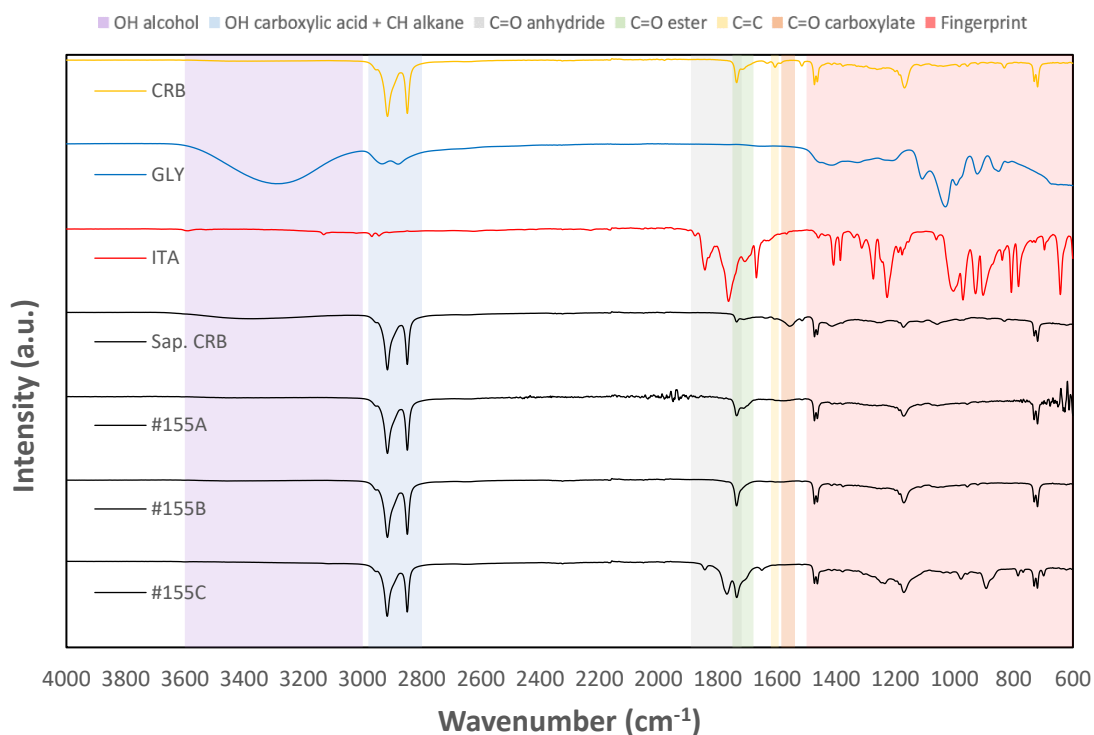
Figure 65 - #155 FTIR spectra (R4.0)
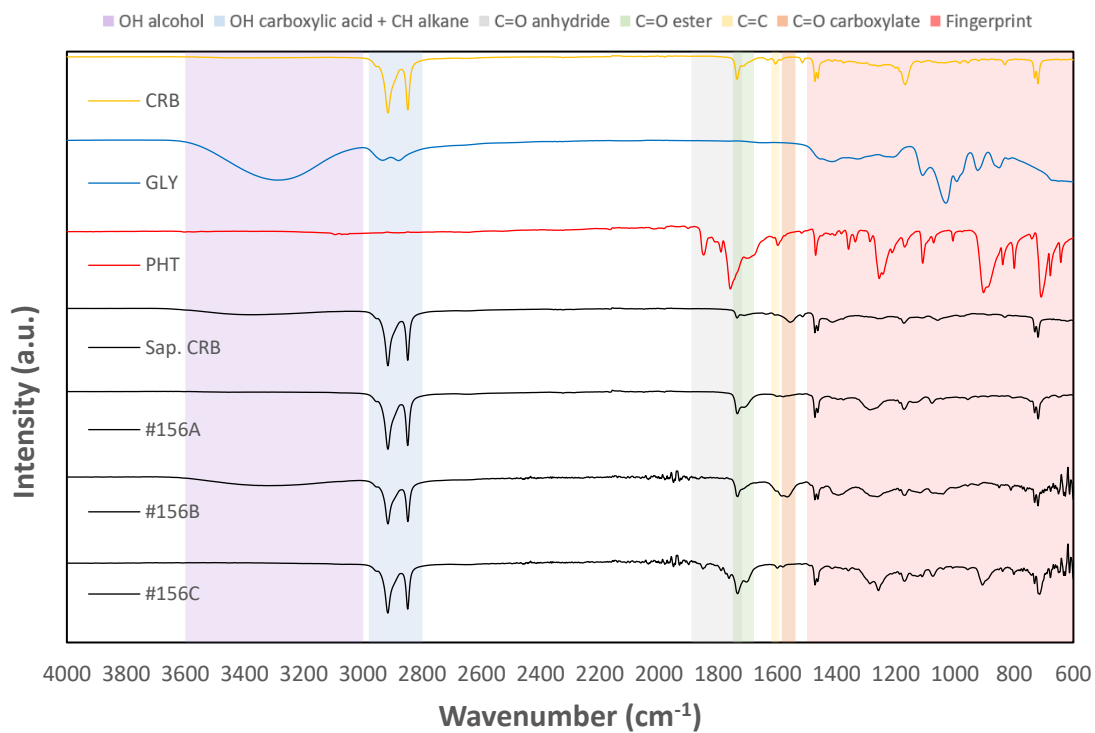
Figure 66 - #156 FTIR spectra (R4.0)
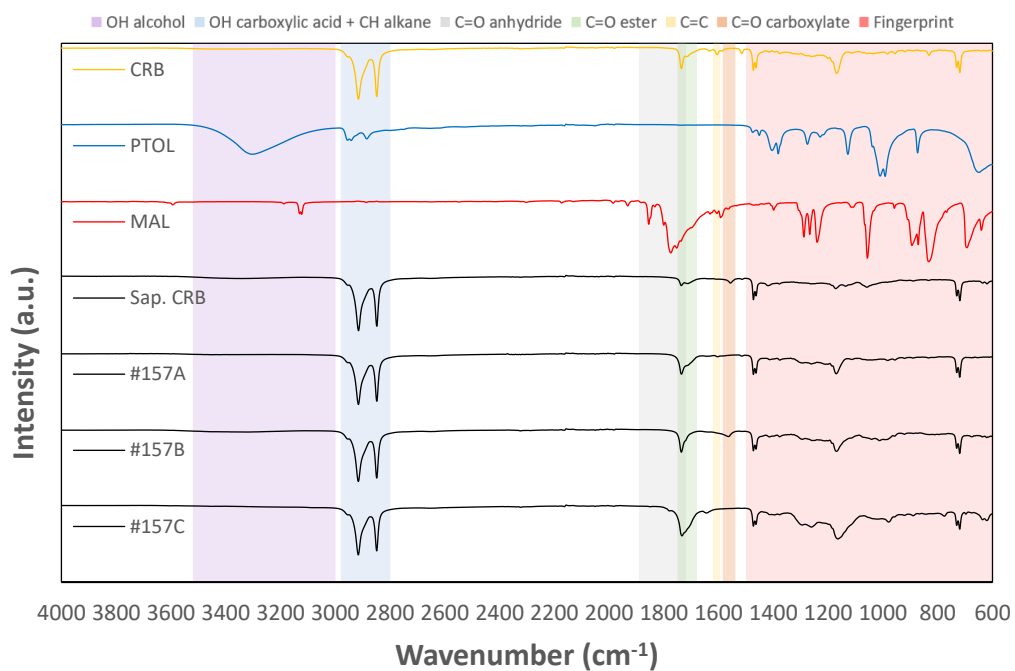
Figure 67 - #157 FTIR spectra (R4.1)
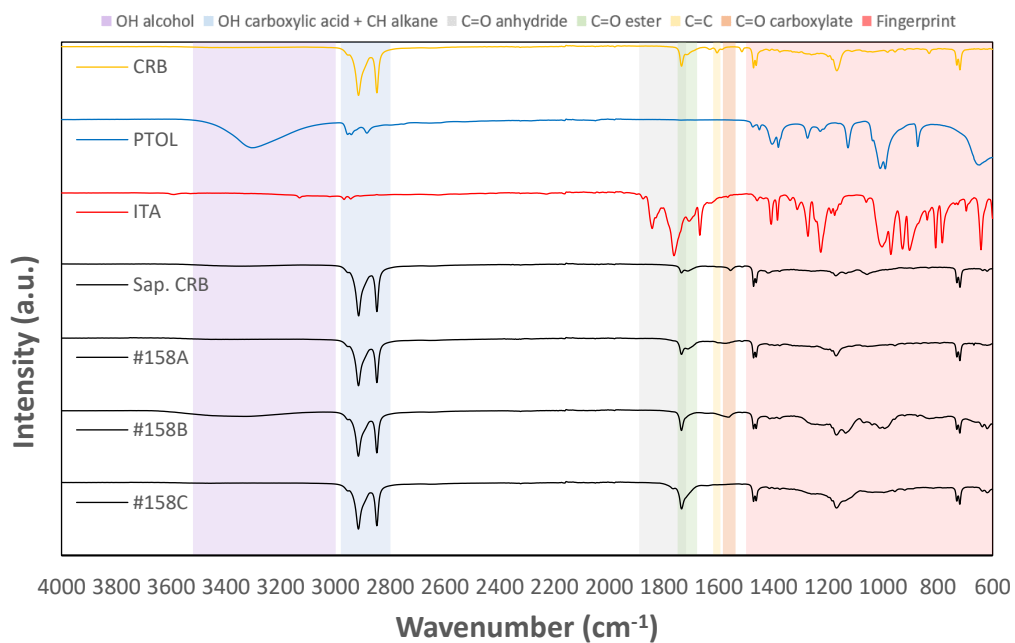
Figure 68 – #158 FTIR spectra (R4.1)
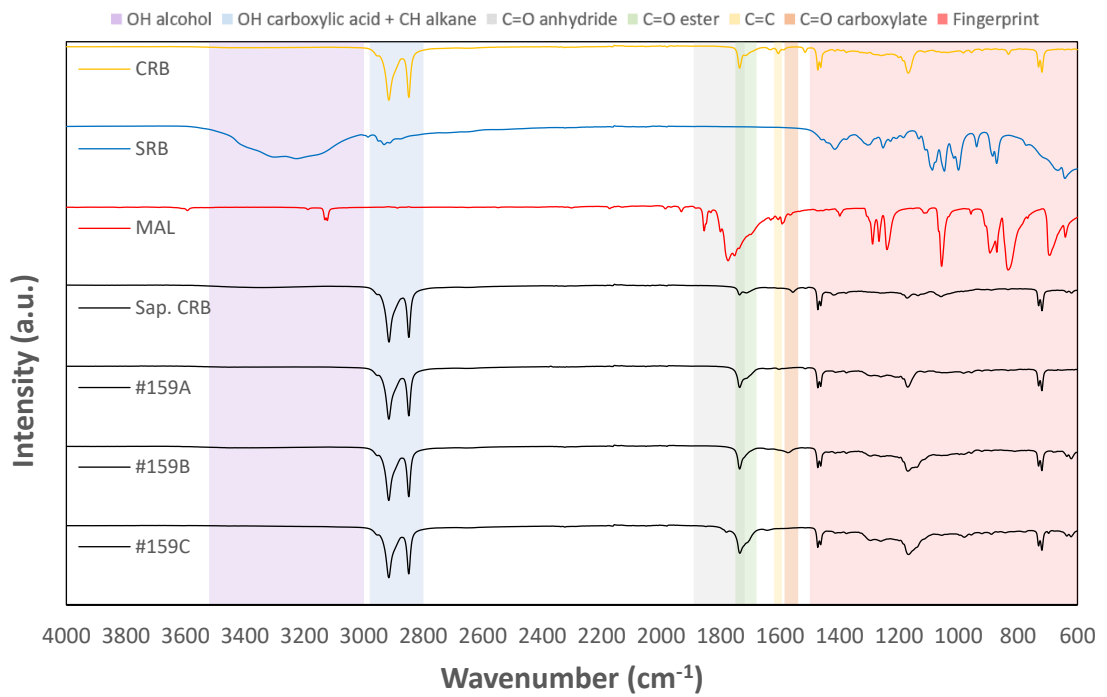
Figure 69 – #159 FTIR spectra (R4.1)
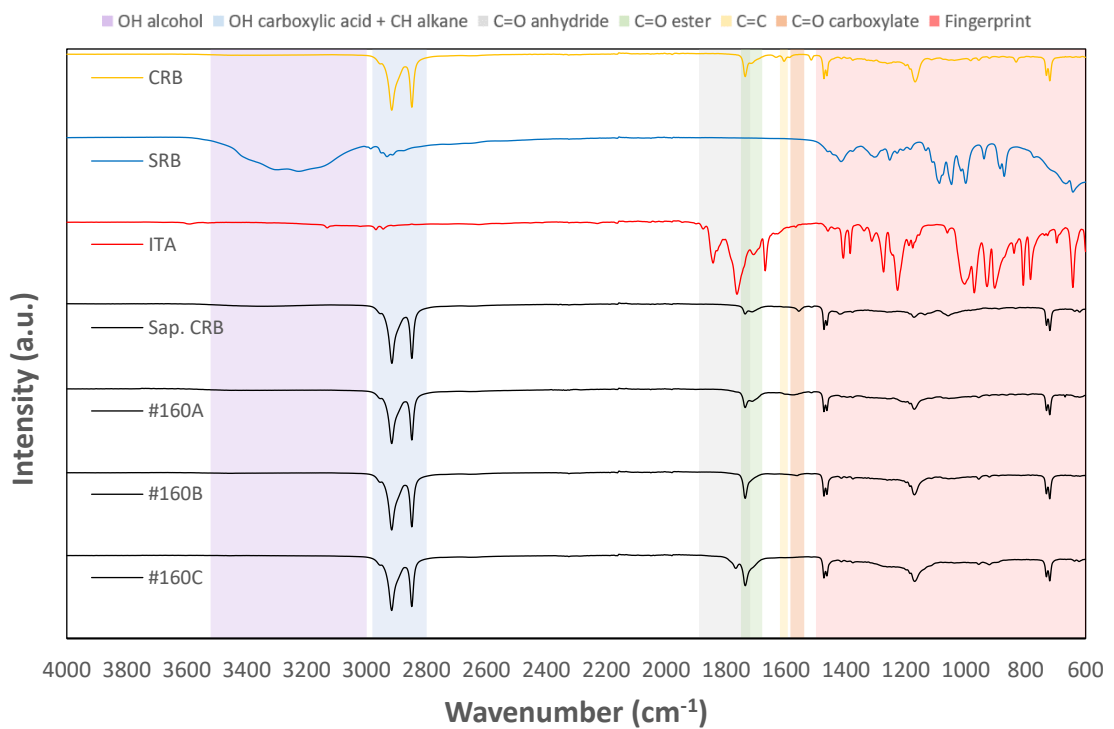
Figure 70 – #160 FTIR spectra (R4.1)

Table 68 – Film thickness measurements

Sample	Film	Thickness (µm)					Mean (µm)
CRB	S1	215.80 ✓	180.85 ✓	192.34 ✓	242.29 ✓	255.42 ✓	217.34
	S2	212.92 ✓	173.15 ✓	188.89 ✓	163.91 ✓	219.57 ✓	191.69
#161	S1*	284.52 ✓	280.66 ✓	280.95 ✓	306.16 ✗	274.42 ✗	282.04
	S2	347.18 ✓	350.00 ✓	329.20 ✓	372.83 ✗	336.92 ✓	340.83
	S3	329.70 ✓	335.12 ✓	295.75 ✓	281.86 ✓	273.88 ✓	303.26
	S4	306.92 ✓	314.49 ✓	343.46 ✓	314.95 ✓	336.33 ✓	323.23
#162	S1*	264.92 ✓	244.82 ✗	259.57 ✓	260.39 ✓	268.50 ✓	263.35
	S2*	272.60 ✓	284.15 ✓	253.64 ✗	276.77 ✓	269.46 ✓	275.75
	S3*	251.75 ✗	263.53 ✓	262.64 ✓	277.34 ✗	264.32 ✓	263.50
	S4	299.38 ✓	250.16 ✓	260.68 ✓	253.09 ✓	241.48 ✓	260.96
#163	S1	248.45 ✗	265.95 ✓	267.95 ✓	273.96 ✓	273.92 ✓	270.45
	S2*	292.55 ✓	283.48 ✓	268.16 ✓	272.99 ✓	316.45 ✗	286.73
	S3	256.04 ✓	281.81 ✗	261.68 ✓	260.44 ✓	249.67 ✓	256.96
	S4*	253.68 ✓	270.09 ✓	261.66 ✓	281.88 ✓	287.48 ✓	270.96
#164	S1	237.22 ✓	271.86 ✗	247.44 ✓	231.45 ✓	236.53 ✓	238.16
	S2	235.02 ✓	225.52 ✓	256.50 ✓	242.41 ✓	251.11 ✓	242.11
	S3	241.87 ✓	247.95 ✓	214.43 ✓	247.61 ✓	226.19 ✓	235.61
	S4	217.43 ✓	228.69 ✓	211.08 ✓	214.36 ✓	234.76 ✓	221.26

*the film broke during the test and it was not considered for the evaluation of WVP